The Solution Conformations of Macrocycles

Applications in the exploration of weak interactions and in drug development

Emma Danelius

UNIVERSITY OF GOTHENBURG

Department of Chemistry and Molecular Biology
University of Gothenburg
2017

DOCTORAL THESIS
Submitted for fulfilment of the requirements for the degree of
Doctor of Philosophy in Chemistry

The Solution Conformations of Macrocycles

Applications in the exploration of weak interactions and in drug development

ISBN: 978-91-629-0274-2 (Print)
ISBN: 978-91-629-0275-9 (PDF)
http://hdl.handle.net/2077/52335

Department of Chemistry and Molecular Biology
SE-41296 Göteborg
Sweden

Printed by Ineko AB
Kållered, 2017

To my family

Abstract

Understanding the solution conformation and dynamics of molecules with biological relevance, as well as the impact of their conformation stabilizing weak interactions, is for example important for drug design. Macrocycles have attractive pharmaceutical properties, and are of special interest as drug leads for targets with large, flat and featureless binding sites like protein-protein interfaces. As they are usually flexible and adopt a variety of solution geometries, the description of their ensembles is of high value. Most macrocyclic drugs are peptides or macrolides. Peptides, and in particular β-hairpin peptides, are suitable model systems for studying weak interactions. Due to their resemblance to proteins, studying peptides by solution state experiments provides knowledge gained in a biologically relevant environment. In this thesis, nuclear magnetic resonance (NMR) spectroscopy has been used for investigation of the solution ensembles of various macrocycles. Using a cyclic β-hairpin model system and NMR analysis of molecular flexibility in solution (NAMFIS), a single interstrand hydrogen bond was shown to provide significant stabilization of the folded conformation. In addition, it was shown that a chlorine-centered halogen bond stabilizes the β-hairpin to a comparable extent. Further, the solution ensembles of four cyclic β-hairpin inhibitors of the MDM2/p53 protein-protein interaction were described, and a higher conformational flexibility was found to correlate with an increased inhibitory activity. In contrast, for cyclic azapeptide inhibitors of the cluster of differentiation 36 (CD36) receptor, higher flexibility correlated to decreased inhibitory activity. An increased population of one of the conformational families in solution was found to be beneficial for the CD36 inhibitory activity. Lastly, roxithromycin, a macrolide antibacterial agent, was described to convert from a more open conformation in polar media to a more closed and less flexible conformation in non-polar media. This thesis demonstrates that macrocycles are applicable as model systems for the study of weak interaction forces, which have a large influence on their conformational behavior. Furthermore, the obtained results show that the conformational stability of macrocycles vastly influences their bioactivity.

Keywords: Macrocycles, cyclic peptides, NMR, solution conformational analysis, NAMFIS, β-hairpin, weak interactions, halogen bonding, protein-protein interaction, bioactive conformation, macrolides, cell permeable conformation.

List of publications

The thesis is based on the following papers and manuscripts, which are referred to in the text by their Roman numerals.

I **Insight into β-Hairpin Stability: Interstrand Hydrogen Bonding**
Emma Danelius, Ulrika Brath, Máté Erdélyi
Synlett, **2013**, *24,* 2407–2410

II **Assessing the Ability of Spectroscopic Methods to Determine the Difference in the Folding Propensities of Highly Similar β-Hairpins**
Hanna Andersson, Emma Danelius, Patrik Jarvoll, Stephan Niebling, Ashley J. Hughes, Sebastian Westenhoff, Ulrika Brath, Máté Erdélyi
ACS Omega, **2017**, *2*, 508–516

III **Halogen Bonding: a Powerful Tool for Modulation of Peptide Conformation**
Emma Danelius, Hanna Andersson, Patrik Jarvoll, Kajsa Lood, Jürgen Gräfenstein, Máté Erdélyi
Biochemistry, **2017**, *56*, 3265–3272

IV **Flexibility is Important for Inhibition of the MDM2/p53 Protein−Protein Interaction by Cyclic β-Hairpins**
Emma Danelius, Mariell Pettersson, Matilda Bred, Jaeki Min, M. Brett Waddell, R. Kiplin Guy, Morten Grøtli, Máté Erdélyi
Organic and Biomolecular Chemistry, **2016**, *14*, 10386–10393

V **Conformational Preferences of Macrocyclic Azapeptide Inhibitors of CD36 in Aqueous Solution**
Emma Danelius, Ahsanullah Ahsanullah, Máté Erdélyi, William Lubell
Manuscript

Publications not included but referred to in this thesis:

The Impact of Interchain Hydrogen Bonding on β-Hairpin Stability is Readily Predicted by Molecular Dynamics Simulation

Stephan Niebling, Emma Danelius, Ulrika Brath, Sebastian Westenhoff, Máté Erdélyi

Peptide Science, **2015**, *104*, 703–706

Conformational Analysis of Macrocyclic Drugs that Adapt to their Environment

Vasanthanathan Poongavanam, Lilian Alcaraz, Emma Danelius, Giulia Caron, Paul Jackson, Máté Erdélyi, Stanislaw Wlodek, Paul C. D. Hawkins, Giuseppe Ermondi, Jan Kihlberg

Manuscript

Contribution to papers I-V

I Performed or supervised the synthesis. Performed the NMR-analysis and interpreted the results, and did parts of the conformational analysis. Wrote the manuscript draft.

II Performed some of the NMR-experiments and contributed to interpretation of the results. Performed the conformational analysis. Provided minor contribution to writing the manuscript.

III Performed or supervised parts of the synthesis. Performed the NMR-analysis and interpreted the results, and performed the conformational analysis. Wrote the manuscript draft.

IV Performed or supervised the synthesis. Performed the NMR-analysis and interpreted the results, and performed the conformational analysis. Wrote the manuscript draft together with MP.

V Performed the NMR-analysis and the conformational analysis. Wrote the manuscript draft.

List of abbreviations

2D NMR	Two-dimensional NMR
AA	Amino acid
Abu	Aminobutyric acid
Ala	Alanine
Asn	Asparagine
Asp	Aspartic acid
Arg	Arginine
Bn	Benzyl
Boc	*tert*-Butyloxycarbonyl
bRo5	Beyond rule of five
CD	Circular dichroism
CD36	Cluster of differentiation 36
Cryo-EM	Cryo-electron microscopy
CSD	Cambridge structural database
Cys	Cysteine
DCC	*N,N*'-Dicyclohexylcarbodiimide
DCM	Dichloromethane
DIC	*N,N*'-Diisopropylcarbodiimide
DIPEA	*N*,*N*-Diisopropylethylamine
DMF	Dimethylformamide
DMSO	Dimethyl sulfoxide
DNA	Deoxyribonucleic acid
Fmoc	9-Fluorenylmethoxycarbonyl
FP	Fluorescence polarization
GH	Growth hormone
GHRP	Growth hormone releasing peptide
GHS-R1a	Growth hormone secretagogue receptor 1a
Gln	Glutamine
Glu	Glutamic acid
Gly	Glycine
HATU	1-[Bis(dimethylamino)methylene]-1*H*-1,2,3-triazolo[4,5-*b*]pyridinium 3-oxide hexafluorophosphate
HBA	Hydrogen bond acceptors
HBD	Hydrogen bond donors
HBTU	3-[Bis(dimethylamino)methyliumyl]-3*H*-benzotriazol-1-oxide hexafluorophosphate
His	Histidine

HOAt	1-Hydroxy-7-azabenzotriazole
HOBt	1-Hydroxybenzotriazole
Ile	Isoleucine
IR	Infrared
Leu	Leucine
MCMM	Monte Carlo molecular mechanics
MD	Molecular dynamics
MDM2	Mouse double minute 2 homolog
MM	Molecular mechanics
NAMFIS	NMR analysis of molecular flexibility in solution
n.d.	Not determined
NMR	Nuclear magnetic resonance
NOE	Nuclear Overhauser effect
NOESY	Nuclear Overhauser effect spectroscopy
oxLDL	Oxidized low density lipoproteins
p53	Tumor protein p53
Pbf	2,2,4,6,7-Pentamethyl-2,3-dihydrobenzofuran-5-sulfonyl
PDB	Protein data bank
PEG	Polyethylene glycol
Phe	Phenylalanine
ppb	Parts per billion
PPI	Protein-protein interaction
ppm	Parts per million
Pro	Proline
PS	Polystyrene
PSA	Polar surface area
pyBOP	Benzotriazol-1-yl-oxytripyrrolidinophosphonium hexafluorophosphate
RMSD	Root-mean-square deviation
RNA	Ribonucleic acid
Ser	Serine
SPPS	Solid phase peptide synthesis
SPR	Surface plasmon resonance
TBTU	3-[Bis(dimethylamino)methyliumyl]-3*H*-benzotriazol-1-oxide tetrafluoroborate
t-Bu	*tert*-Butyl
TFA	Trifluoroacetic acid
Thr	Threonine
TIPS	Triisopropylsilane
TMP	2,4,6-Trimethylpyridine

TOCSY	Total correlation spectroscopy
Trp	Tryptophan
Trt	Trityl
Tyr	Tyrosine
Val	Valine
VT CD	Variable temperature circular dichroism
VT NMR	Variable temperature NMR

Table of Contents

1. General introduction 1

2. Macrocycles 3

2.1 Solution conformation 4

2.1.1 The β-hairpin structural motif 4

2.1.2 Design of β-hairpins stable in solution 5

2.1.2.1 Turn sequence 5

2.1.2.2 β-sheet forming propensities of amino acids 6

2.1.2.3 Interactions between side chains 6

2.1.2.4 Backbone hydrogen bonds 6

3. Conformational analysis of flexible systems 7

3.1 Peptide NMR spectroscopy 7

3.1.1 Peptide ^{1}H NMR assignment 8

3.1.2 Chemical shift and coupling constants related to secondary structure 9

3.1.3 Measuring interproton distances from NOESY 9

3.1.4 Variable temperature NMR spectroscopy 10

3.1.5 Backbone hydrogen bonding 11

3.2 NMR analysis of molecular flexibility in solution 12

4. Peptide synthesis 15

4.1 Solid phase peptide synthesis 15

4.2 The Fmoc/*t*-Bu method 17

4.3 Resins and linkers 18

4.4. Coupling reagents 19

4.5 Peptide cyclization 21

5. Aims of the thesis 23

6. Investigation of weak interactions using cyclic β-hairpin peptides as model systems (Papers I–III) 25

6.1 Weak interactions in biological systems 25

6.1.1 Hydrogen bonding 25

6.1.2 Halogen bonding 26

6.2 Evaluation of the impact of interstrand hydrogen bonding on β-hairpin stability (Paper I) 26

6.2.1 Results and discussion Paper I 28

6.2.2 Summary Paper I 32

6.3 Evaluation of the ability of spectroscopic methods to assess the difference in folding of β-hairpins (Paper II) 32

6.3.1 Results and discussion Paper II 33
6.3.2 Summary Paper II 36
6.4 Evaluation of the impact of interstrand halogen bonding on β-hairpin stability (Paper III) 36
6.4.1 Results and discussion Paper III 36
6.4.2 Summary Paper III 44
7. Conformational analysis of β-hairpin inhibitors of the MDM2/p53 protein-protein interaction (Paper IV) 45
7.1 The protein-protein interaction 45
7.2 The MDM2/p53 interaction 45
7.3 Constrained bioactive peptides 46
7.4 Methods used for biological evaluation 47
7.4.1 Surface plasmon resonance 47
7.4.2 Fluorescence polarization 47
7.5 Evaluation of the flexibility of cyclic β-hairpins inhibitors of the MDM2/p53 protein-protein interaction (Paper IV) 48
7.5.1 Results and discussion Paper IV 49
7.5.2 Summary Paper IV 53
8. Conformational analysis of CD36 modulating cyclic azapeptides (Paper V) 55
8.1 The cluster of differentiation 36 receptor 55
8.2 Growth hormone releasing peptides 55
8.3 Azapeptides 56
8.4 Conformational preferences of macrocyclic azapeptide inhibitors of CD36 in aqueous solution (Paper V) 56
8.4.1 Results and discussion Paper V 57
8.4.2 Summary Paper V 60
9. The solution conformations of roxithromycin adapting to the environment 61
9.1 Cell permeability of macrocycles 61
9.2 Roxithromycin 61
9.3 Solvent dependence of the conformations of roxithromycin 62
10. Concluding remarks 67
11. Acknowledgement 69
12. References 73
13. Appendices 81

1 GENERAL INTRODUCTION

Life is all about molecular motion. The conformational behavior and the interactions of complex molecules in a three-dimensional space run nearly every aspect of biology. If we can describe the dynamics and the interactions of biomolecules and their ligands we gain valuable information that can be used, for example, in the design of drugs. The conformational change of biological molecules in solution is a result of forming and breaking a number of weak interactions such as hydrogen bonds, hydrophobic interactions, and π-stacking. Since these interactions are weak, biological systems are flexible. These cooperatively acting weak forces and the conformational dynamics generated are to a large extent responsible for the function of biological systems. The same is true when a ligand/drug molecule binds to a biological target macromolecule. In order for the ligand to bind with high affinity, these precise interactions have to be generated and the ligand has to be able to adopt the 3D conformations required to fit into the binding pocket of the macromolecule. In drug design, drug candidates are optimized with respect to this bioactive conformation and to the corresponding interactions to the target macromolecule, which is typically a protein. Obtaining information of the biologically active conformation and the interactions involved is therefore of high importance.

There are several methods available for collecting information about the structure, conformation and interactions of molecules with biochemical relevance, including X-ray diffraction, Raman spectroscopy, infrared (IR) spectroscopy, molecular mechanics (MM) and molecular dynamics (MD) calculations, optical rotation and circular dichroism (CD) spectroscopy, single particle cryo-electron microscopy (cryo-EM), and nuclear magnetic resonance (NMR) spectroscopy. The two that have found the most widespread use are X-ray diffraction and NMR spectroscopy. X-ray diffraction provides crystal structures with detailed atomic-level information of the 3D structure of molecules in the solid state. This technique is without doubt the most powerful tool to obtain information about the 3D geometry. However, since measured in the solid state, the generated structure is static and not dynamic as it would be in solution. On the other hand, NMR spectroscopy can be measured in solution and thereby gives information on the dynamics and conformational

behavior of the studied molecule, as well as on their interactions, in a context that better resembles a biological environment. Both X-ray diffraction and NMR spectroscopy have been awarded with several Nobel prizes.[1,2]

2 MACROCYCLES

Classical drug development has focused on small molecule drugs with properties within the Lipinski rule of five,[3] in other words with molecular weight ≤ 500 Da, cLogP ≤ 5, hydrogen bond donors (HBD) ≤ 5, and hydrogen bond acceptors (HBA) ≤ 10. Lipinski's rules can be viewed as guidelines for oral bioavailability, and they have been extended to include polar surface area (PSA) ≤ 140 Å^2 and number of rotatable bonds ≤ 10.[4,5] There are also larger protein-based biological therapeutics, typically with molecular weight > 5000 Da.[6] These biological drugs have been successfully used to modulate targets with exceptional specificity and potency. However, they violate Lipinski's rules resulting in poor cell permeability and low bioavailability, and they are typically administrated intravenously.[6,7] Since a large part of the human proteome has been classified as difficult to modulate using small molecules,[8] a lot of effort is presently put into bridging the gap of small molecules and biologics.[6,9-11] One strategy for this is to use macrocycles, that is cyclic compounds comprising of 12 atoms or more.[12] Macrocycles usually have molecular weights >500 Da and offer an alternative to small molecule drug candidates, providing high specificity, affinity and chemical diversity but still have a better chance of cell permeability than the biologics.[7,11,13] They are often referred to as beyond rule of five (bRo5) ligands since they have properties outside Lipinski's rule of five,[10,14] and they are of special interest as drug leads for non-conventional targets with large, flat and featureless binding sites like protein-protein interactions (PPIs).[10,12,13] As most macrocyclic drugs are cyclic peptides or macrolides,[13] macrocycles are commonly classified as peptidic or non-peptidic natural products, synthetic peptides or synthetic macrocycles.[15] Cyclic peptides have attained increased attention for their attractive pharmaceutical properties as compared to their linear analogues.[7, 16] Since peptides commonly require constrains to retain their 3D structure in water and usually have low bioavailability, peptide cyclization is frequently used to increase their folding. Cyclization leads to minimized metabolic degradation in the gut, blood and tissues as a result of removing the cleavable *N*- and *C*-termini. In addition, the generated conformations often have decreased exposure of polar atoms to the surroundings, which might increase oral bioavailability.[7] Likewise, cyclization is also commonly utilized in order to lock the peptide in the bioactive conformation, and thereby increase the bioactivity.[17] Even

though there are issues such as poor bioavailability and propensity to be rapidly metabolized, over 100 peptidic and macrocyclic drugs are currently on the market,[6,18,19] and the present approval rate of peptide drugs is twice as high as that of small molecule-based drugs.[20] Owing to the fast growing attention of bridging the gap between traditional small molecule and large biological drugs, the understanding and the ability of predicting the behavior of cyclic peptides and other macrocycles is of utmost importance.

2.1 Solution conformation

Macrocycles are usually flexible molecules and a variety of conformers are thus present in solution. It has been shown that due to this flexibility, the population of the bioactive conformation of macrocycles can be as small as 4% in solution.[21] Further, in contrast to small molecule-based drugs, the solution conformations of peptidic drugs have been proposed to be even more important than their physiochemical properties in order to gain high bioactivity and bioavailability.[17] Truncated peptide fragments from proteins usually do not retain their native conformation and consequently lose their binding affinity. Therefore, peptides are often modified with the aim of reinforcing their native conformation and of restoring their binding affinity towards their protein targets, for example via cyclization.[16] There are numerous examples of the introduction of conformational constrains that lock them into a defined secondary structure,[17,22] including stapled α-helices[23,24] azide-alkyne 1,3-dipolar cycloaddition[25] and cysteine- or triazole-bridged β-hairpins.[26] Since most of the work in this thesis is based on the β-hairpin secondary structure, it is described in more detail below.

2.1.1 The β-hairpin structural motif

A β-hairpin consists of two antiparallel hydrogen bonded β-strands, connected by a type I' (ϕ_{i+1} = 60°, ψ_{i+1} = 30°, ϕ_{i+2} = 90°, ψ_{i+2} = 0°) or a type II' (ϕ_{i+1} = 60°, ψ_{i+1} = -120°, ϕ_{i+2} = -80°, ψ_{i+2} = 0°) β-turn (Figure 1).[27] It is a common motif in proteins, often involved in molecular recognition events such as protein-DNA, protein-RNA, and protein-protein recognition.[28,29] β-Hairpins have, for example, been studied as inhibitors of PPIs,[30] antimicrobial agents,[31] and protease inhibitors.[32]

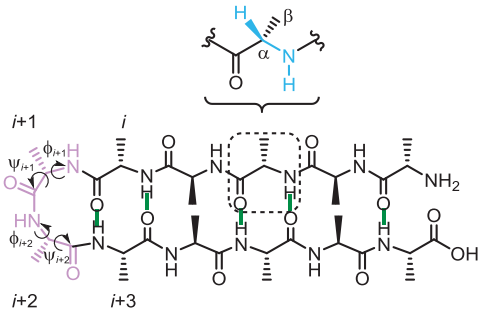

Figure 1. Schematic representation of a β-hairpin. The loop positions are shown in purple and backbone hydrogen bonds in green. The backbone dihedral angle used in the Karplus equation ($J_{HH'}$ = A + B cos ϕ + C cos 2ϕ) is shown in blue.

In addition, β-hairpins are suitable model systems for studying the early stages of protein folding[33] and as models for investigation of weak interactions.[34,35] The first small linear peptide that folds into β-hairpin in solution was reported in 1993,[36] and since then a large number of β-hairpin models have been described.[27,28,33] However, the high tendency to aggregate and the low conformational stability of isolated linear β-hairpins, makes their investigation challenging. Consequently, large efforts have been made to determine the driving forces of β-hairpin folding and to find β-hairpin stabilizing elements, some of which are described below.

2.1.2 Design of β-hairpins stable in solution

β-Hairpin formation is the result of the cooperative interplay of several factors.[27,33] These include the conformational directing ability and rigidity of the β-turn, the propensity of the strand residues to adopt an extended conformation, the presence of stabilizing side chain cross strand interactions, and backbone hydrogen bonds.

2.1.2.1 Turn sequence

The β-turn has a backbone hydrogen bond between residues *i* and *i*+3, as illustrated in Figure 1.[37] There are several types of turn structures with a variety of amino acid combinations known to have high propensity of forming β-turns. Some common examples are D-Pro-Gly,[38,39] Gly-Asp,[40] Asn-Gly,[39] and D-Pro-L-Pro.[28,41,42] The turn sequence is proposed to play a major role in the folding propensity for β-hairpins.[37,38]

2.1.2.2 β-Sheet forming propensities of amino acids

Various amino acids have a different tendency to form the β-sheets of β-hairpins. Especially β-branched amino acids such as Val, Ile and Thr favor β-sheet formation.[43,44] Other amino acids that are also commonly found in β-sheets are Phe, Tyr and Trp. The amino acids with least β-sheet forming tendency are Ala, Asp, Gly, and Pro,[43] which, on the other hand, are commonly found in β-turns.

2.1.2.3 Interactions between side chains

Cross strand side chain to side chain interactions are commonly used to improve β-hairpin stability.[45] These interactions can be either hydrophobic or polar, and some common examples are the "tryptophan zipper" encompassing cross strand tryptophan residues,[46] aromatic π-interactions,[47] and electrostatic interactions.[27,33,48]

2.1.2.4 Backbone hydrogen bonds

The backbone hydrogen bonds of β-hairpins usually only have a weak stabilizing role, and their influence is not fully understood.[27,33] The stabilization of backbone hydrogen bonds are related mainly to the turn regions.[33] Nevertheless, backbone hydrogen bonding is part of the definition of the β-hairpin structural element, as shown in Figure 1.

3 CONFORMATIONAL ALALYSIS OF FLEXIBLE SYSTEMS

Some commonly used techniques to gain insight into the conformational behavior of molecules are X-ray diffraction,[49] Raman spectroscopy,[50] IR spectroscopy,[51] MM and MD calculations,[52-54] CD spectroscopy,[42,55] cryo-EM,[56] and NMR spectroscopy.[57] Of the experimental methods, CD and IR/Raman give information on the overall conformation, whereas NMR and X-ray diffraction provide atomic level data. Cryo-EM also gives detailed information, although this rather new technique has not yet found the same widespread use as NMR spectroscopy and X-ray diffraction.[56,58] The bioactive conformation of ligands is usually derived from X-ray crystallography, but the flexibility of a molecule in solution is better explored by NMR spectroscopy. An important and often ignored aspect of NMR spectroscopy is that the signals are averages of all the conformations of the studied molecule that are present, weighted with their corresponding molar fractions. Therefore, when presuming a single conformation only, NMR data in combination with MM or MD calculation may give misleading geometries. For its proper interpretation, the observed data have to be analyzed as the population averaged sum of the data of single conformations.[59,60] The NMR analysis of molecular flexibility in solution (NAMFIS)[61] method can deconvolute the NMR data into the present conformers, as described in section 3.2 below.

3.1 Peptide NMR spectroscopy

The two most commonly used 2D NMR techniques for studying the primary structure of peptides are Total Correlation Spectroscopy (TOCSY) and Nuclear Overhauser Effect Spectroscopy (NOESY).[59] TOCSY gives correlations for all protons that belong to the same spin system, in other words through-bond correlations via spin-spin coupling. NOESY correlates protons through dipolar couplings in space, i.e. protons that are not covalently bonded. The NOE effect is scaled by $1/r^6$, where r is the distance between two protons and typically distances up to ~5 Å can be detected. The NOE signal also depends on the motion of the molecule, which is dependent on the size and the shape of the molecule, viscosity of the solution, temperature, and magnetic field strength.[62] The signal dependence of the molecular motion is illustrated in Figure 2 A. The phase of small, fast tumbling molecules is usually of opposite sign as compared to the diagonal peaks

and the NOE has a maximum possible value of +0.5. For large slow tumbling molecules the phase is usually of the same sign as compared to the diagonal peaks and the NOE has a maximum of -1.0. As shown in Figure 2 A. intermediate size molecules (~1000–2000 Da) might give very weak or no NOE signals at all.[62] Due to the $1/r^6$ signal dependence of the NOE signal, interproton distances can be calculated from NOE measurements (Figure 2 B), as described in section 3.1.3 below.

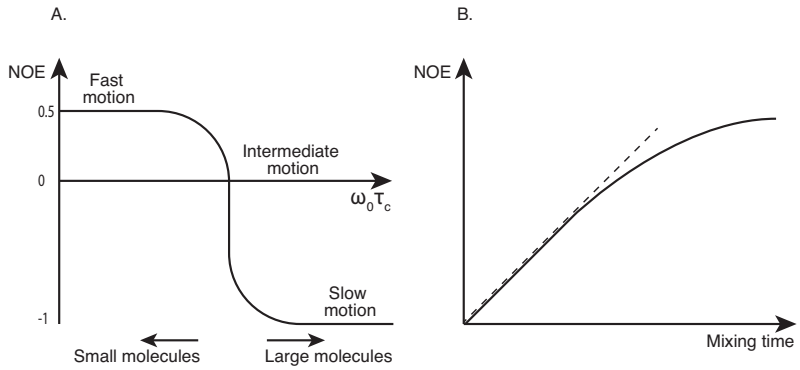

Figure 2. The magnitude of NOE depends on molecular and experimental factors. **A**. The dependence of the signal intensity on molecular motion (τ_c = correlation time, i.e. the time required for a molecule to rotate one radian ($2\pi/360°$), ω_0 = spectrometer observation frequency). Small molecule NOE signals are positive with a maximum possible value of +0.5 (+50%). Large molecule NOE signals are negative with a maximum possible value of -1 (-100%). Intermediate size molecules might give zero NOE. **B**. The build-up of the NOE signal as a function of mixing time (full line) and the initial rate approximation (dashed line).

3.1.1 Peptide ^{1}H NMR assignment

The chemical shift of peptide protons are usually assigned with the TOCSY-NOESY sequential backbone walk.[63] A TOCSY spectrum gives characteristic peak patterns for each amino acid in the peptide. Starting from an NH diagonal peak following f1 or f2, all cross peaks in the spin system for a given amino acid can be detected. Correlations to the next amino acid in the sequence can then be found in the corresponding NOESY spectrum, and in this way all peptide protons can be assigned by "walking" through the backbone.

3.1.2 Chemical shift and coupling constants related to secondary structure

Proton chemical shifts are affected by the electron distribution, bond hybridization, proximity to polar groups, nearby aromatic rings, and bond magnetic anisotropy, but are also sensitive to molecular conformation and environment.[64,65] The ^{1}H and ^{13}C chemical shifts of peptides give information on their secondary structure. Protons in β-strands are more deshielded (higher chemical shifts), as compared to the chemical shifts of random coils. Analogously, protons in α-helices are more shielded (lower chemical shifts), as compared to those of random coils.[64] There is also a relationship between $^{3}J_{NHC\alpha H}$ coupling constants and secondary structure: larger couplings are obtained for β-sheets as compared to α-helices.[66] The $^{3}J_{NHC\alpha H}$ for peptides can be transformed to the corresponding dihedral angles (Figure 1, blue atoms) via a modified Karplus equation ($^{3}J_{HH'} = A + B \cos \phi + C \cos 2\phi$)[67,68] with A, B and C-constants optimized for amino acid side chain substitute effects.[69]

3.1.3 Measuring interproton distances from NOESY

The NOE is the result of dipolar cross-relaxation from nearby spins with perturbed energy levels. The magnitude of the observable NOE is proportional to the cross-relaxation rate (σ) between the interacting spins.[62] In the NOESY experiment there is a delay for evolution of the NOE transfer, in other words NOE signal build-up. This delay is also referred to as mixing time. As illustrated in Figure 2 B, the initial build-up (dashed line) is linear at short mixing times at which the observed signal intensity is determined by the cross-relaxation process. At longer mixing times, other relaxation mechanisms, such as spin diffusion, influence the relaxation and consequently the dependence of NOE intensity on the mixing time deviates from the initial linearity (Figure 2 B full line).[59] In practice, a series of NOESY experiments with an array of mixing times are measured and the normalized peak areas for each mixing time at the initial linear part of the buildup curve calculated according to eq. 1[70]

$$\text{Peak Area} = \left(\frac{\text{Cross peak 1} \times \text{Cross peak 2}}{\text{Diagonal peak 1} \times \text{Diagonal peak 2}}\right)^{0.5} \qquad \text{(eq. 1)}$$

and then plotted against the mixing times. The slope of the initial linear part of the build-up curve (Figure 2 B, dashed line) corresponds to the cross-relaxation rate σ, and from this the interproton distances can be calculated according to eq. 2

$$r_{ij} = r_{ref} \times \left(\frac{\sigma_{ref}}{\sigma_{ij}}\right)^{(1/6)} \qquad \text{(eq. 2)}$$

where r_{ij} is the distance between protons *i* and *j*, r_{ref} is the distance for a pair of reference protons (geminal CH_2 = 1.78 Å or aromatic H-C=C-H = 2.51 Å), and σ_{ref} and σ_{ij} are the corresponding build-up rates.

3.1.4 Variable temperature NMR spectroscopy

The temperature dependence of the chemical shift of the proton of a peptide involved in a two-state equilibrium process can be measured by variable temperature NMR (VT NMR), as is illustrated in Figure 3 (dashed curve). Peptides are typically flexible and exist as an ensemble of conformations in solution, and accordingly their observed chemical shifts are the population weighted averages of all conformations that are present at a certain temperature.[59] Upon temperature variation, they show broad transition curves where the fully folded state is usually not reached even at low temperatures. Large proteins are typically less dynamic with well-defined folding states (solid curve, Figure 3),[71] and it is therefore easier to determine their melting temperature (T_m). Even if the complete unfolded/folded states may not be reached for a small peptide fragment within an experimentally acsessible temperature interval, the data can be fitted to the equation describing the temperature dependence of the chemical shift (eq. 3). The melting temperature (transition temperature) T_m can thus be derived from

$$\delta_{obs} = \delta_U + \frac{\delta_F - \delta_U}{\exp\left[-\frac{\Delta H_m}{R}\left(\frac{1}{T} - \frac{1}{T_m}\right)\right] + 1} \qquad \text{(eq. 3)}$$

where δ_{obs} is the observed chemical shift in ppm at the different temperatures (T), δ_F and δ_U are the chemical shift for the folded and unfolded states, respectively, and ΔH_m is the enthalpy change for unfolding at the melting temperature T_m.[72]

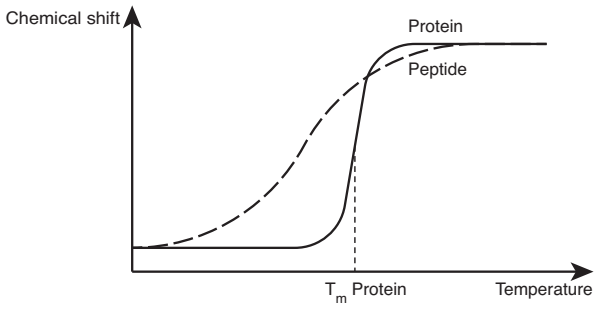

Figure 3. The chemical shift temperature dependence of proteins and peptides involved in a two-state conformational equilibrium process. T_m= unfolding temperature/melting temperature, i.e. the temperature at which 50% of the protein/peptide is unfolded.

3.1.5 Backbone hydrogen bonding

There are two routinely used methods to investigate backbone hydrogen bonding in peptides. The first method is by measuring the amide proton temperature coefficients ($\Delta\delta_{NH}/\Delta T$), which are derived from the correlation of ^{1}H NMR chemical shift and temperature. $\Delta\delta_{NH}/\Delta T$ of the backbone NH are obtained from $(\delta_{T,high}-\delta_{T,low})/(T_{high}-T_{low})$ and typically provides negative values, which are conventionally reported as positive numbers.[59] $\Delta\delta_{NH}/\Delta T < 3$ indicates a strong intramolecular hydrogen bond, $\Delta\delta_{NH}/\Delta T = 3–5$ indicates that the amide proton is in equilibrium between a solvent exposed and an intramolecular hydrogen bond, and $\Delta\delta_{NH}/\Delta T > 5$ that the amide proton is solvent exposed.[59,73,74] The temperature dependence is usually linear to about 15 °C below the melting temperature for the peptide (Figure 3).[65] The change in chemical shift is a result of the change in shielding of the proton due to the hydrogen bond. Hence, a hydrogen bonded backbone amide causes the proton to be deshielded. Increasing the temperature leads to weakening of the hydrogen bond interaction, higher shielding of the amide proton, and a lower chemical shift.[65] The change in amide proton shift is typically also a result of loss in secondary structure, in other words unfolding of the peptide.
The second method to obtain information about backbone hydrogen bonds is by measuring the amide exchange rate, i.e. the exchange rate of the amide protons for deuterium when adding a deuterated protic solvent.[59] Exchange rates are sensitive to pH and local structure fluctuations, and are best used in combination with amide proton temperature coefficients.[65]

3.2 NMR analysis of molecular flexibility in solution

Molecules exist in a variety of conformations in solution. The molar fractions of these conformations (the Boltzmann distribution), are determined by their relative free energies. This means that the solution conformation cannot be accurately represented by a single structure derived from experimentally restrained structure calculations[60] such as restrained MD or MM, but rather by a solution conformational ensemble. The NAMFIS method[61] deconvolutes time-averaged NMR variables (NOE distances and scalar couplings) into the solution ensemble, fulfilling all structural restraints. In practice, NAMFIS varies the mole fraction of each conformer in a computed theoretical input ensemble until the best possible fit to the experimental data is obtained. In this way, those conformers that exist in solution are given a probability that corresponds to their molar fraction, and all other conformations are assigned zero probability. In contrast to conformational analysis using NMR data as constrains in the computation, providing one averaged, possibly unreal conformation, NAMFIS finds all conformations that exist in the solution ensemble (Figure 4). Since energies are not considered in the NAMFIS analysis, the "energy catastrophe", i.e. energy misevaluation introduced by long-range interactions among polar functionalities, is avoided.[75] NAMFIS has previously been utilized to determine the solution conformation of peptides,[76,77] macrocycles[21,78,79] and small molecules.[75,80,81]

The reliability of the NAMFIS analysis depends on the quality of the NMR-derived distances and dihedral angles, as well as that of the theoretical ensembles.[75] In order to obtain high quality NOE-based distances, the following should be implemented:

- At least 4 different mixing times.
- All NOESY experiments should be run subsequently, in a queue.
- The mixing times should be alternated to get rid of systematic errors.
- Applied parameters have to be identical, as do the processing of spectra.
- Temperature control should be active and water presaturation should be avoided.

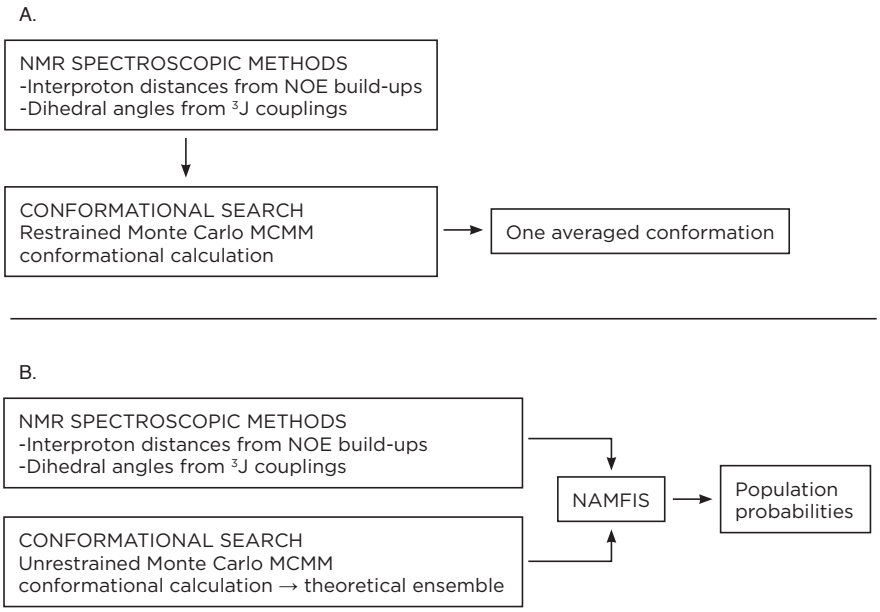

Figure 4. Comparison of methods for analysis of solution conformation. **A.** Constrained computational conformational analysis. **B**. NAMFIS.

The conformational search, giving the theoretical input ensemble for NAMFIS analysis, should cover the entire available conformational space. In practice this is challenging, but a large number of steps and a reasonable energy window should capture most of the possible conformations. To estimate the probability that a conformational search is complete the equation $1-(1-(1/N))^M$ can be used, where N is the total number of conformers and M is the number of search steps.[75] Moreover, finding the 10 "lowest energy" conformations at least 5 times each is a reasonable indicator that a sufficient conformational search has been performed.

4 PEPTIDE SYNTHESIS

Peptides are synthesized by linking two amino acids (Appendix I) by an amide bond in a condensation reaction. The general peptide coupling reaction of two amino acids, generating a dipeptide, is outlined in Scheme 1.

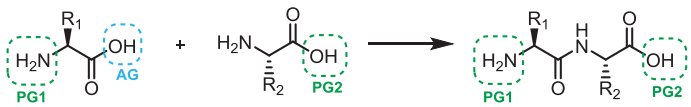

Scheme 1. General outline of the peptide bond formation. AG = activating group, PG = protecting group.

At ambient temperature, the reaction can only occur if the carboxy component of one of the participating amino acids is activated as a good leaving group (Scheme 1, blue square, AG = activating group), and can then react with the amino component of the other amino acid and form the amide bond.[82] Activation can be achieved by the use of coupling reagents, as described in section 4.4 below. In order to get a controlled reaction with only the desired product, all other amino and carboxy functions in the reaction have to be protected (Scheme 1, green square, PG = protecting group). This is also true for reactive groups at side chain positions (Scheme 1, R_1 and R_2). The most commonly used protecting group strategy, the Fmoc/*t*-Bu method, is described in section 4.2 below. For side chain protection there are a large number of protecting groups to choose from.[83]

4.1 Solid phase peptide synthesis

Solid phase peptide synthesis (SPPS) was first described by Bruce Merrifield in 1962,[84] and he was later awarded the Nobel Prize for this discovery. Today, SPPS is the most common strategy for peptide synthesis.[85,86] In SPPS (Scheme 2) the first amino acid of the growing peptide chain is attached to an insoluble solid support via a linker. The advantage, as compared to solution phase peptide synthesis, is that byproducts and reagents can be washed off via filtration after each coupling, and time-consuming purification and isolation of intermediates can be avoided. The first step in SPPS is attachment of the *C*-terminus of the first amino acid to the linker. Subsequent deprotection of its *N*-terminal amine and coupling to the next

amino acid in the sequence gives the dipeptide, as illustrated in Scheme 2. The carboxyl group of the added amino acid is activated prior to the addition. After the coupling, the α-amino group is deprotected and can thus be coupled to the next amino acid. The procedure is repeated until the full linear sequence is obtained, and the resin is filtered and washed between each step.

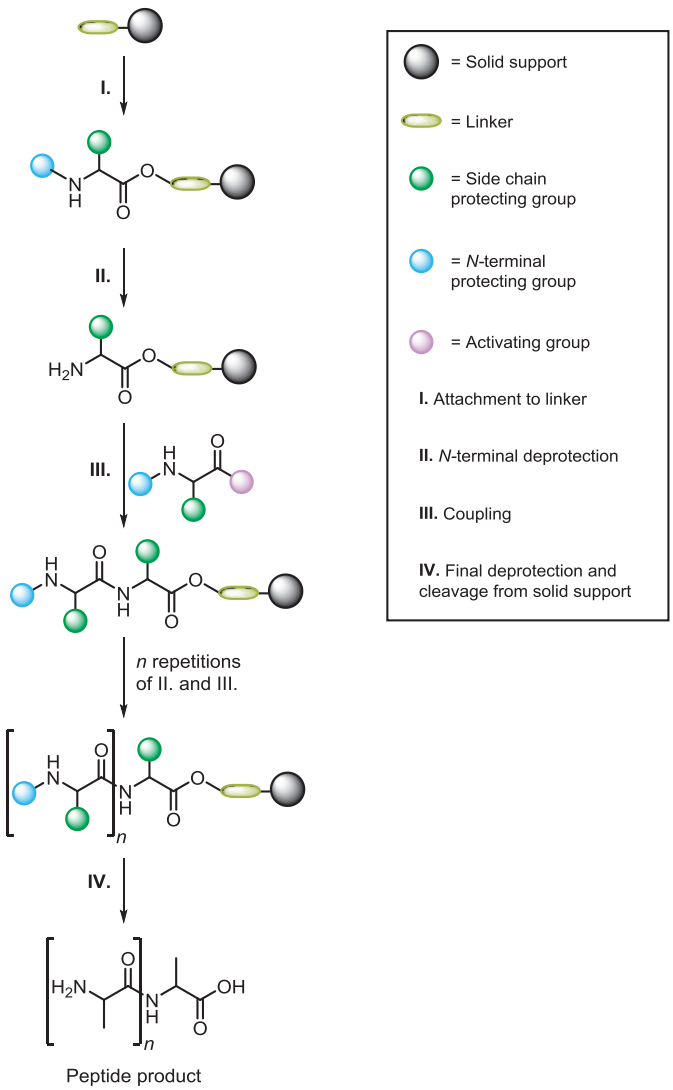

Scheme 2. General outline of solid phase peptide synthesis (SPPS).

Lastly, the peptide is cleaved from the solid support and final deprotection of side chain protecting groups is performed. When a cyclic peptide is the final product, the side chain protecting groups are usually removed after cyclization.

4.2 The Fmoc/*t*-Bu method

As outlined in Scheme 2, the α-amino protecting group is removed after each coupling step and should therefore be orthogonal to the side chain protecting groups and the linker, in other words they should not be cleaved under the same reaction conditions. There are two commonly used protecting group strategies for SPPS: the Fmoc/*t*-Bu strategy and the Boc/Bn strategy (Figure 5).

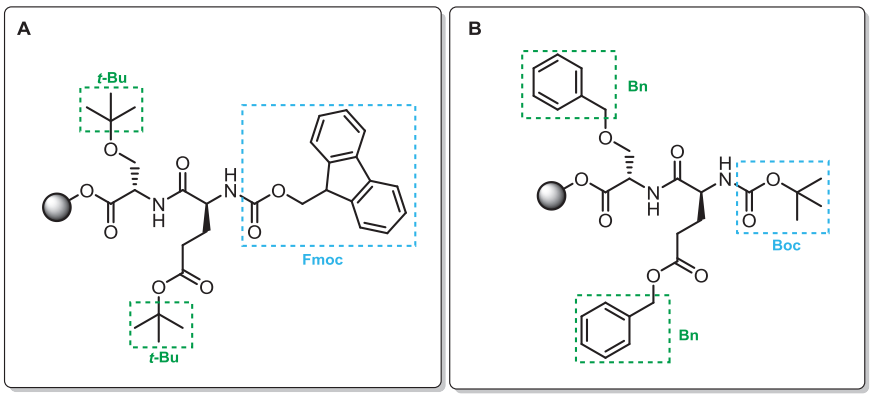

Figure 5. **A**. The Fmoc group is removed by base whereas the *t*-Bu side chain protection groups are removed under acidic conditions. Cleavage of the peptide is also performed under acidic conditions. **B**. The Boc group is removed under acidic conditions and the Bn group by palladium-catalyzed hydrogenation or strong acids. The peptide is cleaved from the resin using strong acid, typically HF.[83]

Protecting the α-amino group with Fmoc provides an orthogonal deprotection scheme since Fmoc is deprotected with bases, usually piperidine, while the side chain protecting groups and the linker is normally cleaved under acidic conditions. In addition, removal of the Fmoc group is performed under milder conditions than the Boc group, which requires strong acid such as trifluoroacetic acid (TFA).[85] Since the Fmoc strategy has been used for the SPPS in this thesis, it is the only strategy that will be discussed further. Common side chain protection groups in the

Fmoc/*t*-Bu strategy includes trityl (Trt for Asn, Cys, Gln, His), *t*-Bu (for Asp, Glu, Ser, Thr, Tyr), Boc (for Lys, Trp), and pentamethyl-2,3-dihydrobenzofuran-5-sulfonyl (Pbf, for Arg).[83,86] During SPPS, the Fmoc group is commonly removed by piperidine, which also acts as a scavenger for the generated dibenzofulvene.[87] The mechanism for Fmoc cleavage is shown in Scheme 3.

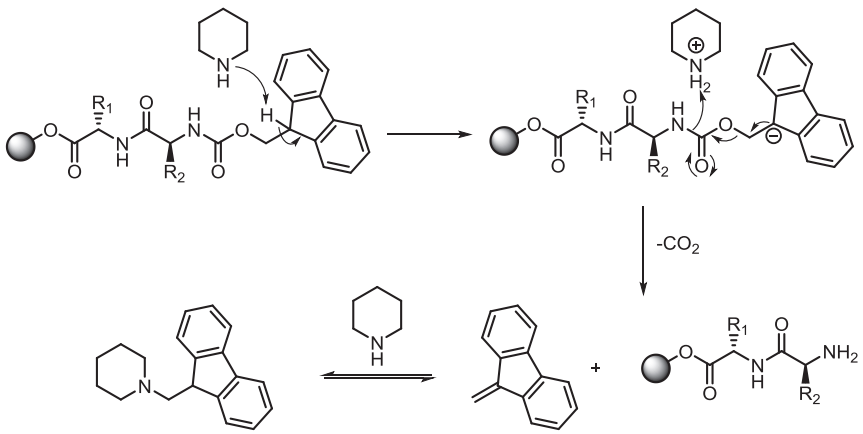

Scheme 3. Deprotection of the Fmoc group using piperidine as base and scavenger for the dibenzofulvene, which reacts with piperidine to form the fulvene-piperidine adduct.

4.3 Resins and linkers

The resins used in SPPS are usually polystyrene (PS)- or polyethylene glycol (PEG)-based, and are available in different mesh sizes and with different linkers attached.[85] Before the first coupling the resin is allowed to swell in a suitable solvent. For PS resin, swelling is most effective in dichloromethane (DCM). Dimethylformamide (DMF) can also be used, which is also the preferred solvents for the coupling reactions. As illustrated in Scheme 2, the peptide is attached to the resin via a linker. There are a large number of linkers available for SPPS,[85,86,88] and they differ in cleavage conditions, loading, distance between peptide and resin, and the *C*-terminal functionality of the peptide product.[86] Two common examples of PS-based resins are shown in Figure 6. The 2-chlorotrityl linker is commonly cleaved under mild acidic conditions (1% TFA) providing a *C*-terminal carboxylic acid. The Rink amide resin is cleaved using higher concentrations of acid (50% TFA)

providing the C-terminal amide. Both the 2-chlorotrityl and Rink amide resins have been utilized in this work.

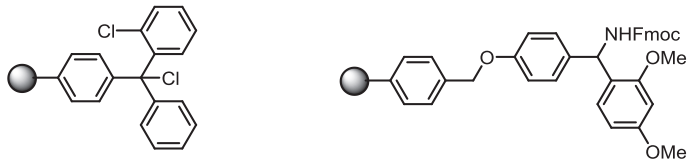

2-Chlorotrityl chloride resin Rink amide resin

Figure 6. Two commonly used resins for SPPS. The 2-chlorotrityl chloride linker provides the C-terminal acid and Rink amide resin provides the C-terminal amide.

4.4. Coupling reagents

As mentioned above, coupling reagents are used for activation of the carboxylic acid. The acid is transformed to an activated ester by introducing an electron withdrawing group that acts as a better leaving group (X, Scheme 4). The carbonyl is thereby available for reaction with the nucleophilic amine of the next amino acid.

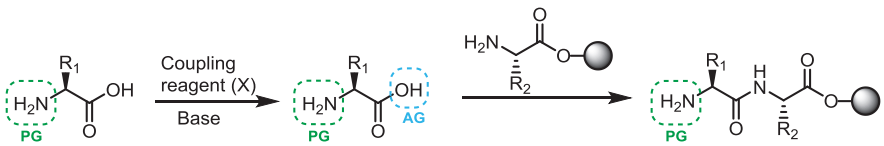

Scheme 4. The coupling reaction in SPPS, using a coupling reagent (X) in the presence of base to activate the carboxylic acid. AG = activating group, PG = protecting group.

There is a large number of commercially available coupling reagents.[89] Examples of coupling reagents often used are shown in Figure 7. The carbodiimides *N,N*'-diisopropylcarbodiimide (DIC) and *N,N*'-dicyclohexylcarbodiimide (DCC) belong to the first generation of coupling reagents, and are often used together with racemization suppressants such as 1-hydroxybenzotriazole (HOBt) and 1-hydroxy-7-azabenzotriazole (HOAt).[86] As shown in the coupling mechanism in Scheme 5, uronium/aminium-based 3-[bis(dimethylamino)methyliumyl]-3*H*-benzotriazol-1-oxide tetrafluoroborate (TBTU) or 3-[bis(dimethylamino)methyliumyl]-3*H*-benzotriazol-1-oxide hexafluorophosphate (HBTU) generate HOBt in situ. Similarly, for 1-[bis(dimethylamino)methylene]-1*H*-1,2,3-triazolo[4,5-*b*]pyridinium 3-oxide hexafluorophosphate (HATU), HOAt is generated in the reaction.

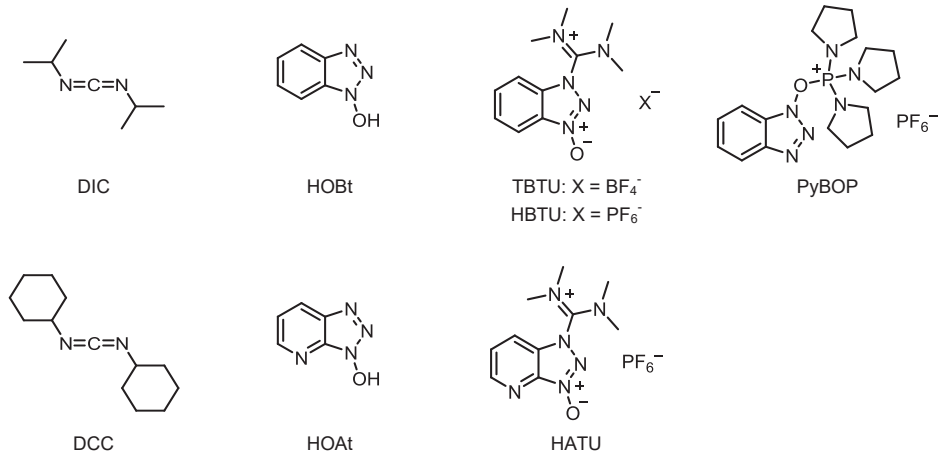

Figure 7. Examples of peptide coupling reagents.

The uronium/aminium-based coupling reagents are commonly used together with a tertiary amine such as diisopropyl ethyl amine (DIPEA). HATU is more reactive than TBTU and HBTU and as a result epimerization is therefore often avoided.[85] These reagents were first assigned as the *O*-isomers (uronium salts) but it was later shown that they exist as the *N*-isomer (aminium salt, Figure 7) both in solid state and in solution.[90] Phosphonium salts such as benzotriazol-1-yl-oxytripyrrolidinophosphonium hexafluorophosphate (PyBOB, Figure 7) are also common coupling reagents.

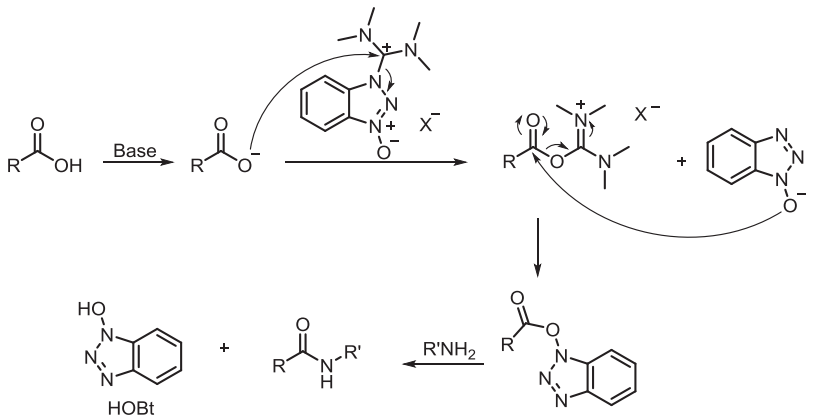

Scheme 5. Proposed mechanism of HBTU (X=PF_6-)/TBTU (X=BF_4-) activation.[85]

4.5 Peptide cyclization

As discussed in Chapter 2, there are several beneficial properties gained by forming cyclic peptides and, as a result, they are valuable target molecules for medicinal chemists. Peptide cyclization is often difficult, mainly due to the entropically disfavored pre-cyclization conformation that the linear peptide needs to adopt, bringing the reactive ends in close spatial proximity, prior to cyclization.[91] As a result dimerization or polymerization is often favored over cyclization. However, this can be avoided by running the cyclization reaction at low concentration. For peptide cyclization in solution, high dilution can be accomplished with slow addition by the use of syringe pumps. Pseudodilution can also be achieved using solid supported macrocyclization.[92,93] Peptide cyclization can be performed head-to-tail, side chain-to-tail, head-to-side chain or side chain-to-side chain.[91,94]

5 AIMS OF THE THESIS

The overall aim of this thesis work was to investigate the solution ensembles of macrocycles in order to gain knowledge on the conformation stabilizing effects of weak interactions and to evaluate the role of flexibility in bioactivity.

The specific objectives were to:

- design a cyclic β-hairpin model system for investigation of weak interactions.
- investigate the ability of various methods for evaluation of this model system.
- use the model system to study the impact of hydrogen and halogen bonding on β-hairpin folding.
- investigate cyclic β-hairpins as inhibitors of the MDM2/p53 interaction and, in particular, examine if there is a correlation between activity and solution conformation.
- describe the solution conformational ensembles of CD36 modulating macrocyclic azapeptides.
- evaluate the conformational change of roxithromycin dependent on the hydrophobicity of the environment.

6 INVESTIGATION OF WEAK INTERACTIONS USING CYCLIC β-HAIRPIN PEPTIDES AS MODEL SYSTEMS (PAPERS I–III)

6.1 Weak interactions in biological systems

Molecular recognition of a ligand by its protein target relies on specific attractive weak interactions such as hydrogen bonding, hydrophobic forces, π-stacking, and halogen bonding.[95,96] In drug design these interactions are optimized with the intention to improve affinity and selectivity, resulting in drug candidates with higher efficacy and fewer side effects. Weak interactions also direct protein folding. Since peptides are smaller, yet resemble proteins, they are commonly used as model systems for investigation of protein folding.[27,33,97] Further, peptides have been used as models for investigations of weak interactions.[34,35,98] Studying peptides by solution state experiments provides knowledge gained in a biological relevant environment. The information from studying weak interactions is useful, for example, for parametrization of the computational force fields for MD and MM algorithms and scoring functions for docking programs.[99]

6.1.1 Hydrogen bonding

A hydrogen bond is an attractive interaction between a hydrogen bond donor X-H and a hydrogen bond acceptor.[100] Hydrogen bonds are the most frequently occurring interactions in biological recognition. Even though hydrogen bonds contribute to specificity for the target, the effect on the binding free energy is often low.[95] This is due to the energy cost of desolvation of donors and acceptors that must take place before the binding event. Intramolecular hydrogen bonding can be utilized to increase membrane permeability of ligands.[101] A survey of hydrogen bonds in the Cambridge Structural Database (CSD) and the Protein Data Bank (PDB) showed a median donor-acceptor distance of 2.75 Å for amide C=O and OH, and 2.9 Å for C=O and NH.[95] The angle for donor–hydrogen···acceptor is generally above 150°.[95]

6.1.2 Halogen bonding

A halogen bond is an attractive interaction between an electron-poor region of a halogen atom and an electron donor.[102] The electropositive region is termed a σ-hole[103,104] and is illustrated in Figure 8. The directionality and strength of halogen bonds can be tuned by changing the halogen atom (F ≪ Cl < Br < I). This is because the size of the σ-hole increases with polarizability and decreases with electronegativity.[105] Generally, fluorine does not have a σ-hole and there are no examples of fluorine-mediated halogen bonds in biological systems. Given the relatively recent discovery of this interaction,[102] the halogen bond is not as well described as the hydrogen bond. However, both theoretical and experimental studies have shown that the halogen bond is more directional than the hydrogen bond, and that the directionality also follows the trend Cl < Br < I, with donor-acceptor angles approaching 180°.[105] Halogen bonds were found in protein-ligand complexes,[106-108] and over 50% of molecules in high throughput screening and ~20% of all drugs are halogenated,[109,110] motivating the investigation of this interaction. The σ-holes of chloro-, bromo- and iodo-substituted benzene are shown in Figure 8.

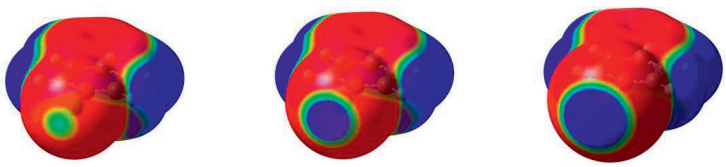

Figure 8. The electropositive region (blue/green), i.e. the σ-hole, of chloro-, bromo- and iodo-substituted benzene, from left to right.

6.2 Evaluation of the impact of interstrand hydrogen bonding on β-hairpin stability (Paper I)

A peptidic model system (Figure 9 A) was designed for investigation of weak interactions. A ten amino acid cyclic β-hairpin was predicted to be a suitable model system, possessing two strands of three amino acids each connected by the two turns. Accordingly, if the β-hairpin conformation is adopted, the interaction site of interest (R_3–R_8) is positioned on one face of the peptide, as illustrated in Figure 9B.

This design permits the selective study of the R_3–R_8 interaction without the influence of competing side chain to side chain interactions from other residues. Since the R_3–R_8 interaction is intramolecular, this model system offers an entropic advantage that allows the characterization of very weak forces.

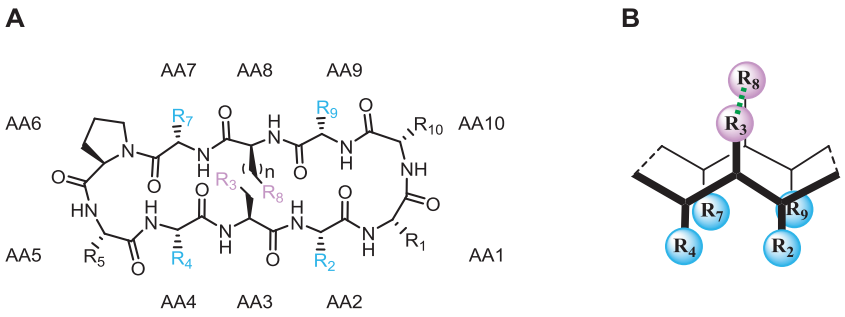

Figure 9. **A**. The β-hairpin model system with the interaction site R_3–R_8 in purple and other strand residues in blue. **B**. General outline of the β-hairpin model system shown from the side, with R_3–R_8 on one face of the peptide. For the hydrogen bonding peptide **1** R_3=OH and R_8=OH, and for the reference peptide **2** R_3=OH and R_8=Me. n=1 for **1** and **2**. The amino acid (AA) position numbering is used for all peptides in Chapter 6.

As a first step towards a β-hairpin model for investigation of halogen bonding, a system with a possible interstrand hydrogen bond was designed (**1**, Figure 9, R_3=OH, R_8=OH). The assumption that a R_3–R_8 hydrogen bond could be formed in this system was based on Monte Carlo molecular mechanics[52] (MCMM) calculations. For examination of the stabilizing role of this single interstrand hydrogen bond on β-hairpin formation, peptide **1** was studied together with a reference containing a methyl at the R_8-position (**2**, Figure 9, R_3=OH, R_8=Me), in which the R_3–R_8 interstrand hydrogen bond is absent. Any observed difference in the β-hairpin conformational stability of **1** and **2** is therefore expected to originate from the R_3–R_8 hydrogen bond of **1**.

The successful application of this model system relies on formation of a β-hairpin structure, and the first step was therefore to design a peptide that folds into this conformation. The structures of the hydrogen bond forming peptide **1** (R_3= OH and R_8=OH) and its reference **2** (R_3=OH and R_8=Me) are shown in Figure 10. In the design, the D-Pro–Gly turn inducer[33,38] and a possible Val7 to Ala4 interstrand

hydrophobic interaction were included, which have previously been shown to be favorable for β-hairpin stabilization.[33] In addition, since β-branched amino acids have shown high propensity in β-strands,[43,44] an additional Val residue was incorporated. The model peptides were cyclized via a Gly–Asn weak turn inducer,[40] which was expected to increase the solubility of the peptides in polar solvents, as well as stabilize β-hairpin formation.

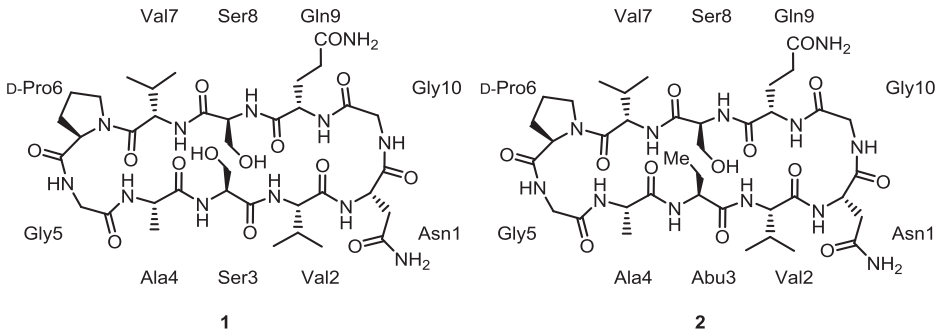

Figure 10. The peptides used for investigation of the impact of an interstrand hydrogen bond on β-hairpin formation. Amino acids are given with three letter codes and residue positions. Abu = L-2-aminobutyric acid.

6.2.1 Results and discussion Paper I

The linear precursors of **1** and **2** were prepared by automated SPPS using an automated benchtop peptide synthesizer, on a 2-chlorotrityl resin following the Fmoc–*t*-Bu–Trt strategy.[83,111] The peptide couplings were performed in DMF using the coupling reagent TBTU and the base DIPEA. Following cleavage of the *t*-Bu/Trt-protected peptides from the solid phase with 1% TFA in DCM, the linear decapeptides were cyclized utilizing a "pseudo-high-dilution" procedure[112] with HATU as the coupling reagent. Peptide cyclization is usually performed at submillimolar concentration in order to avoid dimerization or polymerization[91] leading to impractically high solvent volumes. By slow (10 μL/min) addition of the linear peptide precursor and the coupling reagent to the reaction mixture, low in situ concentration was obtained and minimal volume of solvent could be used. The side chain protecting groups were removed by TFA, and **1** and **2** were isolated following purification by reversed phase high performance liquid chromatography on a C18 column. The synthesis of **1** and **2** is outlined in Scheme 6.

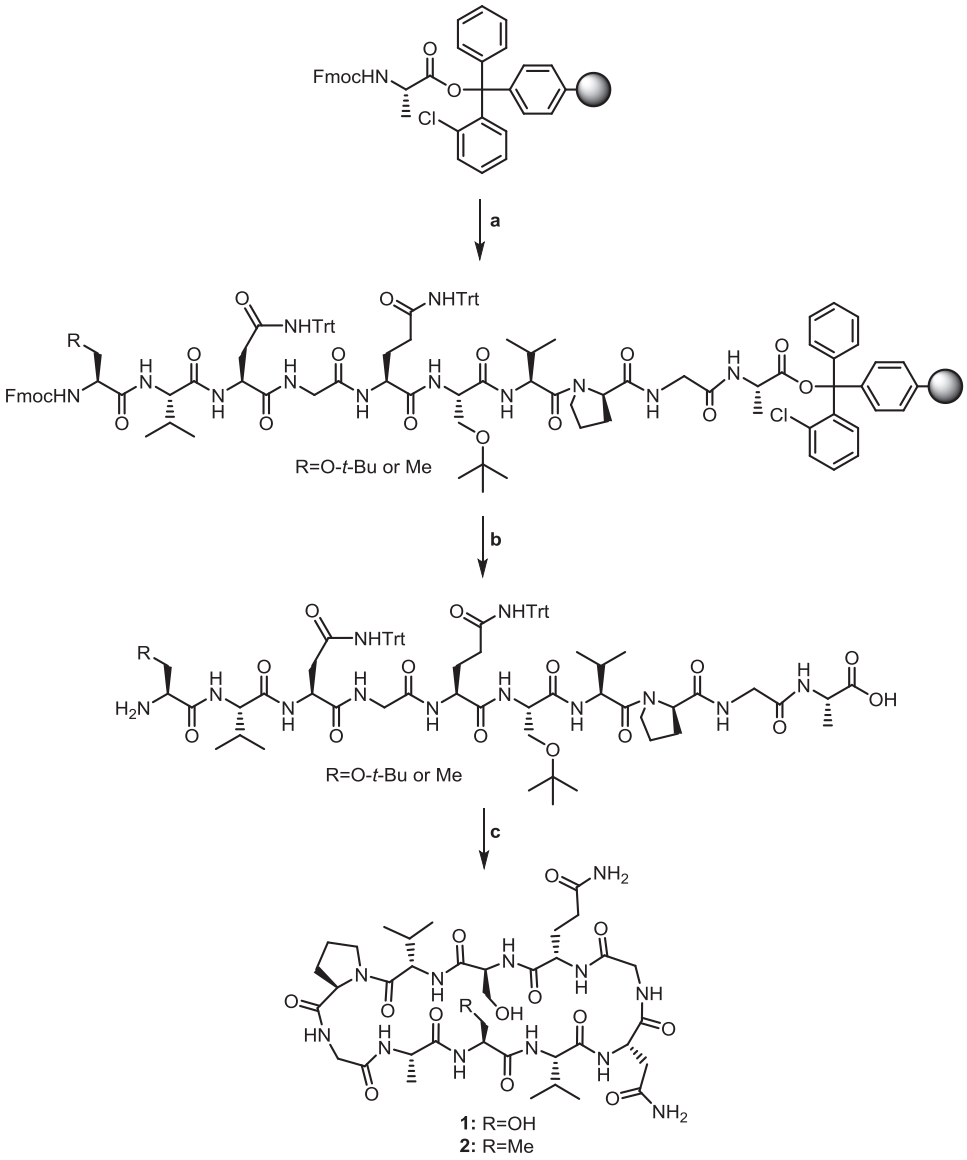

Scheme 6. Synthesis of **1** and **2**. Reagents: (**a**) (i) 20% piperidine in DMF. (ii) Fmoc-AA-OH, TBTU, DIPEA. (iii) Acetic anhydride. Nine consecutive cycles with: Fmoc-Gly-OH, Fmoc-D-Pro-OH, Fmoc-Val-OH, Fmoc-Ser(*t*-Bu)-OH, Fmoc-Gln(Trt)-OH, Fmoc-Gly-OH, Fmoc-Asn(Trt)-OH, Fmoc-Val-OH, Fmoc-Ser(*t*-Bu)-OH (**1**) or Fmoc-Abu-OH (**2**) (**b**) (i) 20% piperidine in DMF. (ii) 1% TFA in DCM. (**c**) (i) HATU, DIPEA, DMF. (ii) TFA/H_2O/TIPS (95:2.5:2.5).

Structural assignment was carried out by the TOCSY-NOESY sequential backbone walk described in section 3.1.1. Due to the low water solubility, the experiments were performed in DMSO-d_6. Both peptides had Hα chemical shifts and $^3J_{CH\alpha NH}$ coupling constants (Table 1), as well as a NOE coupling pattern (Figure 11), compatible with β-hairpin conformation. Further, the low amide temperature coefficients ($\Delta\delta_{NH}/\Delta T$) observed for Ala4 and Gln9 (Table 1 and Figure 11) confirmed formation of the two turn regions,[65,73,113] as shown in Figure 11.

Table 1. Hα proton chemical shifts (ppm), $^3J_{CH\alpha NH}$ coupling constants (Hz) and $\Delta\delta_{NH}/\Delta T$ backbone amide temperature coefficients (ppb K^{-1}) for **1** and **2** in DMSO-d_6.

Residue position[a]	**$\delta_{H\alpha}$ (ppm)**		**$^3J_{CH\alpha NH}$ (Hz)**		**$\Delta\delta_{NH}/\Delta T$ (ppb K^{-1})**[b]	
	1	2	1	2	1	2
Asn1	4.09	4.05	–	5.8	10.6	9.1
Val2	4.18	4.20	8.6	8.9	6.5	5.7
Ser3/Abu3	4.81	4.83	9.0	7.7	6.5	6.5
Ala4	4.59	4.60	9.2	7.3	0.9	1.0
Gly5	3.75, 3.51	3.75, 3.48	–	–	6.4	6.4
D-Pro6	4.27	4.27	–	–	–	–
Val7	4.29	4.30	9.5	9.7	6.4	5.7
Ser8	4.49	4.51	–	7.8	7.3	7.1
Gln9	4.51	4.55	9.2	–	1.3	1.1
Gly10	3.85, 3.25	3.78, 3.22	4.4	5.8	4.1	5.2

[a]Residue position according to Figure 9 A. [b]The amide temperature coefficients are derived as negative numbers but reported as positive numbers. $\Delta\delta_{NH}/\Delta T < 3$ indicates a strong intramolecular hydrogen bond, $\Delta\delta_{NH}/\Delta T = 3–5$ indicates that the amide proton is in equilibrium between a solvent-exposed and intramolecular hydrogen bonded, and $\Delta\delta_{NH}/\Delta T > 5$ indicate that the amide proton is solvent-exposed.

To investigate the impact of the R_3–R_8 hydrogen bond on β-hairpin formation, the NAMFIS methodology, described in section 3.2, was used. Interproton distances and backbone CαH-NH dihedral angles were used as experimental input together with a theoretical MCMM-based ensemble of conformers. As described above, any difference of the β-hairpin population of **1** and **2** is presumed to result from the R_3–R_8 interstrand hydrogen bond.

Interproton distances were measured from NOESY build-ups acquired with mixing times of 200, 400, 600, 700, 800, and 1000 ms, without solvent suppression, on a 500 MHz spectrometer. The distances were calculated from the linear part of the

build-ups (mixing time <800 ms), as described in section 3.1.3, using the geminal methylene protons Gly5-Hα, Gly10-Hα and Ser3-Hβ (1.78 Å) as internal distance references. The dihedral angles were calculated from $^{3}J_{CH\alpha NH}$ using the Karplus equation developed specifically for peptides,[69] as described in section 3.1.2.

The theoretical conformational ensembles of **1** and **2** were generated by restraint-free MCMM conformational searches with molecular mechanics energy minimization using the OPLS-2005 force field.[114] Conformations within 42 kJ/mol of the global minimum were retained. The ensembles from the MCMM were then reduced by redundant conformation elimination with a root-mean-square deviation (RMSD) cutoff of 3 Å for heavy atoms. The derived ensembles were used together with the calculated backbone dihedrals and NOE build-up distances for the backbone positions of **1** and **2** in the subsequent NAMFIS analysis. Distances for side chain positions were not included in the initial run since the flexible side chains are not as well predicted as the backbone by MCMM calculations.[52]

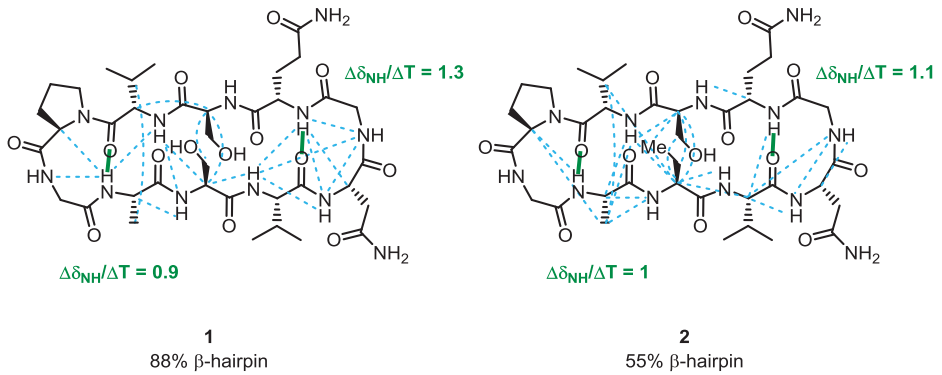

Figure 11. The NOE coupling pattern measured at 500 MHz (blue dotted lines) and amide backbone hydrogen bonds (green lines) for **1** and **2**.

NAMFIS analysis indicated peptides **1** and **2** to be folded into β-hairpin in 88% and 55% molar fraction, respectively, in solution. This suggests that a single interstrand hydrogen bond provides a significant stabilization of this β-hairpin conformation. The β-hairpin conformation of **1**, with the R_3–R_8 hydrogen bond, is shown in Figure 12 A. It should be noted that both peptides have unusually high tendency to fold, as previously described small peptides typically show <40% folding into β-hairpin conformation in solution.[33,73] The NAMFIS analysis was validated using

standard methods, that is by random removal of experimental data, by adding random noise to the data, and by comparison of the experimental and back calculated distances and dihedrals. As shown in Figure 12 B, the folded conformations of **1** and **2** are highly similar.

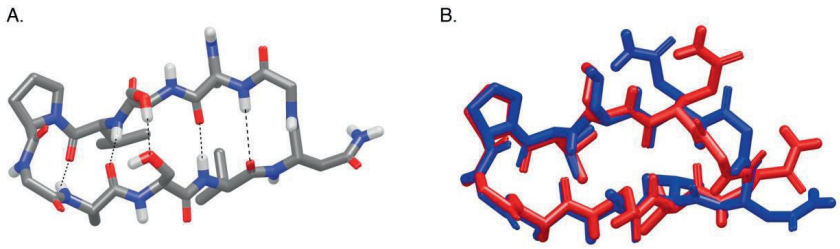

Figure 12. **A**. The β-hairpin conformation of **1**, as selected by the NAMFIS analysis. **B**. Overlay of the major conformations of **1** (red) and **2** (blue).

Attempts to derive the ^{1}HNMR chemical shift temperature dependence of **1** and **2** failed due to signal overlaps and small chemical shift changes for the available temperature interval. The T_m could only be derived for a limited number of residues and with large standard errors.

6.2.2 Summary Paper I

Two cyclic peptides, **1** and **2**, differing only in an OH-to-Me substitution were synthesized and analyzed by NMR spectroscopy. Their solution conformational ensembles were derived from NAMFIS analysis, and it was shown that a single interchain hydrogen bond provided significant stabilization of the β-hairpin conformation. These results confirm that a cyclic β-hairpin model system is suitable for the investigation of weak interactions.

6.3 Evaluation of the ability of spectroscopic methods to assess the difference in folding of β-hairpins (Paper II)

The next pair of cyclic peptides that were designed, synthesized and evaluated is shown in Figure 13. As a step towards a model system for the investigation of halogen bonding, the R_8 OH of **1** and **2** were substituted for OMe, generating peptides **3** and **4** (Figure 13). This design prevents competing hydrogen bonding

when R_3 is halogenated. However, this model system was first used for evaluating the ability of chemical shift melting curve analysis, as well as CD spectroscopy to quantitatively evaluate minor differences in hairpin folding. We have previously shown that MD calculations are capable to quantitatively predict the β-hairpin population of **1** and **2** by validation against experimental data, i.e. NAMFIS analysis.[115]

6.3.1 Results and discussion Paper II

Peptides **3** and **4** were synthesized as described in section 6.2.1 and their synthesis is shown in Appendix II. Analogously to peptides **1** and **2** described above, **3** and **4** (Figure 13) differ only in their R_3 substituent (Figure 9). OH-substituted **3** can form a hydrogen bond with OMe at R_8, whereas the Me-substituted **4** cannot. Similar to peptides **1** and **2** described above, any difference in their folding is assumed to be a result of the capability to form the R_3–R_8 interstrand hydrogen bond.

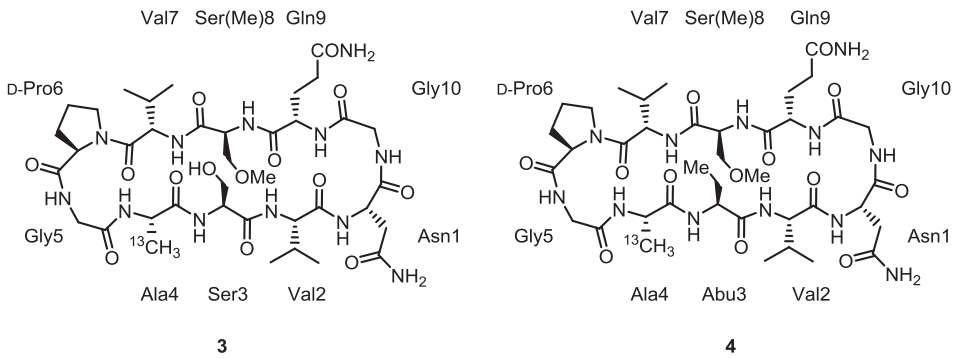

Figure 13. The peptides used for evaluation of the ability of spectroscopic methods to determine the difference in folding. Amino acids are given with three letter codes and residue positions. Abu = L-2-aminobutyric acid.

As previously described, conformations with ≥3 interstrand hydrogen bonds were defined as folded,[115] and the MD calculation for this peptide pair proposed the β-hairpin population to be 64% for **3** and 43% for **4**. Peptides **3** and **4** were evaluated using NAMFIS, similarly to **1** and **2** as described above. NOESY data were collected at a 900 MHz spectrometer and the interproton distances were determined from build-ups acquired with mixing times of 100, 200, 400, 500, 600,

and 700 ms. The NOE coupling pattern and amide backbone hydrogen bonds for **3** and **4** are shown in Figure 14. Theoretical ensembles were derived in the same way as described above, with MCMM conformational searching using OPLS-2005 and AMBER* force fields. The subsequent NAMFIS analysis showed 29% difference in folding of **3** (58% folded) and **4** (29% folded). The folded conformations selected by NAMFIS are shown in Figure 15.

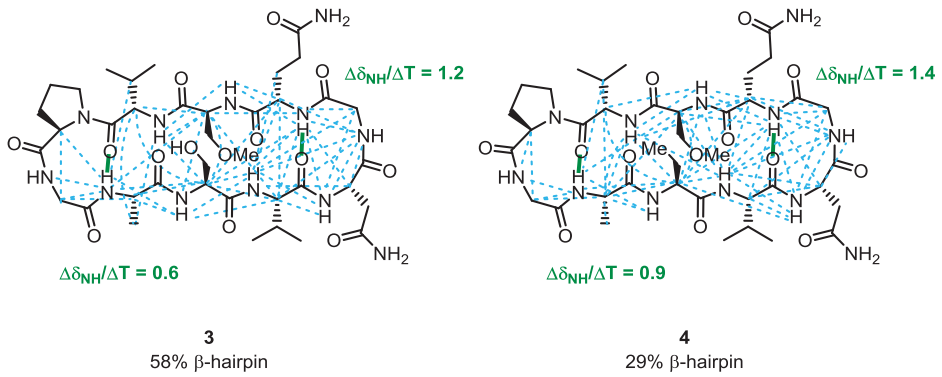

Figure 14. The NOE coupling pattern measured at 900 MHz (blue dotted lines) and amide backbone hydrogen bonds (green lines) for **3** and **4**.

The CD spectrum of **3** shows a double minimum at 205 nm and 223 nm. Although sometimes mistaken for a helical peptide spectrum, the double minimum is common for β-hairpins with strong type II' β-turns, where the 205 nm absorption band is from the II' β-turn and the 223 nm band from the β-sheet.[42] On the other hand, the CD spectrum of **4** does not show this double minimum, and in addition, **3** shows a stronger molar ellipticity in the 220 nm region as compared to **4**. These data indicate that **3** is folded into a β-hairpin to a higher degree than **4**. To quantify the folded populations of **3** and **4**, CD spectra were measured at 200-260 nm at a temperature interval of 80 ºC. The variable temperature CD (VT CD) spectra were deconvoluted into β-hairpin and random coil components using principal component analysis (PCA). For both **3** and **4**, the β-hairpin CD band at 220 nm

loses intensity at higher temperature, while the random coil band at 200 nm gains in intensity. The PCA analysis showed 13% more folded structure for **3** as compared to **4**.

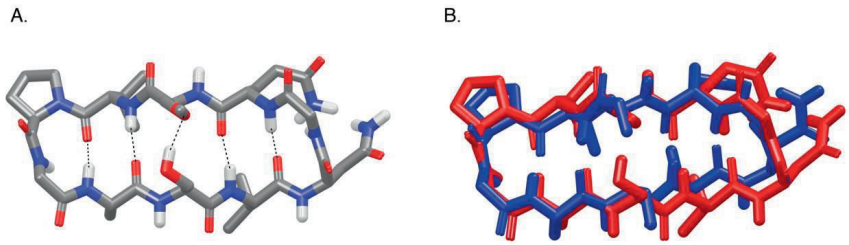

Figure 15. The β-hairpin conformation of **3**, as selected by the NAMFIS analysis. **B**. Overlay of the major conformations of **3** (red) and **4** (blue).

The chemical shift temperature dependence of **3** and **4** was measured and analyzed using the chemical shift melting curve analysis method reported by Honda *et al.*,[116] which was described in section 3.1.4. Due to signal overlaps and small chemical shift changes for the available temperature interval, the ^{1}H NMR data could not be used. Instead, the VT NMR analysis was based on the ^{13}C labeled β-carbon of alanine in position 4 (Figure 13). The temperature dependence was studied at 25–130 ºC and the data were fitted to eq. 3 (section 3.1.4) using computationally predicted chemical shifts for the fully folded and unfolded states (δ_F and δ_U), i.e. the endpoints of the melting curve. Only a small part of the unfolding curve could be detected in the experimentally available temperature interval. The relative thermodynamic stability of **3** and **4** was obtained as the ratio of the unfolding constants $K_U = K_U^3/K_U^4$. K_U was derived from equation 4.

$$K_U \left(\delta_U^3 - \delta_{obs}^3\right)\left(\delta_{obs}^4 - \delta_F^4\right) = \left(\delta_{obs}^3 - \delta_F^3\right)\left(\delta_U^4 - \delta_{obs}^4\right) \qquad \text{(eq. 4)}$$

The plot of $(\delta_U^3 - \delta_{obs}^3)(\delta_{obs}^4 - \delta_F^4)$ versus $(\delta_{obs}^3 - \delta_F^3)(\delta_U^4 - \delta_{obs}^4)$ gives a close to linear correlation with the slope K_U. The analysis suggests **4** to have 37% higher stability than **3**. This is in disagreement with the outcome of the NAMFIS, MD and VT CD analyses. A likely explanation is that the first three methods describe the overall conformational change, whereas the chemical shift melting curve analysis of a

single nucleus might predominantly report on local conformational changes, rather than on overall folding.

6.3.2 Summary Paper II

Evaluation of the ability of chemical shift and CD melting curve analyses to estimate the β-hairpin folding propensity, validated against MD and NAMFIS, suggest that the methods detecting the overall conformation (MD, VT CD and NAMFIS) detect **3** to be folded to a higher degree than **4**. In contrast, chemical shift analysis of a single nucleus gave the opposite result. Hence, the method used for estimation of β-hairpin population must be chosen with care, and methods that may report on local rather than global conformational changes should be avoided.

6.4 Evaluation of the impact of interstrand halogen bonding on β-hairpin stability (Paper III)

Approximately 20% of all marketed drugs are halogenated.[110] However, halogen bonding is not as well described in the literature as for example hydrogen bonding. So far, most studies of halogen bonds have been performed in the solid state (X-ray) or by computations.[105] The reported solution experiments have typically used small perfluorinated organohalides,[117-119] which are not directly relevant for biological systems. Halogen bonding has to some extent also been studied in biological systems, for example in ligand-receptor recognition[106] and to induce DNA junctions,[120] but never before to modulate the conformation of a peptidic model system in solution.

6.4.1 Results and discussion Paper III

In addition to the peptides described in sections 6.2 and 6.3, two additional peptide pairs (**5**–**6** and **7**–**8**, Figure 16) were evaluated as possible models for studying halogen bond interactions. Their synthesis is outlined in Appendices III-IV. Hydrogen bonding peptide **5** and its reference **6**, as well as hydrogen bonding peptide **7** and its reference **8**, were designed to gain an overall increased flexibility as compared to peptides **1**–**4**. In addition, an L-methoxy serine to L-methoxy homoserine substitution was performed, extending the side chain of R_8 with an

extra carbon (n=2, Figure 9 A and Figure 16). However, these changes led to a substantial destabilization of the peptides (Table 3). Linear peptides **5** and **6** do not fold into β-hairpin to a measurable extent, and cyclic peptides **7** and **8** do not show

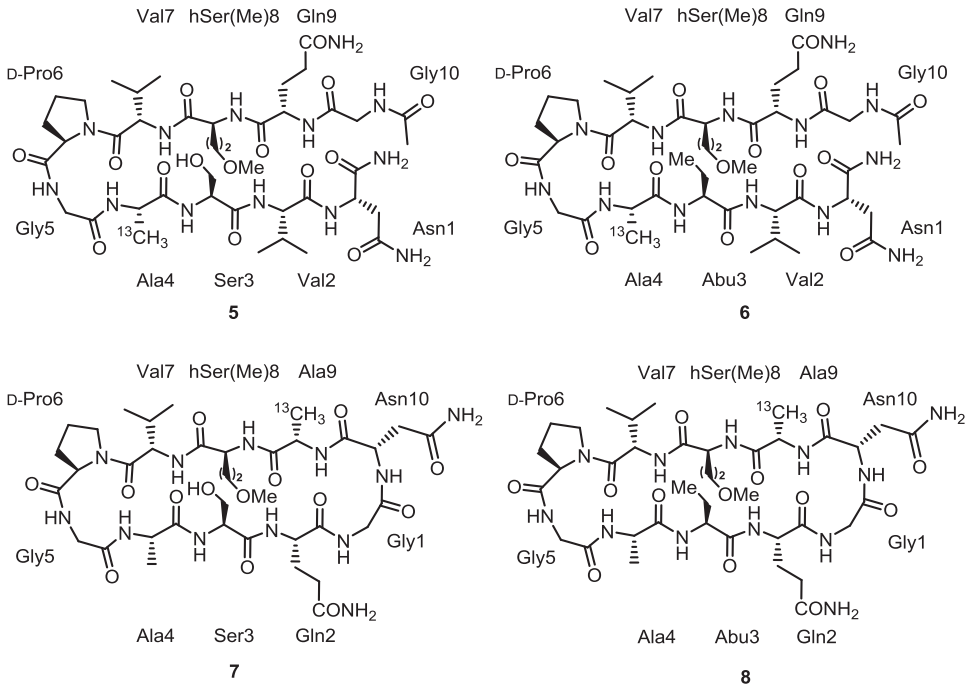

Figure 16. The additional peptides evaluated as possible halogen bond models. Amino acids are given with three letter codes and residue positions. Abu = L-2-aminobutyric acid.

a sufficient difference in folding for the hydrogen bonding peptide (**7**, R_3=OH, 36%) and the reference (**8**, R_3=Me, 30%), suggesting that the interstrand R_3–R_8 hydrogen bond in this case is not formed. The NOESY coupling pattern and backbone NH coefficients of **5**–**8** are shown in Figure 19, and the results of all peptides (**1**–**8**) described so far are shown in Table 3. Considering all information collected for **1**–**8**, peptide **3** was used as a template for the halogen bonding analogues. With 58% β-hairpin stability in solution for **3** (R_3=OH, R_8=OMe) as compared to 29% for the reference **4** (R_3=Me, R_8=OMe), this peptide pair is in a suitable folding region for a model system. Its chlorine- and bromine-substituted

analogues (**9** and **10**, Figure 17) were therefore synthesized, and subsequently evaluated using NAMFIS.

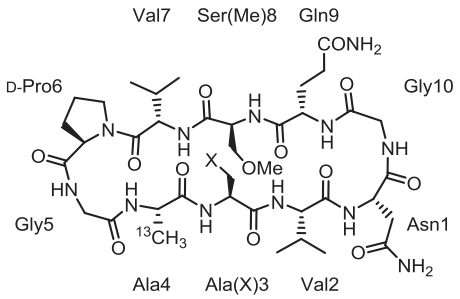

Figure 17. The halogenated analogues of **3**. Amino acids are given with three letter codes and residue positions.

The synthesis of the chlorine-substituted analogue **9** is outlined in Scheme 7. The first eight amino acids were coupled using SPPS, with an automated synthesizer, as described above. In order to avoid elimination of the Cl-atom, the last two couplings were performed manually under optimized conditions. HATU in combination with 2,4,6-trimethylpyridine (TMP) was found to give full conversion without any elimination product, as detected by LCMS. For removal of the Fmoc protecting group, a quick addition of 20% piperidine (1 min) in DMF gave the best result, however, still with some β-eliminated byproduct. After the last coupling the peptide was cleaved from the solid support as described above and was cyclized in solution using the same pseudo high dilution protocol[112] as before, and HATU/TMP as reagents. The Hα chemical shifts, the $^{3}J_{CH\alpha NH}$ coupling constants (Table 2) and the NOE coupling pattern (Figure 19) of **9** were in good agreement with a β-hairpin conformation. Ala4 and Gln9 showed low amide temperature coefficients ($\Delta\delta_{NH}/\Delta T$, Table 2 and Figure 19), which confirmed the presence of the two β-turn regions, and hence a similar folding to the previously synthesized analogues.

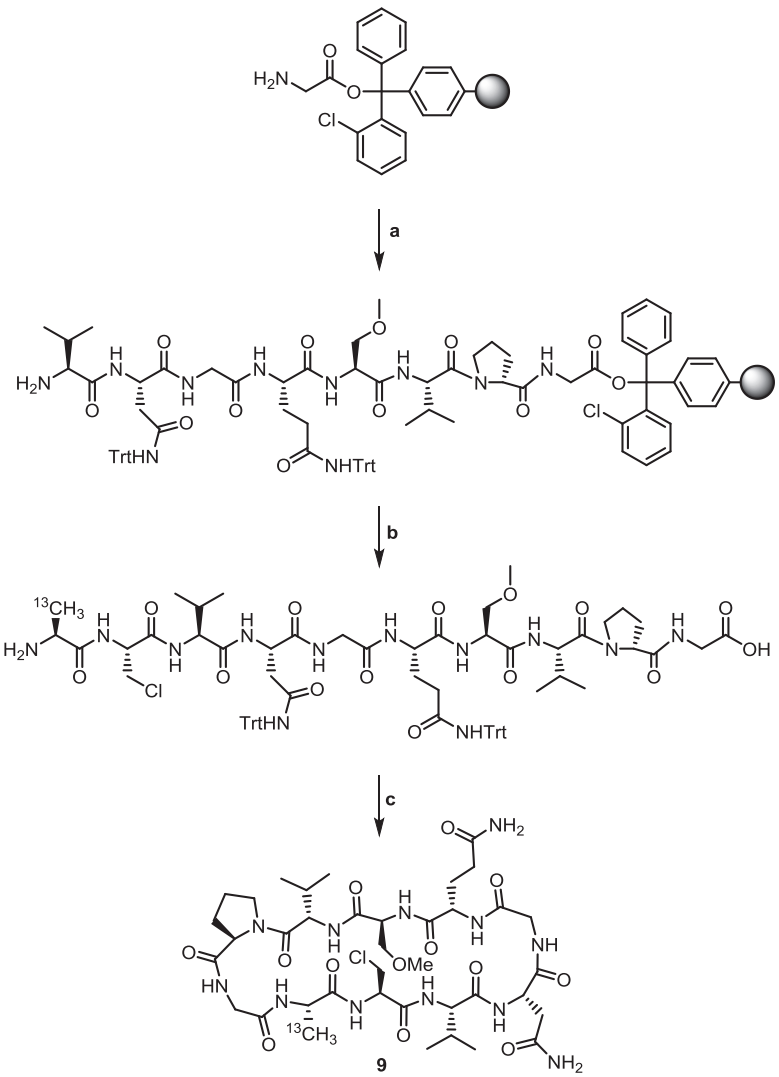

Scheme 7. Synthesis of **9**. Reagents and reaction conditions: (**a**) (i) Fmoc-AA-OH, TBTU, DIPEA. (ii) Acetic anhydride. (iii) 20% piperidine in DMF. Seven consecutive cycles with: Fmoc-D-Pro-OH, Fmoc-Val-OH, Fmoc-Ser(Me)-OH, Fmoc-Gln(Trt)-OH, Fmoc-Gly-OH, Fmoc-Asn(Trt)-OH, Fmoc-Val-OH, (**b**) (i) Fmoc-Ala(3-Cl)-OH, HATU, TMP. (ii) 20% piperidine in DMF, 1 min. (iii) Fmoc-[3-^{13}C]-Ala-OH, HATU, TMP. (iv) 20% piperidine in DMF, 1 min. (v) 1% TFA in DCM. (**c**) (i) HATU, TMP, DMF. (ii) TFA/H_2O/TIPS (95:2.5:2.5).

Table 2. Hα proton chemical shifts (ppm), $^3J_{CH\alpha NH}$ coupling constants (Hz), and $\Delta\delta_{NH}/\Delta T$ backbone amide temperature coefficients (ppb K^{-1}) for **9** in DMSO-d_6.

Residue position[a]	$\delta_{H\alpha}$ (ppm)	$^3J_{CH\alpha NH}$ (Hz)	$\Delta\delta_{NH}/\Delta T$ (ppb K^{-1})[b]
Asn1	4.07	6.75	6.52
Val2	4.19	8.44	3.44
Ala(Cl)3	5.25	8.45	5.20
Ala4	4.66	8.28	1.28
Gly5	3.84, 3.39	–	3.40
D-Pro6	4.29	–	–
Val7	4.30	7.98	3.48
Ser8	4.80	7.80	5.36
Gln9	4.53	8.44	1.68
Gly10	3.84, 3.25	–	6.68

[a]Position according to Figure 9 A. [b]The amide temperature coefficients are derived as negative numbers but reported as positive numbers. $\Delta\delta_{NH}/\Delta T < 3$ indicates a strong intramolecular hydrogen bond, $\Delta\delta_{NH}/\Delta T = 3–5$ indicates that the amide proton is in equilibrium between a solvent-exposed and an intramolecular hydrogen bond, and $\Delta\delta_{NH}/\Delta T > 5$ indicate that the amide proton is solvent-exposed.

The solution conformational ensemble of **9** was derived by NAMFIS analysis, as described for the other peptides. Interproton distances were calculated from NOESY build-ups acquired with mixing times 200, 300, 400, 500, 600, and 700 ms, at a 900 MHz spectrometer. To generate the theoretical conformational ensemble, MCMM calculations were performed, using OPLS-2005, AMBER* and OPLS-3 force fields. OPLS-3 is the first force field parameterized for halogen bonding, although so far only for halogens attached to aromatic rings.[121] Due to the lack of force field parameters for aliphatic halogens, no conformations with the R_3–R_8 interstrand halogen bond were observed in the MCMM calculation. Therefore, a β-hairpin conformer encompassing a Cl–OMe distance and angle optimal for halogen bonding, enforced by restraints, was also added to the NAMFIS input ensemble. The total β-hairpin content in solution for **9** (R_3=Cl, R_8=OMe) was estimated by NAMFIS to 74%, which is significantly higher than for the reference (R_3=Me, R_8=OMe, 29%) and close to the hydrogen bonded analogue **3** (R_3=OH, R_8=OMe 58%). For peptide **3**, the main conformer selected by NAMFIS is the one with a R_3–R_8 hydrogen bond interaction, even when data derived only from backbone positions is used. In the NAMFIS analysis of **9**, the conformer minimized with a constrained Cl–OMe distance and angle (Figure 18) was found to have a content of

9%. However, with the ensemble of **3** as input the conformation with the R_3–R_8 interaction is selected as the major one.

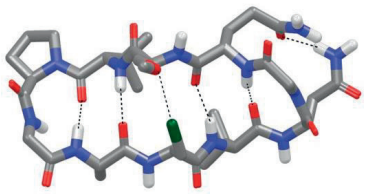

Figure 18. The solution conformer with an interstrand Cl···O halogen bond.

To further analyze the presence of an R_3–R_8 halogen bond, a NAMFIS analysis was carried out with the NMR data of these residues only. A β-hairpin conformation that was obtained in the initial NAMFIS analysis was selected, and its R_3 and R_8 side chains were rotated around their Cα–Cβ bond to generate the gauche$^+$, gauche$^-$, and trans conformers, providing an input ensemble of nine conformers (Appendix V). Independently of the NMR data assignment of the β-hydrogens (2 × 2 possible solutions) the conformation with the MeO and Cl facing each other was found to have >90% probability. In addition, the methyl group of the R_8-OCH_3 was used as a reporter for the $R_3X\cdots R_8OCH_3$ interaction (X = OH (**3**), Me (**4**) or Cl (**9**)). Since the chemical shift of nuclei neighboring an equilibrium process is expected to show comparably high temperature dependence, the chemical shift of the R_8OCH_3-protons was monitored for peptides **3**, **4** and **9** in the temperature interval 25–100 °C. The temperature coefficients ($\Delta\delta_{CH3}/\Delta T$) were calculated to 0.07 ppb/K for **4**, 0.19 ppb/K for **3**, and 0.32 ppb/K for **9**. Following the trends observed by NAMFIS for the β-hairpin solution population of the peptides, these data support the conclusion that a R_3–R_8 halogen bond is formed. This result was further confirmed by density functional theory calculations that showed that a σ-hole is present on the Cl-atom of **9**, and estimated the bond energy to be 6.1 kJ/mol, which is in good agreement with the literature.[122]

Since aliphatic carbon-bromine bonds are not compatible with the conditions for SPPS, the bromine atom of **10** was introduced in the last step via reaction of **3** with a Vilsmeier reagent (Scheme 8).

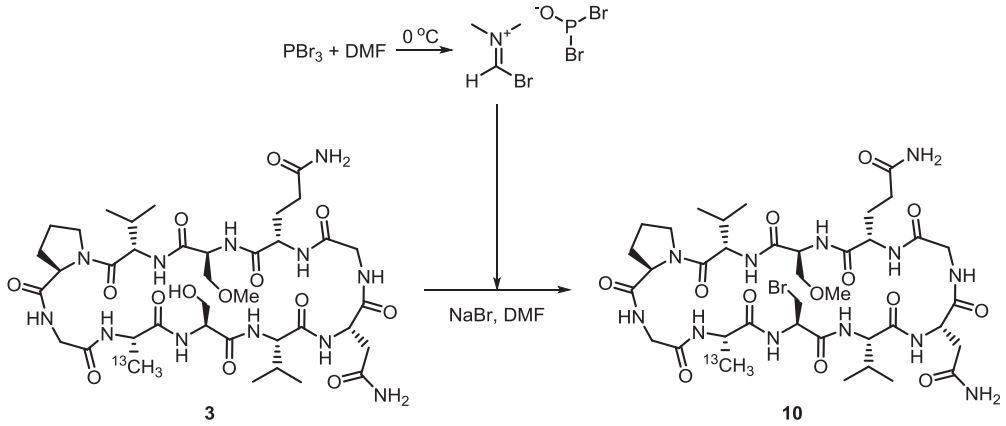

Scheme 8. Outline of the synthesis of **10** encompassing a bromo-substituent in position R_3.

The bromo-substituted peptide **10** was found to be unstable at room temperature and was therefore analyzed at -10 ºC, in DMF-d_7. The NOESY coupling pattern of **10** is shown in Figure 19. No interstrand NOEs indicating β-hairpin folding were observed. The backbone NH coefficients could not be derived due to the rapid degradation of **10** upon increasing the temperature. Likewise, the solution conformational ensemble could not be obtained since no reliable distances could be measured from the NOESY spectrum of **10** at -10 ºC. It was concluded that in the case with R_3 = Br, the peptide is most likely not folded as a β-hairpin. This might be due to the size of the Br that does not allow interstrand interactions with a reasonable geometry for a β-hairpin.

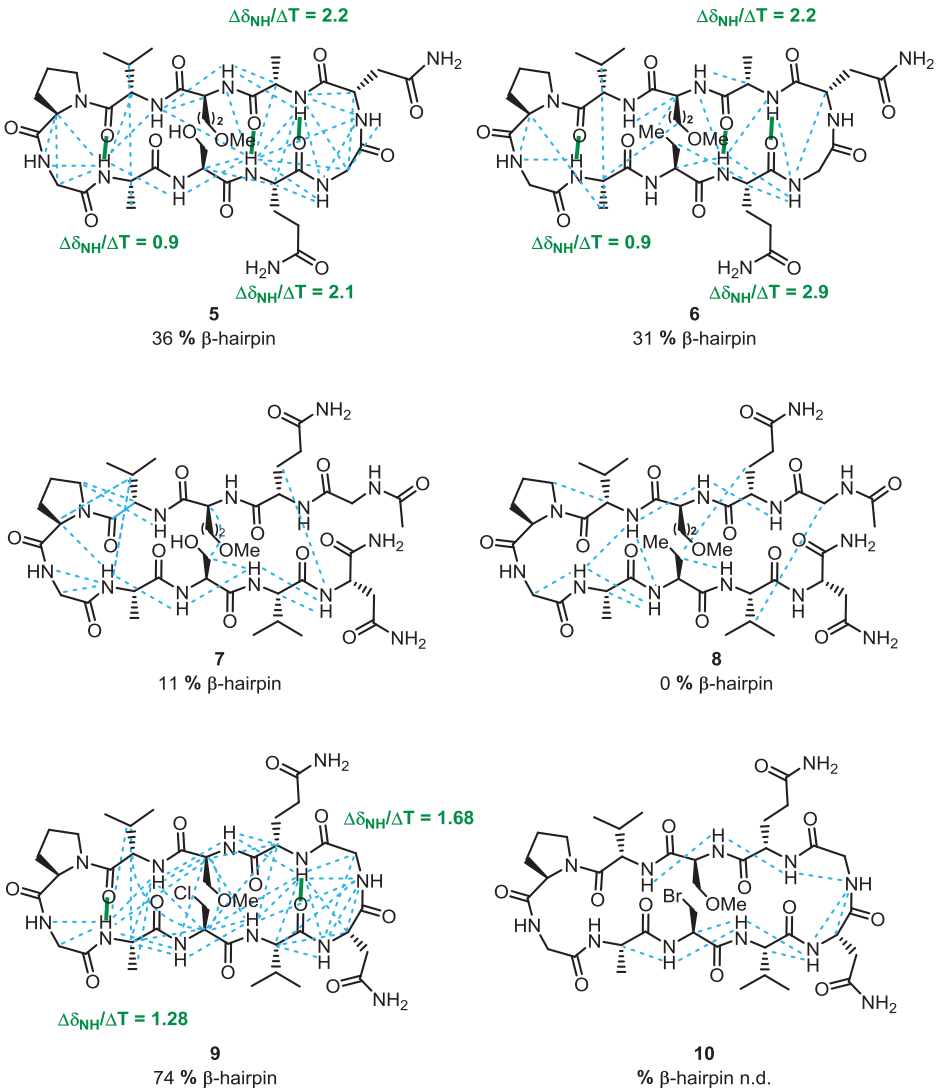

Figure 19. The NOE coupling pattern (blue dotted lines) and amide backbone hydrogen bonds (green lines) for peptides **5–9** were measured in DMSO-d_6 at room temperature at a 900 MHz spectrometer. The NOE coupling pattern (blue dotted lines) for peptide **10** was measured at -10 ºC in DMF-d_7 at a 500 MHz spectrometer. Amide backbone hydrogen bonds were not obtained for **10** due to rapid decomposition at temperatures > -10 ºC.

Table 3. Summary of the results of the conformational analysis of peptides **1–10**.

Peptide	Sequence[a]	R_3[b]	R_8[b]	n[c]	$\Delta\delta_{NH}/\Delta T < 3$[d]	% β-hairpin[e]
1	c(NVSAGD-PVSQG)	OH	OH	1	AA4, AA9	88
2	c(NVXAGD-PVSQG)	Me	OH	1	AA4, AA9	50
3	c(NVSAGD-PVS(Me)QG)	OH	OMe	1	AA4, AA9	58
4	c(NVXAGD-PVS(Me)QG)	Me	OMe	1	AA4, AA10	29
5	NVSAGD-PVhS(Me)QG-Ac	OH	OMe	2	–	11
6	NVXAGD-PVhS(Me)QG-Ac	Me	OMe	2	–	0
7	c(GQSAGD-PVhS(Me)AN)	OH	OMe	2	AA2, AA4, AA9	36
8	c(GQXAGD-PVhS(Me)AN)	Me	OMe	2	AA2, AA4, AA9	31
9	c(NVA(Cl)AGD-PVS(Me)QG)	Cl	OMe	1	AA4, AA9	74
10	c(NVA(Br)AGD-PVS(Me)QG)	Br	OMe	1	n.d.	n.d.

[a]One letter amino acid acronyms are given in Appendix I. Peptide sequence is given according to the numbering in Figure 9 A. X = Abu (L-2-aminobutyric acid), S(Me) = *O*-methyl-L-serine, hS(Me) = *O*-methyl-L-homoserine. [b]When R_3=OH the R_3–R_8 hydrogen cross strand interaction is possible. When R_3=Cl/Br the R_3–R_8 halogen cross strand interaction is possible. When R_3=Me the cross strand interaction cannot occur, and the peptides with R_3=Me serves as references. [c]Number of carbons in the R_8 side chain, see Figure 9. [d]$\Delta\delta_{NH}/\Delta T < 3$ indicate a strong intramolecular hydrogen bond (see section 3.1.5). AA positions are given in Figure 9. [e]The % β-hairpin in the solution ensemble as determined by NAMFIS analysis. Peptide **10** could not be evaluated due to rapid degradation at room temperature and low quality spectrum at low temperatures.

6.4.2 Summary Paper III

The impact of halogen bonding on β-hairpin formation in solution was studied by NMR, and it was concluded that a chlorine-centered halogen bond stabilizes a β-hairpin to a comparable degree to an equivalent hydrogen bond. Since chlorine has poor NMR properties, the halogen bond was detected indirectly from ^{1}H NOE/ NAMFIS ensemble analysis and VT NMR experiments. This is, to the best of our knowledge, the first example of a stabilizing halogen bond interaction in a peptidic system in solution.

7 CONFORMATIONAL ANALYSIS OF β–HAIRPIN INHIBITORS OF THE MDM2/P53 PROTEIN-PROTEIN INTERACTION (PAPER IV)

7.1 The protein-protein interaction

Protein-protein interactions (PPIs) regulate numerous essential cellular pathways such as cell growth, DNA replication, transcriptional activation, energy production, protein folding, and transmembrane signaling, and are therefore important targets for the development of new therapeutics.[123] However, due to their typically large and flat interaction sites, lacking well-defined buried cavities that are common for conventional targets, the activity of PPIs is often difficult to modulate by small molecules.[124] In contrast to protein-small ligand interactions, which are typically mediated by a few specific chemical forces, the protein-protein complex formation is usually driven by a large number of weak interactions that are often hydrophobic. Peptides with well-defined secondary structures have been shown useful for modulation of targets with featureless and flat binding sites, like PPIs.[16,125] This is because they can address the demand for higher molecular complexity that is necessary for targeting PPIs and hence reproduce the specific interactions involved, and thereby bind with high specificity to the flat protein interface.[16] The identification of hot spots, that is regions of the binding site that significantly contribute to the binding free energy, has been demonstrated to be a fruitful strategy for the identification of PPI modulators.[126] Many PPI drug targets have hot spot regions with well-defined secondary structures such as α-helices and β-sheets. One example is the MDM2/p53 PPI site, where an α-helix of p53 binds to MDM2 via a "hot spot triad" involving the three hydrophobic residues Phe19, Trp23 and Leu26 aligned on one face of the α-helical fragment (Figure 20 A and B).[127]

7.2 The MDM2/p53 interaction

The transcription factor and tumor suppressor p53 is activated in response to DNA damage and cellular stress. p53 induces cell cycle arrest and apoptosis, and thereby protects cells from malignant transformation.[128] MDM2 serves as a negative regulator of the expression of p53.[129] Inactivation of p53 by mutation or

overexpression of MDM2 is one of the most common defects in human cancers.[130] The pharmacological disruption of the MDM2/p53 PPI may therefore allow p53 induced cell cycle arrest and apoptosis, providing a strategy for treating this important class of tumors.

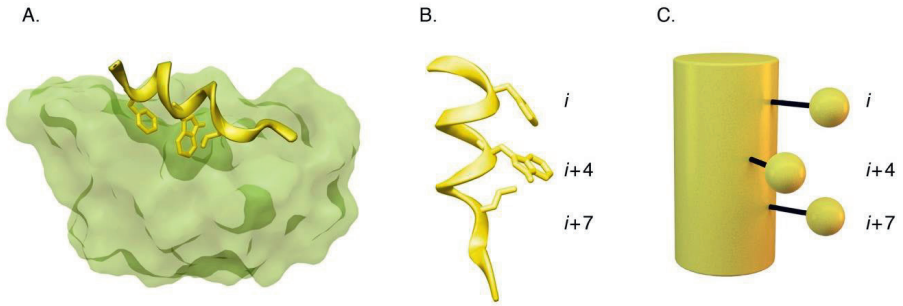

Figure 20. **A**. Crystal structure of the α-helix of p53 binding to MDM2. The "hot spot triad" consisting of residues Phe19 (*i*), Trp23 (*i*+4) and Leu26 (*i*+7) of p53 are shown (PDB code: 1YCR).[127] **B**. The α-helical part of p53 that binds to MDM2, with *i, i*+4 and *i*+7 residues. **C**. Schematic illustration of an MDM2 inhibitor as a cylinder and the positions of the *i, i*+4 and *i*+7 triad shown as spheres.

A large number of inhibitors of the MDM2/p53 interaction have been developed, including small molecules[131-133] and peptides.[125] Although these inhibitors vary in structure they all orient the interacting substituents in the *i*, *i*+4 and *i*+7 positions as illustrated in Figure 20 C.

7.3 Constrained bioactive peptides

Constraining the peptide conformation can be a useful strategy in order to increase both bioactivity and bioavailability. In fact, the conformation has been suggested to be the most important factor for the bioactivity and bioavailability of peptides.[17] Since peptides are usually flexible, binding to the target receptor is associated with an energy penalty due to the loss in entropy. By locking the peptide into the bioactive conformation this penalty will be smaller. Some examples of different ways to constrain peptides are hydrocarbon stapling,[134] backbone cyclization,[91] and azide-alkyne cyclization.[22,25] However, for non-conventional targets like PPIs this approach has been discussed,[10,135-137] and it has been proposed that bRo5-ligands,

for example peptides, should have an appropriate balance between flexibility and rigidity to bind to their targets.[10]

7.4 Methods used for biological evaluation

7.4.1 Surface plasmon resonance

In the surface plasmon resonance (SPR) experiment direct binding of a ligand to its receptor is measured. The general principle is outlined in Figure 21. A gold coated glass chip immobilized with the protein is illuminated with polarized light. Part of the light is penetrating the surface as a so-called evanescent wave, and the energy of this wave is missing in the detector in a certain angle (SPR angle, Figure 21 A), which can be measured.[133] The SPR angle is directly proportional to the amount of material on the surface. When a ligand is added the SPR angle is increased. This angle dependence is detected over time as illustrated by the sensogram in Figure 21 B, from which the on- and off-rates can be extracted and thereby also the dissociation constant (K_D).[99]

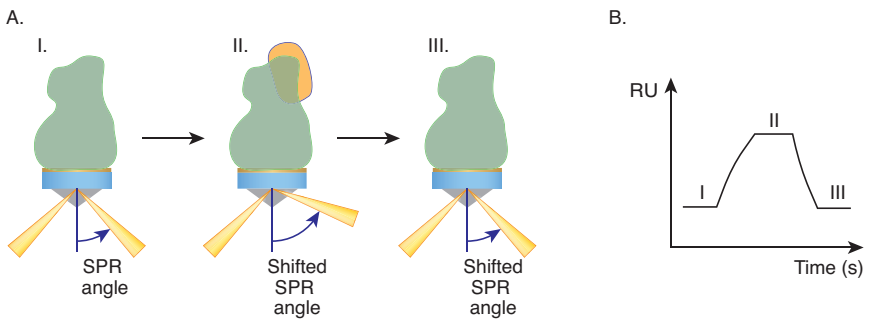

Figure 21. Schematic illustration of the SPR experiment. **A**. I. The protein immobilized on the surface. II. Addition of a binding ligand leads to an increased SPR angle. III. The angle is decreased when the ligand is removed by washing. **B**. SPR sensogram. The change is measured in resonance units (RU, 1 RU = 1 pg/mm^2).

7.4.2 Fluorescence polarization

In the fluorescence polarization (FP) experiment (Figure 22) fluorescently labeled ligands are excited with linear polarized light. Due to the movement of the molecules in solution between the excitation and emission, the light emitted by the ligands is of a different polarization.[133] The change in polarization is proportional to

molecular tumbling in solution. This means that a fluorescently labeled ligand-protein complex emits light of different polarization than the free ligand, which tumbles faster in solution. Adding a fluorescently labeled ligand to the protein and then exchanging it for the ligands of interest provides a measure of exchange rate. In contrast to SPR, the FP experiment can therefore be used to measure competitive binding of a ligand to its receptor.[99]

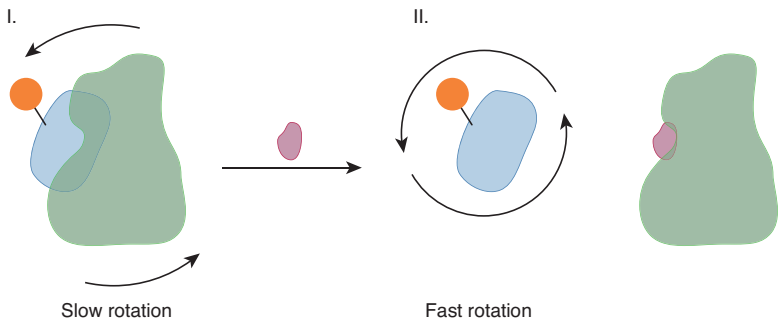

Figure 22. Schematic illustration of the FP-experiment. A fluorescently labeled ligand rotates faster when it is not bound to the protein.

7.5 Evaluation of the flexibility of cyclic β-hairpin inhibitors of the MDM2/p53 protein-protein interaction (Paper IV)

β-Hairpin peptides, similar to the ones described in Chapter 6, have been used as α-helical mimetics to inhibit the MDM2/p53 interaction.[30] A crystal structure of the peptide with highest affinity (**11**, Figure 23) of the investigated compounds showed that the binding conformation is a β-hairpin placing the interacting side chains in the *i*, *i*+4 and *i*+7 positions.[30] Due to the similarity to our previously described peptides, and the fact that the interstrand hydrogen bond can be used for stabilization of β-hairpins, we decided to study whether the inhibitory potency of the β-hairpin inhibitors of the MDM2/p53 PPI depends on their flexibility.

7.5.1 Results and discussion Paper IV

The previously reported **11** (Figure 23)[30,138] was used as a starting point for the design of new β-hairpin inhibitors of the MDM2/p53 PPI. Based on conformational analysis of several cyclic peptides by MCMM, **12** (Figure 23) was selected for its predicted high propensity to fold into a β-hairpin conformation.

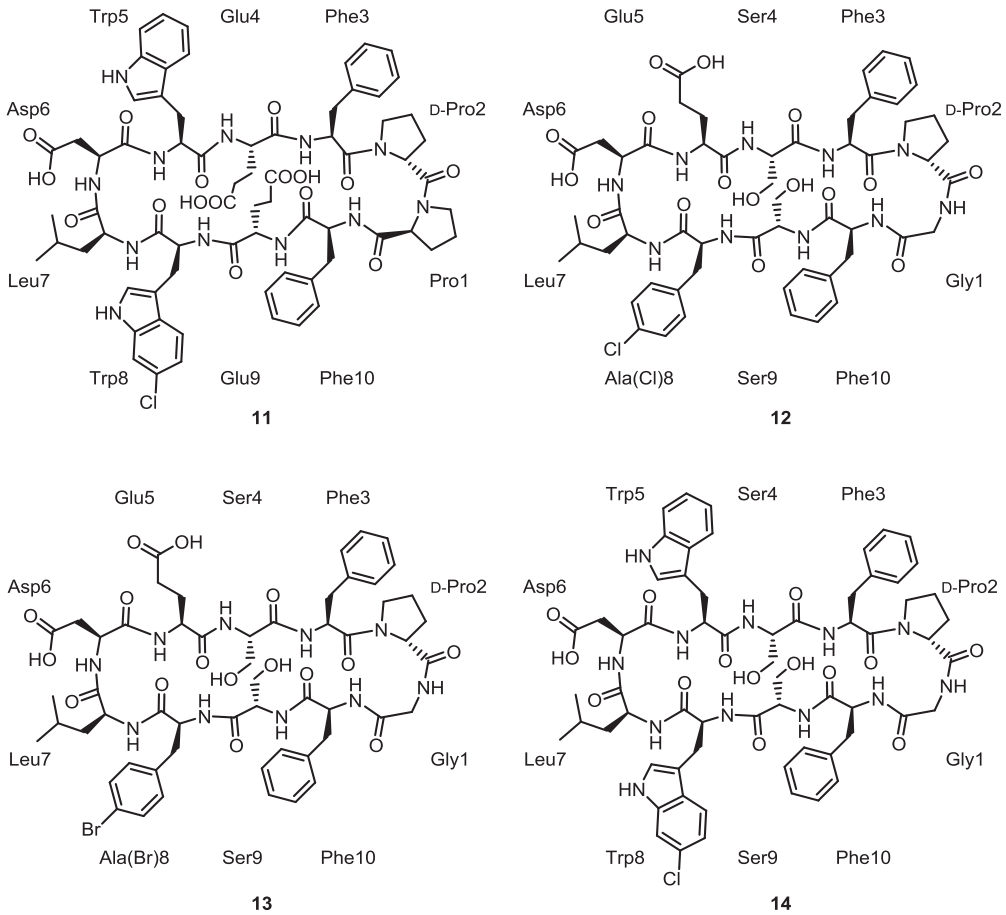

Figure 23. Structures of cyclic peptides studied as inhibitors of the MDM2/p53 interaction. Amino acids are given with three letter codes and residue positions (*i* = position 10, *i*+4 = position 8 and *i*+7 = position 7).

Several small molecule inhibitors of MDM2/p53 have a 4-chlorophenyl in the *i*+4 position, and it has been speculated that the chlorine atom is involved in a halogen

bond with MDM2. Therefore, 4-chloro-L-phenylalanine was incorporated at the *i*+4 position in **12**, and an analogue with the stronger halogen bond donor bromine at the same position, i.e. 4-bromo-L-phenylalanine (**13**, Figure 23), was also prepared. For comparison to previous data, **14** (Figure 23) was also included in the analysis. Peptides **12–14** all have the possible cross strand hydrogen bond as well as the D-Pro-Gly β-turn inducer that was used in our previous peptides (Figure 10 and Figure 13).

Peptides **11–14** were prepared by SPPS as described in section 6.2.1, and their synthesis is outlined in Appendices VI–VIII. Likewise, structural assignment, NOE build-up-based distances, amide temperature coefficients, and MCMM ensembles were derived as described above. The Hα chemical shifts, the $^3J_{CH\alpha NH}$ coupling constants (Table 4) and the NOE coupling pattern (Figure 24) were in good agreement with a β-hairpin conformation for all peptides. The amide temperature coefficients ($\Delta\delta_{NH}/\Delta T$, Table 4 and Figure 24) were > 3, indicating that the backbone hydrogens are in equilibrium between intra- and intermolecular (solvent) hydrogen bonding; however, the coefficients are lowest at the turn positions, indicating formation of stable β-turns.

Table 4. Hα proton chemical shifts (ppm), $^3J_{CH\alpha NH}$ coupling constants (Hz) and $\Delta\delta_{NH}/\Delta T$ backbone amide temperature coefficients (ppb K^{-1}) for **11–14** in DMSO-d_6.

Residue	**$\delta_{H\alpha}$ (ppm)**				**$^3J_{CH\alpha NH}$ (Hz)**				**$\Delta\delta_{NH}/\Delta T$ (ppb K^{-1})[b]**			
position[a]	**11**	**12**	**13**	**14**	**11**	**12**	**13**	**14**	**11**	**12**	**13**	**14**
1	4.22	3.51	3.52	3.52	–	–	–	–	–	9.3	8.1	10.0
2	4.46	4.22	4.22	4.20	–	–	–	–	–	–	–	–
3	4.90	4.78	4.79	4.68	–	7.8	7.5	–	5.7	7.4	7.6	8.1
4	4.83	4.85	4.86	4.70	–	–	7.3	7.4	8.8	9.4	9.6	11.8
5	4.76	4.56	4.56	4.67	8.4	7.4	8.2	–	4.8	3.2	3.1	5.5
6	4.27	4.37	4.37	4.33	7.7	6.2	8.0	6.8	10.0	7.1	7.2	8.2
7	3.48	3.65	3.64	3.64	–	–	–	–	8.2	9.3	8.6	10.1
8	4.67	4.54	4.54	4.57	7.3	7.4	8.6	7.3	6.7	6.2	6.1	8.5
9	5.02	4.70	4.71	4.80	7.9	–	7.3	6.6	9.1	10.5	9.8	8.5
10	4.82	4.78	4.78	4.77	8.9	7.5	9.2	8.5	3.7	3.5	3.7	3.7

[a]Residue position according to Figure 23. [b]The amide temperature coefficients are derived as negative numbers but reported as positive numbers. $\Delta\delta_{NH}/\Delta T$ < 3 indicates a strong intramolecular hydrogen bond, $\Delta\delta_{NH}/\Delta T$ = 3–5 indicates that the amide proton is in equilibrium between a solvent-exposed and an intramolecular hydrogen bond, and $\Delta\delta_{NH}/\Delta T$ > 5 indicates that the amide proton is solvent-exposed.

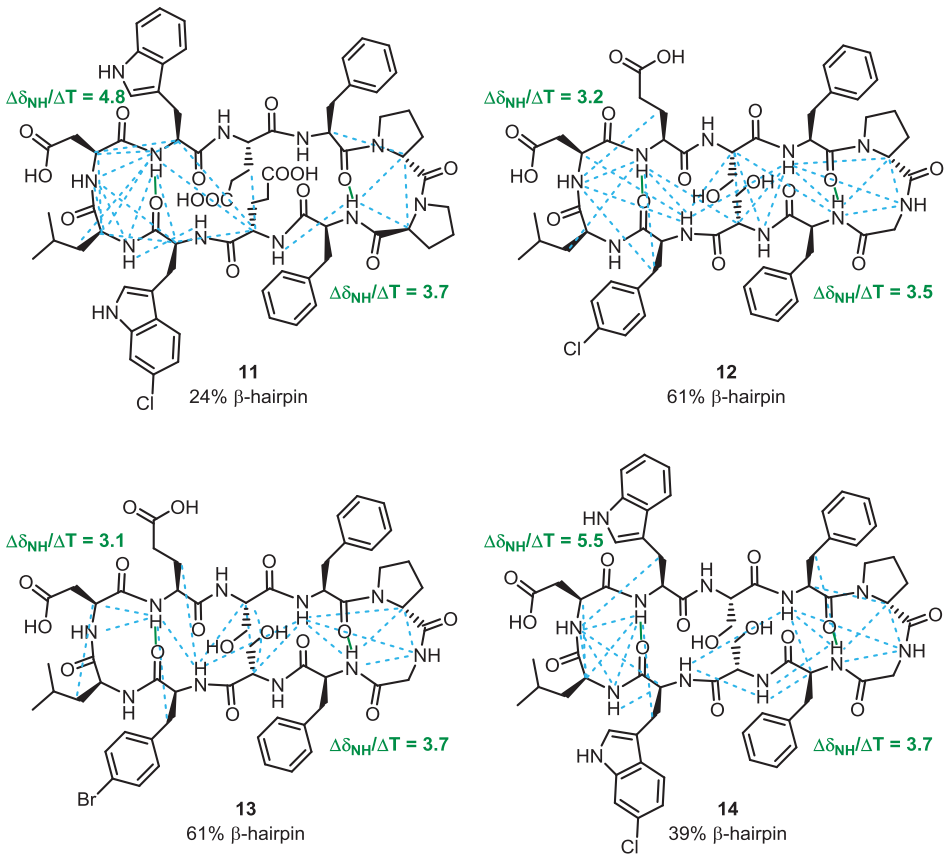

Figure 24. The NOE coupling pattern measured at 900 MHz (blue dotted lines) and amide backbone hydrogen bonds (green lines) for **11–14**.

The NAMFIS analysis revealed the folding propensity to follow the order **12** ≈ **13** > **14** > **11** (Table 5). The main conformations of **11–14** as selected by NAMFIS are shown in Figure 25.

The inhibitory activity was evaluated using FP and SPR assays. The FP assay measures displacement of Texas red labeled wild-type p53 peptide bound to MDM2, and in this case the activity order **11** > **14** > **13** > **12** was observed (Table 5). Hence, the activity increases with increased flexibility of the structurally similar β-hairpins **11–14**. This observation was further supported by the K_D-values

measured by SPR assays (Table 5). Whereas the backbone geometries of the peptides are comparable to the MDM2-bound crystal structure of **11**, as shown in Figure 25, the peptides show different degree of flexibility. Thus, our data indicate that constraining the peptides decreases their affinity to MDM2.

Table 5. The results from the NAMFIS ensemble analysis and the FP and SPR assays for **11–14.**

Peptide	% β-hairpin[a]	IC_{50} (μM) FP-assay[b]	95% CI FP-assay[c]	K_D (μM) SPR-assay[d]
11	24	2.86	1.61-5.10	0.127 ± 0.001
12	61	23.94	7.72-74.30	7.00 ±0.1
13	61	10.10	5.67-17.99	5.73 ±0.09
14	39	7.56	3.42-16.69	2.50 ±0.02

[a]% β-hairpin content in solution as deduced by NAMFIS analysis. [b]MDM2/p53 inhibitory activity observed in a FP-assay. [c]CI = confidence interval. [d]Dissociation constant (K_D) measured using a SPR-assay.

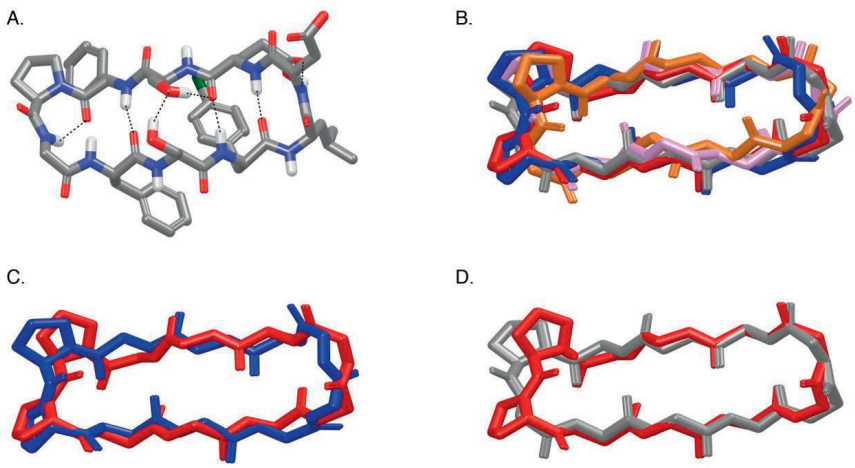

Figure 25. β-Hairpin conformations as selected by NAMFIS. **A**. The main conformation of **12**. **B**. Overlay of conformations **11** (blue), **12** (grey), **13** (orange), **14** (pink), and the MDM2-bound X-ray structure of **11** (red) showing their similarity. **C**. Overlay of the β-hairpin selected for **11** by NAMFIS (blue), and the MDM2-bound crystal structure of **11** (red). **D**. Overlay of the β-hairpin selected for **12** by NAMFIS (grey), and the MDM2-bound crystal structure of **11** (red).

7.5.2 Summary Paper IV

Four peptide inhibitors (**11–14**) of the MDM2/p53 PPI were designed, synthesized and evaluated with respect to their conformational flexibility and inhibitory activity. Constraining the peptides was shown to decrease the affinity towards MDM2. The importance of flexibility of bioactive peptides for an optimal affinity has previously been discussed, especially for difficult protein targets like PPIs.[10] It has been proposed that flexible binding domains might require flexible ligands, and that conformational restrictions could result in overall reduced entropy for the ligand-bound complex.[10,13,15,95] Thus, the binding to a relatively flat surface, such as a PPI binding site, might require sufficient flexibility in order to allow the necessary geometrical adjustments. Stabilizing the bioactive conformation of macrocyclic peptides was previously shown to have either favorable or unfavorable entropic consequences.[136,139]

8 CONFORMATIONAL ANALYSIS OF CD36 MODULATING CYCLIC AZAPEPTIDES (PAPER V)

8.1 The cluster of differentiation 36 receptor

The cluster of differentiation 36 (CD36) receptor is a multiligand transmembrane receptor involved in a number of biological processes, for example atherosclerotic lesion formation,[140] fatty acid signal transduction[141] and angiogenesis.[142] Due to the large range of ligands that bind to the CD36 receptor,[143] including oxidized low density lipoprotein (oxLDL),[140] malaria infected erythrocytes,[144] long-chain fatty acids,[141] hexarelin,[145] and thrombospondins,[142] CD36 is a drug target for several diseases. For instance, binding of oxLDL is one of the initial steps of foam cell formation leading to atherosclerosis.[140] CD36 has multiple ligand binding domains[140] and, for example, oxLDL and thrombospodin-1 bind at different sites.[146] There are only a few crystal structures of CD36 complexes, and for many of its ligands the binding event is not characterized.

8.2 Growth hormone releasing peptides

Growth hormone releasing peptides (GHRPs) are synthetic hexa- or heptapeptides that are known to stimulate growth hormone release by binding the growth hormone secretagogue receptor 1a (GHS-R1a). The synthetic hexapeptide GHRP-6 (His-D-Trp-Ala-Trp-D-Phe-Lys-NH_2, Figure 26) was the first GHRP to be discovered.[147] The 2-metyl-tryptophan analogue of GHRP-6, hexarelin ([2-Me-W2]GHRP-6, Figure 26),[145] was later shown to also bind to the CD36 receptor and

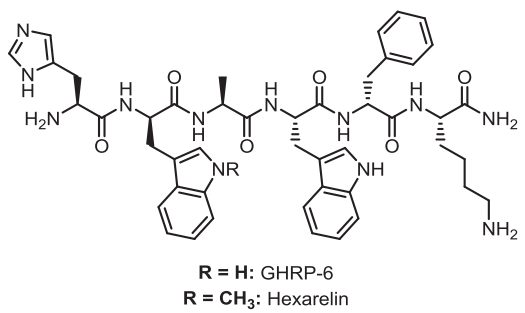

Figure 26. The growth hormone releasing peptides GHRP-6 and hexarelin.

thereby provide cardiovascular protective effects, likely due to inhibition of oxLDL.[143] The bioactive conformation of GHRP-6 analogues has been suggested to adopt a turn motif.[148,149]

8.3 Azapeptides

Azapeptides are peptides with at least one of the amino acid residues substituted for a semicarbazide, in other words one of the α-carbons is replaced with an α-nitrogen (Figure 27). There are several examples of bioactive azapeptide analogues,[150,151] including the marketed HIV-1 protease inhibitor atazanavir.[152] The aza-moiety has typically been incorporated to induce conformational constrains[151] or to increase metabolic stability.[153] The conformational behavior of azapeptides have been studied mostly using small linear peptides, and it has been shown that the aza-moiety can induce β-turns,[74,154] and that the carbonyl–aza-amine (CO–NR) bond can display hindered single bond rotation.[155] However, the solution conformations of azapeptides have in most cases not been described.

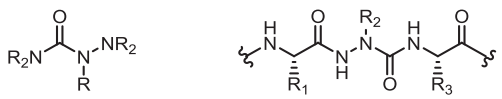

Figure 27. General structures of the semicarbazide moiety and the azapeptide, with a semicarbazide incorporated at one of the amino acid residues (R_2).

8.4 Conformational preferences of macrocyclic azapeptide inhibitors of CD36 in aqueous solution (Paper V)

Linear azapeptide analogues of GHRP-6 have previously been shown to modulate CD36 activity.[156-159] As compared to GHRP-6 and hexarelin, the azapeptide analogue [Aza-Phe[4]]-GHRP-6 (His-D-Trp-Ala-aza-Phe-D-Phe-Lys-NH_2) showed an increased CD36 versus GHS-R1a selectivity, while maintaining a comparable potency for CD36. CD and NMR measurements of this peptide revealed that the aza-moiety induced a β-turn.[156,157] Alanine scans of the linear azapeptide analogues of GHRP-6 revealed that the D-Trp2 residue was important for CD36 inhibitory activity, whereas the His1 residue was not.[158] Macrocyclic azapeptide analogues of

GHRP-6 (**15–17**, Figure 28) were shown to modulate CD36 activity and **15** has the highest potency reported for a GHRP-analogue.[159]

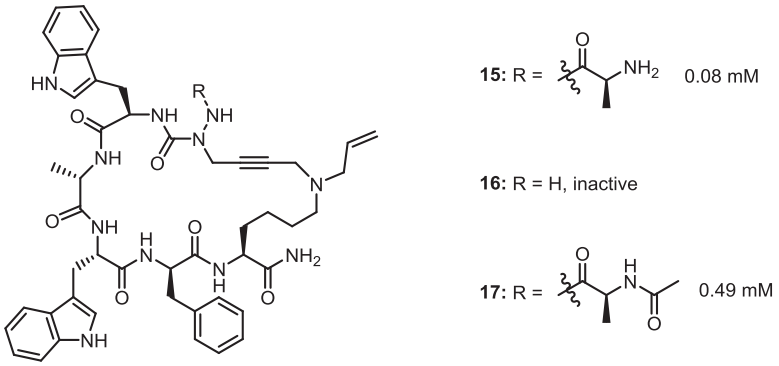

Figure 28. The investigated cyclic azapeptides and their respective IC_{50}-values for CD36.

As mentioned above, little is known about the binding event of CD36 and its ligands. In the case of GHRP-6 analogues, hexarelin has been shown to bind to a lysine-rich domain of CD36, which overlaps with the oxLDL binding site. Although aza-GHRP-6 analogues have been suggested to adopt β-turns, no crystal structure for any of the reported ligands in complex with CD36 is avaiable, and the bioactive conformation and the solution ensembles of these peptides have not yet been studied. Following the presumption that the protein-bound conformation of a flexible ligand is represented in its solution ensemble,[21,160,161] the conformations of the macrocyclic azapeptides **15–17**, in aqueous solution were investigated using the NAMFIS methodology.

8.4.1 Results and discussion Paper V

Due to conformational dynamics of the positions near the 3' amine of azapeptides **15–17**, the ^{1}H NMR assignment of these peptides was challenging. The TOCSY-NOESY backbone walk, as described above, was used in combination with COSY, HSQC and HMBC spectra for the ^{1}H NMR assignment. Compounds **16** and **17** had broader peaks and fewer NOESY correlations than **15**, suggesting higher flexibility. NOE-based distances and MCMM calculated theoretical ensembles of **15–17** were derived as described above. NAMFIS analysis (Table 6) verified the line

broadening-based assumption that **16** and **17** are more flexible than **15**, with the overlaid solution ensembles of these compounds being shown in Figure 29. The ensemble of **16** was identified to contain 9 conformers, as compared to 6 for **15** and **17**, and was therefore concluded to be the most flexible of the three. The ensemble of **17** is more diverse than that of **15** (RMSD = 1.90 and 1.78, respectively). Thus, the flexibility order was found to be **16** > **17** > **15**, which is opposite to the CD36 activity order **15** > **17** > **16**.[159]

Table 6. Results of the NAMFIS analyses for the azapeptides **15**–**17** in D_2O.

15			**16**			**17**		
Conf. no.[a]	% in ensemble[b]	Conf. family[c]	Conf. no.[a]	% in ensemble[b]	Conf. family[c]	Conf. no.[a]	% in ensemble[b]	Conf. family[c]
1	3	A	7	2	A	16	22	A
2	28	A	8	7	C	17	8	B
3	11	B	9	11	C	18	22	-
4	8	B	10	2	D	19	8	-
5	11	B	11	3	C	20	16	-
6	36	B	12	25	-	21	21	D
			13	8	B			
			14	6	-			
			15	33	B			

[a]The overlaid structures of the most populated conformations are shown in Figure 29. [b]Population of the indicated conformer in solution as selected by NAMFIS analysis, all other molar fractions are 1% or less. [c]The conformational families are shown in Figure 30. RMSD overlaying backbone atoms: A = 0.91, B = 1.36, C = 0.53, D = 1.22.

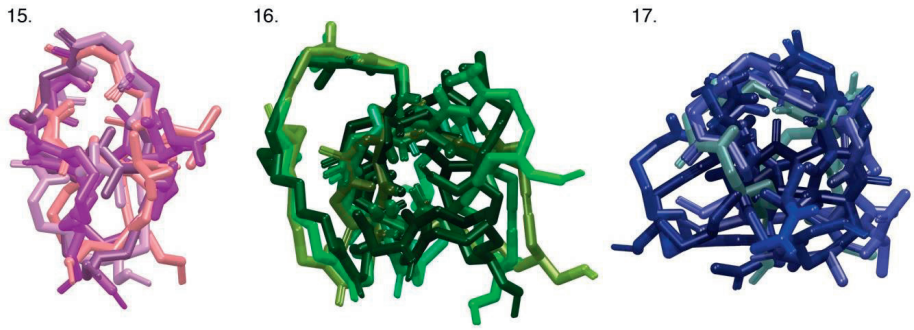

Figure 29. Overlaid backbone conformations (superpositioning α-carbons of Trp-Ala-Trp-Phe) of the solution ensembles of peptides **15**–**17**. RMSD overlaying backbone atoms: 1 = 1.78, 2 = 2.70, 3 = 1.90. Amino acid side chains are omitted for clarity.

The conformations of the solutions ensembles of **15–17** were assigned to conformational families A–D (Table 6 and Figure 30) according to similarities in backbone geometry. Peptide **15** possesses two major conformations, A and B, supporting the previous results suggesting this to be more rigid than **16** and **17**, whose solution conformations were distributed in a larger number of families. Conformational family A was populated to 31% for **15**, 22% for **17**, and 2% for **16**, and thus follow the trend of the CD36 potency (**15** > **17** > **16**). Previous studies of linear azapeptide analogues of GHRP-6 have suggested that the aza-moiety may induce a β-turn.[156,157] Such a turn was not found for any of the conformations among the conformations identified to exist in solution by the NAMFIS analysis. Instead, the conformations in family A displayed a type II' β-turn for residues Ala-D-Trp. As the only difference in the structure of peptides **15–17** is the side chain attached to the aza-nitrogen, this side chain is expected to cause the flexibility difference of the peptides. Stabilizing side chain-to-macrocycle hydrogen bonds were not found for the family A conformations. However, they were found for families B and D, with a higher population for peptide **17** as compared to **15**, which might explain their difference in flexibility.

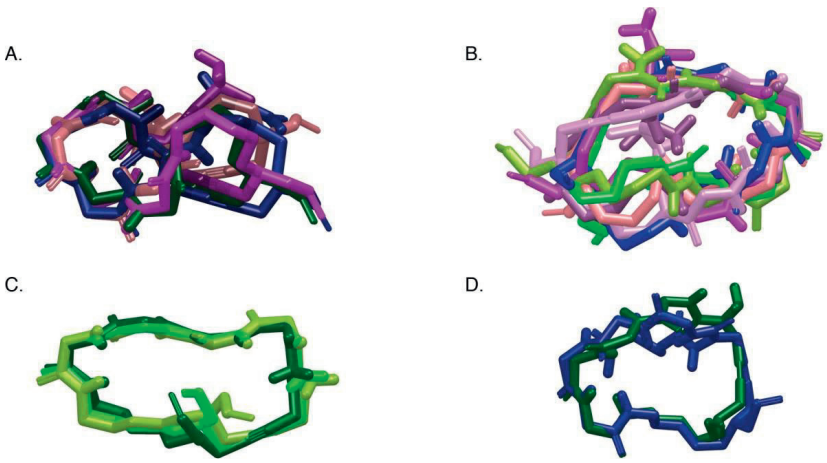

Figure 30. Overlapped backbone conformations of the conformational families A–D of azapeptides **15–17** given in Table 6. Amino acid side chains are omitted for clarity. RMSD overlaying backbone atoms: A = 0.91, B = 1.36, C = 0.53, D = 1.22. Pink/purple conformations represent peptide **15**, green conformations peptide **16**, and blue conformations peptide **17**.

Previous studies of small linear azapeptides showed that the E-configuration along with hindered single bond rotation of the CO-NMe moiety is preferred when one of the aza-nitrogens is methylated, which might also constrain the peptide.[155]

8.4.2 Summary Paper V

Three macrocyclic azapeptides with activity for the CD36 receptor were investigated by NAMFIS. A decreased flexibility and increased solution population of conformational family A was shown to be beneficial for their CD36 inhibitory activity, that is 31% population of A for **15** (IC_{50} 0.08 μM), 22% population of A for **17** (IC_{50} 0.49 μM) and 2% population of A for **16** (no measurable activity).

9 THE SOLUTION CONFORMATIONS OF ROXITHROMYCIN ADAPTING TO THE ENVIROMENT

9.1 Cell permeability of macrocycles

Macrocyclization is commonly used to improve cell permeability. Increased cellular penetration upon cyclization might be due to a decreased flexibility and decreased polarity as a result of formation of intramolecular hydrogen bonds and/or conformational shielding of polar functionalities.[13,14] Although many macrocycles are administrated orally, they generally belong to the bRo5 ligands, and often have both low cellular penetration and low oral bioavailability. However, the analysis of the properties of orally bioavailable drugs in the bRo5-space has shown that, as compared to the Lipinski rules,[3,14] the molecular weight of these compounds may be increased up to 1000 Da, the PSA to 250 $Å^2$ and the number of HBAs to 15.[11,14] For the analysis of macrocyclic peptide conformational preferences in relation to permeability, solution NMR spectroscopy has previously been used, with $CDCl_3$ mimicking the cell membrane and D_2O mimicking the cell surroundings.[162]

9.2 Roxithromycin

Roxithromycin (Figure 31) is a macrocyclic antibacterial agent based on the structure of erythromycin (Figure 31), where replacement of the 9-keto group by the 9-[*O*-(2,5-dioxahexyl)oxime] side chain results in increased metabolic stability and better oral bioavailability.[163] It has been shown using parallel artificial membrane permeability assay (PAMPA) that passive diffusion is higher for roxithromycin than for erythromycin, which might partly explain its higher bioavailability.[164] Roxithromycin and erythromycin belong to the group of macrolides, in other words natural products with a macrocyclic lactone ring of at least 12 atoms. Their antibacterial activity is the result of binding to the bacterial ribosome and thereby inhibit protein biosynthesis.[165] The solution ensemble of roxithromycin has been proposed to contain one major conformation, which is highly similar to the crystal structure,[166] and some minor conformations that could not be identified experimentally due to their low solution populations, in both hydrophilic and hydrophobic solvents.[167-169] The major solution conformation has

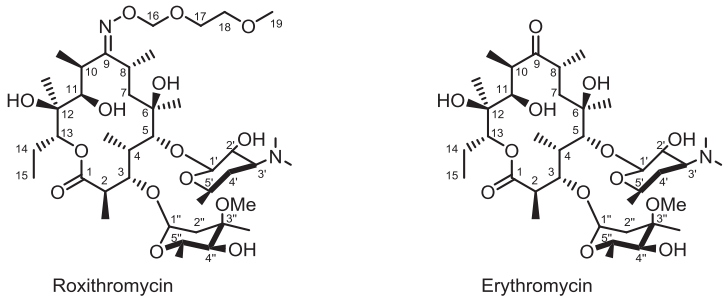

Figure 31. The structures of macrolides roxithromycin and erythromycin.

the oxime chain folded over, and hydrogen bonded to, the macrocycle. However, dependence of the solution conformation ensemble of roxithromycin on its environment has not yet been described in detail. As a part of a project examining the ability of computational techniques to predict the cell permeability of macrocycles, the conformational preferences of roxithromycin were studied by solution NMR spectroscopy in $CDCl_3$, mimicking the cell membrane, and in D_2O, mimicking the cell surroundings.

9.3 Solvent dependence of the conformations of roxithromycin

The proton assignments of roxithromycin in $CDCl_3$ and D_2O (Appendix IX) were derived from TOCSY, NOESY, COSY, and HSQC spectra. Interproton distances (Appendix X) were calculated from NOE build-ups as described above. The NOESY spectrum showed the same phase of the diagonal peaks and cross peaks for roxithromycin in D_2O and the opposite phase for roxithromycin in $CDCl_3$, indicating that roxithromycin interacts more with the solvent in D_2O. Solution conformations were derived by NAMFIS analysis using an input ensemble containing conformers generated by MCMM searches in chloroform and water using the OPLS and Amber* force fields (Appendix XI). Conformers from all individual MCMM searches were combined, and following redundant conformer elimination, comparing heavy atoms, generated the input ensemble for NAMFIS analysis (Appendix XI). The same input ensemble was used for analysis of the data from $CDCl_3$ and from D_2O. In the experimental input only data from the macrocycle, and not the flexible oxime chain or the sugars, were used. The initial

NAMFIS was run with the MCMM generated ensemble. In the following run the crystal structures of roxithromycin[166,170,171] were added to the input ensemble for comparison (Table 7).

The ensemble of roxithromycin in $CDCl_3$ selected by NAMFIS from the MCMM ensemble (Table 7) contains three highly similar conformations (Figure 32 A). In line with previous reports on the solution conformation of roxithromycin,[167-169] the oxime chain was found to be oriented above the macrocycle. When the crystal structures were added to the ensemble, one of them (Figure 32 B)[170] was selected to 100% (Table 7). Adding the crystal structure to the ensemble allowed the correct positioning of the oxime chain and also revealed that the oxime chain is hydrogen bonded to C(6)-OH. As shown by the overlaid conformations in Figure 32 C, the crystal structure and the major conformation from the initial run are highly similar. In conclusion, in chloroform, which was used to mimic the cell membrane, the oxime chain is fully folded over the macrocycle as shown in Figure 32 B. NAMFIS was able to capture the side chain orientation even when only data considering the macrocycle, and not the oxime chain, were used as input.

Table 7. Conformational populations derived by NAMFIS analysis for roxithromycin in $CDCl_3$ and D_2O solutions.

MCMM ensemble[a]				**MCMM ensemble + X-Ray structures[a]**			
$CDCl_3$		D_2O[e]		$CDCl_3$		D_2O[e]	
Conf. No.[b]	%[c]	Conf. No.[b]	%[c]	Conf. No.[b]	%[c]	Conf. No.[b]	%[c]
1	17	*2*	14	*X-ray*[d]	100	4	47
2	12	4	59			5	10
3	71	5	7			6	19
		6	6			9	3
		7	4			*10*	14
		8	8			*X-ray*[d]	6

[a]See Appendix XI. [b]Conformations in *italic* have the oxime chain-to-macrocycle hydrogen bonding. [c]Population of the indicated conformer in solution, as deduced by NAMFIS analysis, all other molar fractions are 1% or less. [d]CSD: KAHWAT. [e]Conformations 2 and 10, 7 and X-ray, 6 and 8, and 9 and 4 are highly similar.

However, although the MCMM conformational search did sample conformations with the oxime chain folded over the macrocycle, it did not sample hydrogen

bonding to C(6)-OH, but only to C(11)-OH. It is well known that MCMM does not describe the orientation of flexible side chains as well as backbone geometry.[52]

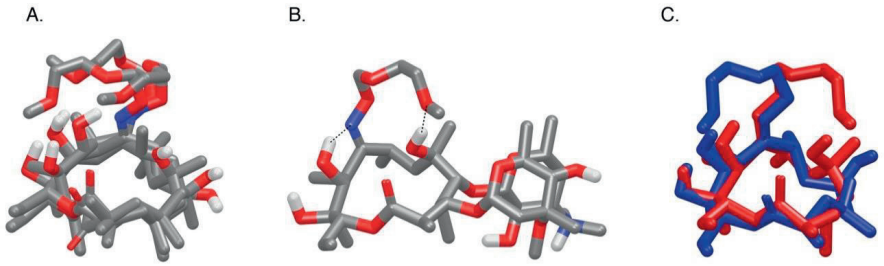

Figure 32. **A**. The conformations of roxithromycin obtained in the NAMFIS analysis of the MCMM ensemble in $CDCl_3$, with hydrogen bonding to C(11)-OH. Sugar residues are omitted for clarity. **B**. The crystal structure selected by NAMFIS from the ensemble containing the three crystal structures, with hydrogen bonding to C(6)-OH (CSD: KAHWAT).[170] **C**. Overlay of the major conformation from **A** (blue) and the crystal structure in **B** (red), showing their similarity in macrocycle geometry and difference in oxime chain orientation. Sugar residues are omitted for clarity.

The aqueous solution ensemble of roxithromycin was, in contrast to previous reports,[167-169] shown to contain several conformers (Table 7). Importantly, the majority of these conformations (80%) did not have the oxime chain oriented over the macrocycle but solvent exposed. As illustrated by the overlaid conformations in Figure 33 A, the aqueous ensemble of roxithromycin shows a relatively diverse set of macrocycle geometries. Similar to the analyses of the $CHCl_3$-data, adding the crystal structures to the ensemble did not change the outcome of the NAMFIS analysis of the D_2O-data significantly. Hence, in both ensembles ~20% of the conformations have the oxime chain over the macrocycle. When the X-ray structures are added 6% of the conformers show hydrogen bonding of the oxime chain to C(6)-OH and the rest to C(11)-OH. The protein-bound conformation of a flexible ligand is expected to be represented in its solution ensemble,[21,160,161] and accordingly the previously published protein bound geometry,[172] identified by X-ray diffraction, was identified to be present in solution. This structure (Figure 33 B) is highly similar to conformation 10 (Figure 33 C), which has a solution population of 14%. The oxime chain is not folded over the macrocycle in the bioactive conformation in which the C(6)-OH, C(11)-OH and C(12)-OH form hydrogen bonds to the ribosome.[172] It should be noted that the major conformation in $CDCl_3$

does not show as high similarity to the bioactive conformation, as it has previously been proposed.[165] Overall, it has been shown that in $CDCl_3$ the oxime chain of roxithromycin is oriented over the macrocycle, with this conformation being dominant in this solvent. In contrast, the solution ensemble of roxithromycin in D_2O consists of six different conformers, and the oxime chain is oriented over the macrocycle only in ~20% of the ensemble. Thus, these data reveal that the structure of roxithromycin converts from a more open conformation in polar media to a more closed and less flexible in non-polar media. Formation of intramolecular hydrogen bonds, as well as reduction of PSA, has been shown to internalize polarity and improve cell permeability and oral bioavailability for bRo5-macrocycles.[11,12] For the roxithromycin ensembles, 66% have macrocycle intramolecular hydrogen bonds in $CDCl_3$ as compared to 60% in D_2O, and the PSA weighted to the molar fractions of the conformers in the two solvents is 169 $Å^2$ and 173 $Å^2$, respectively. Although these differences are small, together with the overall flexibility of roxithromycin they might contribute to an improved passive diffusion as compared to erythromycin. It has previously been suggested that conformational flexibility may be beneficial for permeability by allowing the molecule to adapt to the transitional environment at the water-lipid interface at the boundary of the cell membrane.[162]

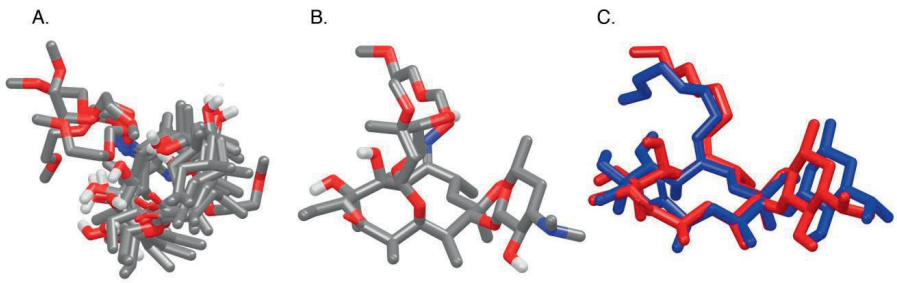

Figure 33. **A**. The solution conformational ensemble of roxithromycin in D_2O as derived by NAMFIS analysis using an ensemble generated by MCMM and including its crystal structures. Sugars are omitted for clarity. **B**. The X-ray structure of roxithromycin bound to the 50S subunit of the eubacterium *Deinococcus radiodurans* (PDB: 1JZZ).[172] **C**. Overlay of **B** and conformation 10, showing their resemblance. The cladinose sugars are omitted for clarity.

10 CONCLUDING REMARKS

This thesis describes the solution conformational ensembles of various macrocycles. Weak interstrand interactions were demonstrated to provide significant stabilization of the β-hairpin conformation. In this respect a halogen bond appears to be just as powerful for conformation direction as a hydrogen bond. Further, the flexibility of bioactive cyclic peptides in relation to their potency was studied and the importance of a balanced flexibility/rigidity for bioactivity was demonstrated. Whereas for one macrocycle rigidification in a presumptive bioactive conformation may provide increased bioactivity, for another it may result in decreased potency. The conformational preference of a macrolide antibiotic in different environments was also examined. Its structure was shown to convert from a more open conformation in a hydrophilic environment to a more closed and less flexible in a hydrophobic environment, proposing this to be the cell-permeable conformation. The information gained in these investigations could provide valuable insight in the process of drug design.

Further investigations of special interest include optimization of the cyclic β-hairpin model system used for investigation of weak interactions. More specifically, we would like to design peptides with bromine and iodine halogen bond donor sites. In addition, we wish to perform further variable temperature NMR studies, preferably in different solvents. Other studies of interest include the evaluation of the conformation and dynamics of erythromycin and other macrolides, using NAMFIS, to gain further insights into their conformational preferences in relation to permeability. Likewise, we would like to continue the conformational evaluation of additional cyclic azapeptides to establish their conformational preferences in correlation to their bioactivity.

11 ACKNOWLEDGEMENT

I have had wonderful years as a PhD student at the University of Gothenburg. The experience has been fun, educational, challenging, and most of the time really exciting. I would like to express my sincere gratitude to everyone who contributed in one way or another during my time as a PhD student. I would especially like to thank the following people.

My supervisor, Prof. **Máté Erdélyi**: Thank you for giving me the opportunity, for your enthusiasm, for all the support you have given me over the years, and for allowing me to try my own ideas – that has meant a lot to me! I have really appreciated working with you all these years.

My co-supervisor, Prof. **Kristina Luthman**: Ever since you were my teacher in the medicinal chemistry courses you have provided me with both great support and great inspiration. Thank you for always being there with good advice, for the great conversations about the research and for being such an excellent role model.

My examiners, Prof. **Morten Grøtli**, Docent **Göran Karlsson** and Prof. **Ann-Therese Karlberg**: Thank you for meaningful discussions, and for providing support in both my research and my career.

My degree project workers, **Nemanja Stanisic**, **Matilda Bred** and **Kajsa Lood**: Thank you for a job well done; you have made a major contribution to this thesis. Master's degree student **Stefan Peintner**: Thank you for your hard work analyzing the NMR data for the Roxithromycin project.

Past and current members of the halogen bonding group: Thank you for your support and helpful input, and for all the fun over the years. A special thank you to my old roommate Dr. **Anna-Carin Carlsson** for the good times we shared both in Gothenburg and Colorado, and to Dr. **Hanna Andersson** for all support, great collaboration on the projects and for your ability to maintain even better order in the lab than I do. My time as a PhD student would never have been the same without you two!

Past and current members of the organic chemistry, medicinal chemistry and dermatochemistry units (eighth and ninth floors): Thank you all for creating a friendly and stimulating work environment, and for the perfect combination of science and friendship, serious discussions and laughs. To all the people who were involved in arranging those lovely pea soup dinners, crab fish and Christmas parties – **Mariell**, **Tina**, **Markus**, **Tobbe**, **Martin**, and others: Thank you, it has been much appreciated!

All co-authors and collaborators. Dr. **Hanna Andersson**, Dr. **Patrik Jarvoll** and Dr. **Ulrika Brath**: Thank you for great teamwork on the various projects and for your invaluable knowledge and experience. Prof. **Jan Kihlberg**: Thank you for all the fruitful discussions about Roxithromycin on Skype. I really look forward to continuing this work after defending my thesis. Prof. **William Lubell**: Thank you for the opportunity to work on the aza-peptide project, which I truly enjoyed. Prof. **Shing Ho**: Thank you for making it possible for me to work in your lab at Colorado State University and for your generosity and kindness. A special thanks to **Rhianon Kay Rowe** for all the help in the lab, and to the rest of the group for making my visit such a wonderful experience. Dr. **Stefan Niebling** and Dr. **Ashley Hughes**: Many thanks for the MD calculations and the CD analysis on the ACS Omega paper. Docent **Jürgen Gräfenstein**: Thank you for your calculations regarding halogen bonding peptide and for providing the great image for my thesis. Dr. **Mariell Pettersson** and Prof. **Morten Grøtli**: Thank you so much for great teamwork on the MDM2/p53 project; I really enjoyed working on the project with you! Thank you also Prof. **Kiplin Guy** and co-workers at St Jude Children's Research Hospital in Memphis for the bioassays in this project. I would also like to thank the Swedish NMR Centre for their generous allotment of spectrometer time.

Máté Erdélyi, **Kristina Luthman**, **Morten Grötli**, **Itedale Namro Redwan**, **Patrik Jarvoll**, **Mariell Pettersson**, and **Stina Westerlund**, who proofread the thesis or manuscript: Many thanks – it has meant so much to me! **Mariell** and **Stina**: Thank you for also being such incredibly good friends, and for always being there to offer support with chemistry and everything else.

Thank you so much **Karin Axell** and **Proper English AB** for language editing. **Noel Danelius**, thank you for providing great pictures for the thesis and the papers.

Swedish Pharmaceutical Society, Olle Engkvist byggmästare foundation, the Royal Society of Arts and Sciences in Gothenburg, Helge Ax:son Johnson foundation, Swedish chemical society, Wilhelm and Martina Lundgrens foundation, Längmanska kulturfonden, Lindhés advokatbyrå – Sigrud and Elsa Goljes foundation, the Jörnvall foundation, the Adlerbert Scholarships, and Iris Jonzén-Sandbloms foundation, are all gratefully acknowledged for providing financial support for my research exchange and conferences. A special thanks to **Mariell**, **Ivana**, **Anna-Carin**, and **Alavi** for being great travel companions and creating wonderful memories. I would also like to thank the Nobel foundation for nominating me for the Lindau Nobel Laurate meeting in chemistry. This was truly a once in a lifetime experience!

The research leading to the results presented in this thesis has received funding from the European Research Council under the European Union's Seventh Framework Programme (FP7/2007-2013): ERC Grant Agreement n° 259638, and from the Swedish Research Council: Grant 2012-3819 and 2016-03602.

Food team members **Markus**, **Mariell**, **Jenny**, **David**, and **Tobbe**: We had some great years preparing food and eating lunch together. Thanks for great conversation, lots of laughs and delicious food.

To my **family** and **friends** who supported me along the way – I'm so lucky to have you in my life.

Noel, you are wonderful! Thank you for everything! Now we are ready for new adventures.

Siri and **Ivar**, you provide me with daily inspiration and you make me a better person. Love you!

12 REFERENCES

1. Boesch, C., Nobel prizes for nuclear magnetic resonance: 2003 and historical perspectives. *J. Magn. Reson. Imaging* **2004**, *20*, 177–179.
2. Galli, S., X-ray crystallography: one century of nobel prizes. *J. Chem. Educ.* **2014**, *91*, 2009–2012.
3. Lipinski, C. A.; Lombardo, F.; Dominy, B. W.; Feeney, P. J., Experimental and computational approaches to estimate solubility and permeability in drug discovery and development settings. *Adv. Drug Deliv. Rev.* **1997**, *23*, 3–25.
4. Palm, K.; Stenberg, P.; Luthman, K.; Artursson, P., Polar molecular surface properties predict the intestinal absorption of drugs in humans. *Pharm. Res.* **1997**, *14*, 568–571.
5. Veber, D. F.; Johnson, S. R.; Cheng, H. Y.; Smith, B. R.; Ward, K. W.; Kopple, K. D., Molecular properties that influence the oral bioavailability of drug candidates. *J. Med. Chem.* **2002**, *45*, 2615–2623.
6. Craik, D. J.; Fairlie, D. P.; Liras, S.; Price, D., The future of peptide-based drugs. *Chem. Biol. Drug Des.* **2013**, *81*, 136–147.
7. Nielsen, D. S.; Shepherd, N. E.; Xu, W.; Lucke, A. J.; Stoermer, M. J.; Fairlie, D. P., Orally absorbed cyclic peptides. *Chem. Rev.* **2017**, *117*, 8094–8128.
8. Hopkins, A. L.; Groom, C. R., The druggable genome. *Nat. Rev. Drug Discov.* **2002**, *1*, 727–730.
9. Waldmann, H.; Valeur, E.; Guéret, S. M.; Adihou, H.; Gopalakrishnan, R.; Lemurell, M.; Grossmann, T. N.; Plowright, A. T., New modalities for challenging targets in drug discovery. *Angew. Chem. Int. Ed.* **2017**, *56*, 10294–10323.
10. Doak, B. C.; Zheng, J.; Dobritzsch, D.; Kihlberg, J., How beyond rule of 5 drugs and clinical candidates bind to their targets. *J. Med. Chem.* **2016**, *59*, 2312–2327.
11. Doak, B. C.; Over, B.; Giordanetto, F.; Kihlberg, J., Oral druggable space beyond the rule of 5: insights from drugs and clinical candidates. *Chem. Biol.* **2014**, *21*, 1115–1142.
12. Yudin, A. K., Macrocycles: lessons from the distant past, recent developments, and future directions. *Chem. Sci.* **2015**, *6*, 30–49.
13. Giordanetto, F.; Kihlberg, J., Macrocyclic drugs and clinical candidates: what can medicinal chemists learn from their properties? *J. Med. Chem.* **2014**, *57*, 278–295.
14. Matsson, P.; Doak, B. C.; Over, B.; Kihlberg, J., Cell permeability beyond the rule of 5. *Adv. Drug Deliv. Rev.* **2016**, *101*, 42–61.
15. Mallinson, J.; Collins, I., Macrocycles in new drug discovery. *Future Med. Chem.* **2012**, *4*, 1409–1438.
16. Tsomaia, N., Peptide therapeutics: targeting the undruggable space. *Eur. J. Med. Chem.* **2015**, *94*, 459–470.
17. Bock, J. E.; Gavenonis, J.; Kritzer, J. A., Getting in shape: controlling peptide bioactivity and bioavailability using conformational constraints. *ACS Chem. Biol.* **2012**, *8*, 488–499.
18. Vlieghe, P.; Lisowski, V.; Martinez, J.; Khrestchatisky, M., Synthetic therapeutic peptides: science and market. *Drug Discov. Today* **2010**, *15*, 40–56.
19. Driggers, E. M.; Hale, S. P.; Lee, J.; Terrett, N. K., The exploration of macrocycles for drug discovery — an underexploited structural class. *Nat. Rev. Drug Discov.* **2008**, *7*, 608–624.
20. Fotouhi, N., Peptide therapeutics. *Peptide chemistry and drug design* **2015**, John Wiley & Sons, Inc, Hoboken, NJ, USA.
21. Thepchatri, P.; Eliseo, T.; Cicero, D. O.; Myles, D.; Snyder, J. P., Relationship among ligand conformations in solution, in the solid state, and at the Hsp90 binding site: geldanamycin and radicicol. *J. Am. Chem. Soc.* **2007**, *129*, 3127–3134.
22. Dharanipragada, R., New modalities in conformationally constrained peptides for potency, selectivity and cell permeation. *Future Med. Chem.* **2013**, *5*, 831–849.
23. Bernal, F.; Wade, M.; Godes, M.; Davis, T. N.; Whitehead, D. G.; Kung, A. L.; Wahl, G. M.; Walensky, L. D., A stapled p53 helix overcomes HDMX-mediated suppression of p53. *Cancer Cell* **2010**, *18*, 411–422.

24. Lau, Y. H.; de Andrade, P.; Wu, Y.; Spring, D. R., Peptide stapling techniques based on different macrocyclisation chemistries. *Chem. Soc. Rev.* **2015**, *44*, 91–102.
25. Cantel, S.; Le Chevalier Isaad, A.; Scrima, M.; Levy, J. J.; DiMarchi, R. D.; Rovero, P.; Halperin, J. A.; D'Ursi, A. M.; Papini, A. M.; Chorev, M., Synthesis and conformational analysis of a cyclic peptide obtained via *i* to *i*+4 intramolecular side-chain to side-chain azide−alkyne 1,3-dipolar cycloaddition. *J. Org. Chem.* **2008**, *73*, 5663–5674.
26. Holland-Nell, K.; Meldal, M., Maintaining biological activity by using triazoles as disufide bond mimetics. *Angew. Chem. Int. Ed.* **2011**, *50*, 5204–5206.
27. Stotz, C. E.; Topp, E. M., Applications of model β-hairpin peptides. *J. Pharm. Sci.* **2004**, *93*, 2881–2894.
28. Robinson, J. A., β-Hairpin peptidomimetics: design, structures and biological activities. *Acc. Chem. Res*. **2008**, *41*, 1278–1288.
29. Cooper, W. J.; Waters, M. L., Molecular recognition with designed peptides and proteins. *Curr. Opin. Chem. Biol*. **2005**, *9*, 627–631.
30. Fasan, R.; Dias, R. L. A.; Moehle, K.; Zerbe, O.; Obrecht, D.; Mittl, P. R. E.; Grütter, M. G.; Robinson, J. A., Structure–activity studies in a family of β-hairpin protein epitope mimetic inhibitors of the p53–HDM2 protein–protein interaction. *ChemBioChem* **2006**, *7*, 515–526.
31. Robinson, J. A.; Shankaramma, S. C.; Jetter, P.; Kienzl, U.; Schwendener, R. A.; Vrijbloed, J. W.; Obrecht, D., Properties and structure–activity studies of cyclic β-hairpin peptidomimetics based on the cationic antimicrobial peptide protegrin I. *Bioorg. Med. Chem.* **2005**, *13*, 2055–2064.
32. Luckett, S.; Garcia, R. S.; Barker, J. J.; Konarev, A. V.; Shewry, P. R.; Clarke, A. R.; Brady, R. L., High-resolution structure of a potent, cyclic proteinase inhibitor from sunflower seeds. *J. Mol. Biol.* **1999**, 290, 525–533.
33. Lewandowska, A.; Ołdziej, S.; Liwo, A.; Scheraga, H. A., β-hairpin-forming peptides; models of early stages of protein folding. *Biophys. Chem.* **2010**, *151*, 1–9.
34. Tatko, C. D.; Waters, M. L., Effect of halogenation on edge−face aromatic interactions in a β-hairpin peptide: enhanced affinity with iodo-substituents. *Org. Lett.* **2004**, *6*, 3969–3972.
35. Tatko, C. D.; Waters, M. L., The geometry and efficacy of cation–π interactions in a diagonal position of a designed β-hairpin. *Protein Science* **2003**, *12*, 2443–2452.
36. Blanco, F. J.; Jimenez, M. A.; Herranz, J.; Rico, M.; Santoro, J.; Nieto, J. L., NMR evidence of a short linear peptide that folds into a β-hairpin in aqueous solution. *J. Am. Chem. Soc.* **1993**, *115*, 5887–5888.
37. Marcelino, A. M. C.; Gierasch, L. M., Roles of β-turns in protein folding: from peptide models to protein engineering. *Biopolymers* **2008**, *89*, 380–391.
38. Haque, T. S.; Gellman, S. H., Insights on β-hairpin stability in aqueous solution from peptides with enforced type I' and type II' β-turns. *J. Am. Chem. Soc.* **1997**, *119*, 2303–2304.
39. Stanger, H. E.; Gellman, S. H., Rules for antiparallel β-sheet design: D-Pro-Gly is superior to L-Asn-Gly for β-hairpin nucleation. *J. Am. Chem. Soc.* **1998**, *120*, 4236–4237.
40. Fisher, M. J.; Gunn, B.; Harms, C. S.; Kline, A. D.; Mullaney, J. T.; Nunes, A.; Scarborough, R. M.; Arfsten, A. E.; Skelton, M. A.; Um, S. L.; Utterback, B. G.; Jakubowski, J. A., Non-peptide RGD surrogates which mimic a Gly-Asp β-turn: potent antagonists of platelet glycoprotein IIb−IIIa. *J. Med. Chem.* **1997**, *40*, 2085–2101.
41. Nair, C. M.; Vijayan, M.; Venkatachalapathi, Y. V.; Balaram, P., X-Ray crystal structure of pivaloyl-D-Pro-L-Pro-L-Ala-*N*-methylamide; observation of a consecutive β-turn conformation. *J. Chem. Soc. Chem. Commun.* **1979**, 1183–1184.
42. Gibbs, A. C.; Bjorndahl, T. C.; Hodges, R. S.; Wishart, D. S., Probing the structural determinants of type II' β-turn formation in peptides and proteins. *J. Am. Chem. Soc.* **2002**, *124*, 1203–1213.
43. Smith, C. K.; Withka, J. M.; Regan, L., A thermodynamic scale for the β-sheet forming tendencies of the amino acids. *Biochemistry* **1994**, *33*, 5510–5517.
44. Minor, D. L.; Kim, P. S., Measurement of the β-sheet-forming propensities of amino acids. *Nature* **1994**, *367*, 660–663.

45. Phillips, S. T.; Piersanti, G.; Bartlett, P. A., Quantifying amino acid conformational preferences and side-chain–side-chain interactions in β-hairpins. *Proc. Natl. Acad. Sci.* **2005**, *102*, 13737–13742.
46. Cochran, A. G.; Skelton, N. J.; Starovasnik, M. A., Tryptophan zippers: stable, monomeric β-hairpins. *Proc. Natl. Acad. Sci.* **2001**, *98*, 5578–5583.
47. Kiehna, S. E.; Waters, M. L., Sequence dependence of β-hairpin structure: comparison of a salt bridge and an aromatic interaction. *Protein Science* **2003**, *12*, 2657–2667.
48. Ciani, B.; Jourdan, M.; Searle, M. S., Stabilization of β-hairpin peptides by salt bridges: role of preorganization in the energetic contribution of weak interactions. *J. Am. Chem. Soc.* **2003**, *125*, 9038–9047.
49. Bunaciu, A. A.; Udriştioiu, E. G.; Aboul-Enein, H. Y., X-ray diffraction: instrumentation and applications. *Crit. Rev. Anal. Chem.* **2015**, *45*, 289–299.
50. Pelton, J. T.; McLean, L. R., Spectroscopic methods for analysis of protein secondary structure. *Anal. Biochem.* **2000**, *277*, 167–176.
51. Vass, E.; Hollósi, M.; Besson, F.; Buchet, R., Vibrational spectroscopic detection of β- and γ-turns in synthetic and natural peptides and proteins. *Chem. Rev.* **2003**, *103*, 1917–1954.
52. Kuczera, K. Molecular modeling in peptide and protein analysis. *Encyclopedia of Analytical Chemistry*, **2006**, John Wiley & Sons, Ltd.
53. Adcock, S. A.; McCammon, J. A., Molecular dynamics: survey of methods for simulating the activity of proteins. *Chem. Rev.* **2006**, *106*, 1589–1615.
54. Mazzanti, A.; Casarini, D., Recent trends in conformational analysis. *Wiley Interdiscip. Rev. Comput. Mol. Sci.* **2012**, *2*, 613–641.
55. Greenfield, N. J., Using circular dichroism spectra to estimate protein secondary structure. *Nat. Protocols* **2007**, *1*, 2876–2890.
56. Nogales, E., The development of cryo-EM into a mainstream structural biology technique. *Nat. Meth.* **2016**, *13*, 24–27.
57. Tormena, C. F., Conformational analysis of small molecules: NMR and quantum mechanics calculations. *Prog. Nucl. Mag. Res. Sp.* **2016**, *96*, 73–88.
58. Frank, J., Advances in the field of single-particle cryo-electron microscopy over the last decade. *Nat. Protocols* **2017**, *12*, 209–212.
59. Williamson, M. P. Peptide structure determination by NMR. *Spectroscopic Methods and Analyses: NMR, Mass Spectrometry, and Metalloprotein Techniques*. **1993**, Humana Press, Totowa, NJ, USA.
60. Jardetzky, O., On the nature of molecular conformations inferred from high-resolution NMR. *Biochim. Biophys. Acta* **1980**, *621*, 227–232.
61. Cicero, D. O.; Barbato, G.; Bazzo, R., NMR analysis of molecular flexibility in solution: a new method for the study of complex distributions of rapidly exchanging conformations. application to a 13-residue peptide with an 8-residue loop. *J. Am. Chem. Soc.* **1995**, *117*, 1027–1033.
62. Claridge, T. D. W., *High-Resolution NMR Techniques in Organic Chemistry*. **2009**, Elsevier Ltd.
63. Jacobsen, N. E., *NMR Spectroscopy Explained: Simplified Theory, Applications and Examples for Organic Chemistry and Structural Biology*. **2007**, John Wiley & Sons, Inc. NJ, USA.
64. Wishart, D. S.; Sykes, B. D.; Richards, F. M., Relationship between nuclear magnetic resonance chemical shift and protein secondary structure. *J. Mol. Biol.* **1991**, *222*, 311–333.
65. Baxter, N. J.; Williamson, M. P., Temperature dependence of ^{1}H chemical shifts in proteins. *J. Biomol. NMR* **1997**, *9*, 359–369.
66. Smith, L. J.; Bolin, K. A.; Schwalbe, H.; MacArthur, M. W.; Thornton, J. M.; Dobson, C. M., Analysis of main chain torsion angles in proteins: prediction of NMR coupling constants for native and random coil conformations. *J. Mol. Biol.* **1996**, *255*, 494–506.
67. Karplus, M., Contact electron-spin coupling of nuclear magnetic moments. *J. Chem. Phys.* **1959**, *30*, 11–15.
68. Karplus, M., Vicinal proton coupling in nuclear magnetic resonance. *J. Am. Chem. Soc.* **1963**, *85*, 2870–2871.
69. Schmidt, J. M., A versatile component-coupling model to account for substituent effects: application to polypeptide ϕ and χ1 torsion related ^{3}J data. *J. Magn. Reson.* **2007**, *186*, 34–50.

70. Macur, S.; Farmer, B. T.; Brown, L. R., An improved method for the determination of cross-relaxation rates from NOE data. *J. Magn. Reson. Imaging* **1986**, *70*, 493–499.
71. Hill, D. J.; Mio, M. J.; Prince, R. B.; Hughes, T. S.; Moore, J. S., A field guide to foldamers. *Chem. Rev.* **2001**, *101*, 3893–4012.
72. Kobayashi, N.; Honda, S.; Yoshii, H.; Munekata, E., Role of side-chains in the cooperative β-hairpin folding of the short *C*−terminal fragment derived from streptococcal protein G. *Biochemistry* **2000**, *39*, 6564–6571.
73. Erdélyi, M.; Langer, V.; Karlen, A.; Gogoll, A., Insight into β-hairpin stability: a structural and thermodynamic study of diastereomeric β-hairpin mimetics. *New J. Chem.* **2002**, *26*, 834–843.
74. Lee, H. J.; Choi, K. H.; Ahn, I. A.; Ro, S.; Jang, H. G.; Choi, Y. S.; Lee, K. B., The β-turn preferential solution conformation of a tetrapeptide containing an azaamino acid residue. *J. Mol. Struct.* **2001**, *569*, 43–54.
75. Nevins, N.; Cicero, D.; Snyder, J. P., A test of the single-conformation hypothesis in the analysis of NMR data for small polar molecules: a force field comparison. *J. Org. Chem.* **1999**, *64*, 3979–3986.
76. Koivisto, J. J.; Kumpulainen, E. T. T.; Koskinen, A. M. P., Conformational ensembles of flexible β-turn mimetics in DMSO-d_6. *Org. Biomol. Chem.* **2010**, *8*, 2103–2116.
77. Andersson, H.; Demaegdt, H.; Vauquelin, G.; Lindeberg, G.; Karlén, A.; Hallberg, M.; Erdélyi, M.; Hallberg, A., Disulfide cyclized tripeptide analogues of angiotensin IV as potent and selective inhibitors of insulin-regulated aminopeptidase (IRAP). *J. Med. Chem.* **2010**, *53*, 8059–8071.
78. Thepchatri, P.; Cicero, D. O.; Monteagudo, E.; Ghosh, A. K.; Cornett, B.; Weeks, E. R.; Snyder, J. P., Conformations of laulimalide in DMSO-d_6. *J. Am. Chem. Soc.* **2005**, *127*, 12838–12846.
79. Erdélyi, M.; Pfeiffer, B.; Hauenstein, K.; Fohrer, J.; Gertsch, J.; Altmann, K.-H.; Carlomagno, T., Conformational preferences of natural and C3-modified epothilones in aqueous solution. *J. Med. Chem.* **2008**, *51*, 1469–1473.
80. Fridén-Saxin, M.; Seifert, T.; Hansen, L. K.; Grøtli, M.; Erdélyi, M.; Luthman, K., Proline-mediated formation of novel chroman-4-one tetrahydropyrimidines. *Tetrahedron* **2012**, *68*, 7035–7040.
81. Grimmer, C.; Moore, T. W.; Padwa, A.; Prussia, A.; Wells, G.; Wu, S.; Sun, A.; Snyder, J. P., Antiviral atropisomers: conformational energy surfaces by NMR for host-directed myxovirus blockers. *J. Chem. Inf. Model.* **2014**, *54*, 2214–2223.
82. Valeur, E.; Bradley, M., Amide bond formation: beyond the myth of coupling reagents. *Chem. Soc. Rev.* **2009**, *38*, 606–631.
83. Isidro-Llobet, A.; Álvarez, M.; Albericio, F., Amino acid-protecting groups. *Chem. Rev.* **2009**, *109*, 2455–2504.
84. Merrifield, R. B., Solid phase peptide synthesis. I. The synthesis of a tetrapeptide. *J. Am. Chem. Soc.* **1963**, *85*, 2149–2154.
85. Palomo, J. M., Solid-phase peptide synthesis: an overview focused on the preparation of biologically relevant peptides. *RSC Adv.* **2014**, *4*, 32658–32672.
86. Mäde, V.; Els-Heindl, S.; Beck-Sickinger, A. G., Automated solid-phase peptide synthesis to obtain therapeutic peptides. *Beilstein J. Org. Chem.* **2014**, *10*, 1197–1212.
87. Fields, G. B. Methods for removing the Fmoc group. *Peptide Synthesis Protocols* **1995**, Humana Press, Totowa, NJ, USA.
88. Guillier, F.; Orain, D.; Bradley, M., Linkers and cleavage strategies in solid-phase organic synthesis and combinatorial chemistry. *Chem. Rev.* **2000**, *100*, 2091–2158.
89. El-Faham, A.; Albericio, F., Peptide coupling reagents, more than a letter soup. *Chem. Rev.* **2011**, *111*, 6557–6602.
90. Carpino, L. A.; Imazumi, H.; El-Faham, A.; Ferrer, F. J.; Zhang, C.; Lee, Y.; Foxman, B. M.; Henklein, P.; Hanay, C.; Mügge, C.; Wenschuh, H.; Klose, J.; Beyermann, M.; Bienert, M., The uronium/guanidinium peptide coupling reagents: finally the true uronium salts. *Angew. Chem. Int. Ed.* **2002**, *41*, 441–445.
91. White, C. J.; Yudin, A. K., Contemporary strategies for peptide macrocyclization. *Nat. Chem.* **2011**, *3*, 509–524.

92. Kates, S. A.; Solé, N. A.; Johnson, C. R.; Hudson, D.; Barany, G.; Albericio, F., A novel, convenient, three-dimensional orthogonal strategy for solid-phase synthesis of cyclic peptides. *Tetrahedron Lett.* **1993**, *34*, 1549–1552.
93. Alcaro, M. C.; Sabatino, G.; Uziel, J.; Chelli, M.; Ginanneschi, M.; Rovero, P.; Papini, A. M., On-resin head-to-tail cyclization of cyclotetrapeptides: optimization of crucial parameters. *J. Pep. Sci.* **2004**, *10*, 218–228.
94. Tapeinou, A.; Matsoukas, M.-T.; Simal, C.; Tselios, T., Review cyclic peptides on a merry-go-round; towards drug design. *Peptide Science* **2015**, *104*, 453–461.
95. Bissantz, C.; Kuhn, B.; Stahl, M., A Medicinal chemist's guide to molecular interactions. *J. Med. Chem.* **2010**, *53*, 5061–5084.
96. Persch, E.; Dumele, O.; Diederich, F., Molecular recognition in chemical and biological systems. *Angew. Chem. Int. Ed.* **2015**, *54*, 3290–3327.
97. Mayo, K. H.; Fields, G. B., Peptides as models for understanding protein folding. *Adv. Mol. Cell. Biol.* **1997**, *22*, 567–612.
98. Searle, M. S., Insights into stabilizing weak interactions in designed peptide β-hairpins. *Peptide Science* **2004**, *76*, 185–195.
99. Du, X.; Li, Y.; Xia, Y.-L.; Ai, S.-M.; Liang, J.; Sang, P.; Ji, X.-L.; Liu, S.-Q., Insights into protein–ligand interactions: mechanisms, models, and methods. *Int. J. Mol. Sci.* **2016**, *17*, e144.
100. Arunan, E.; Desiraju, G. R.; Klein, R. A.; Sadlej, J.; Scheiner, S.; Alkorta, I.; Clary, D. C.; Crabtree, R. H.; Dannenberg, J. J.; Hobza, P.; Kjaergaard, H. G.; Legon, A. C.; Mennucci, B.; Nesbitt, D. J., Defining the hydrogen bond: an account (IUPAC technical report). *Pure Appl. Chem.* **2011**, *83*, 1619–1636.
101. Kuhn, B.; Mohr, P.; Stahl, M., Intramolecular hydrogen bonding in medicinal chemistry. *J. Med. Chem.* **2010**, *53*, 2601–2611.
102. Desiraju, G. R.; Ho, P. S.; Kloo, L.; Legon, A. C.; Marquardt, R.; Metrangolo, P.; Politzer, P.; Resnati, G.; Rissanen, K., Definition of the halogen bond. *Pure Appl. Chem.* **2013**, *85*, 1711–1713.
103. Clark, T.; Hennemann, M.; Murray, J. S.; Politzer, P., Halogen bonding: the σ-hole. *J. Mol. Model.* **2007**, *13*, 291–296.
104. Clark, T., Halogen bonds and σ -holes. *Faraday Discuss.* **2017**, DOI: 10.1039/c7fd00058h .
105. Cavallo, G.; Metrangolo, P.; Milani, R.; Pilati, T.; Priimagi, A.; Resnati, G.; Terraneo, G., The halogen bond. *Chem. Rev.* **2016**, *116*, 2478–2601.
106. Wilcken, R.; Zimmermann, M. O.; Lange, A.; Joerger, A. C.; Boeckler, F. M., Principles and applications of halogen bonding in medicinal chemistry and chemical biology. *J. Med. Chem.* **2013**, *56*, 1363–1388.
107. Scholfield, M. R.; Vander Zanden, C. M.; Carter, M.; Ho, P. S., Halogen bonding (X-bonding): a biological perspective. *Protein Science* **2013**, *22*, 139–152.
108. Ho, P. S., Biomolecular halogen bonds. *Top. Curr. Chem.* **2014**, *358*, 241–276.
109. Erdélyi, M., Halogen bonding in solution *Chem. Soc. Rev.* **2012**, *41*, 3547–3557.
110. Xu, Z.; Yang, Z.; Liu, Y.; Lu, Y.; Chen, K.; Zhu, W., Halogen bond: its role beyond drug–target binding affinity for drug discovery and development. *J. Chem. Inf. Model.* **2014**, *54*, 69–78.
111. Góngora-Benítez, M.; Tulla-Puche, J.; Albericio, F., Handles for Fmoc solid-phase synthesis of protected peptides. *ACS Comb. Sci.* **2013**, *15*, 217–228.
112. Malesevic, M.; Strijowski, U.; Bächle, D.; Sewald, N., An improved method for the solution cyclization of peptides under pseudo-high dilution conditions. *J. Biotechnol.* **2004**, *112*, 73–77.
113. Cierpicki, T.; Otlewski, J., Amide proton temperature coefficients as hydrogen bond indicators in proteins. *J. Biomol. NMR* **2001**, *21*, 249–261.
114. Kaminski, G. A.; Friesner, R. A.; Tirado-Rives, J.; Jorgensen, W. L., Evaluation and reparametrization of the OPLS-AA force field for proteins via comparison with accurate quantum chemical calculations on peptides. *J. Phys. Chem. B.* **2001**, *105*, 6474–6487.
115. Niebling, S.; Danelius, E.; Brath, U.; Westenhoff, S.; Erdélyi, M., The impact of interchain hydrogen bonding on β-hairpin stability is readily predicted by molecular dynamics simulation. *Biopolymers* **2015**, *104*, 703–706.

116. Honda, S.; Kobayashi, N.; Munekata, E., Thermodynamics of a β-hairpin structure: evidence for cooperative formation of folding nucleus. *J. Mol. Biol.* **2000**, *295*, 269–278.
117. Thorson, R. A.; Woller, G. R.; Driscoll, Z. L.; Geiger, B. E.; Moss, C. A.; Schlapper, A. L.; Speetzen, E. D.; Bosch, E.; Erdélyi, M.; Bowling, N. P., Intramolecular halogen bonding in solution: ^{15}N, ^{13}C, and ^{19}F NMR studies of temperature and solvent effects. *Eur. J. Org. Chem.* **2015**, 1685–1695.
118. Chudzinski, M. G.; McClary, C. A.; Taylor, M. S., anion receptors composed of hydrogen- and halogen-bond donor groups: modulating selectivity with combinations of distinct noncovalent interactions. *J. Am. Chem. Soc.* **2011**, *133*, 10559–10567.
119. Sarwar, M. G.; Dragisic, B.; Salsberg, L. J.; Gouliaras, C.; Taylor, M. S., Thermodynamics of halogen bonding in solution: substituent, structural, and solvent effects. *J. Am. Chem. Soc.* **2010**, *132*, 1646–1653.
120. Regier Voth, A.; Hays, F. A.; Ho, P. S., Directing macromolecular conformation through halogen bonds. *Proc. Natl. Acad. Sci.* **2007**, *104*, 6188–6193.
121. Harder, E.; Damm, W.; Maple, J.; Wu, C.; Reboul, M.; Xiang, J. Y.; Wang, L.; Lupyan, D.; Dahlgren, M. K.; Knight, J. L.; Kaus, J. W.; Cerutti, D. S.; Krilov, G.; Jorgensen, W. L.; Abel, R.; Friesner, R. A., OPLS3: A force field providing broad coverage of drug-like small molecules and proteins. *J. Chem. Theory Comput.* **2016**, *12*, 281–296.
122. Riley, K.; Hobza, P., Investigations into the nature of halogen bonding including symmetry adapted preturbation theory analyses. *J. Theory Comput.* **2008**, *4*, 232–242.
123. Stites, W. E., Protein−protein interactions: interface structure, binding thermodynamics, and mutational analysis. *Chem. Rev.* **1997**, *97*, 1233–1250.
124. Scott, D. E.; Bayly, A. R.; Abell, C.; Skidmore, J., Small molecules, big targets: drug discovery faces the protein-protein interaction challenge. *Nat. Rev. Drug Discov.* **2016**, *15*, 533–550.
125. Pelay-Gimeno, M.; Glas, A.; Koch, O.; Grossmann, T. N., Structure-based design of inhibitors of protein–protein interactions: mimicking peptide binding epitopes. *Angew. Chem. Int. Ed.* **2015**, *54*, 8896–8927.
126. Kozakov, D.; Hall, D. R.; Napoleon, R. L.; Yueh, C.; Whitty, A.; Vajda, S., New frontiers in druggability. *J. Med. Chem.* **2015**, *58*, 9063–9088.
127. Kussie, P. H.; Gorina, S.; Marechal, V.; Elenbaas, B.; Moreau, J.; Levine, A. J.; Pavletich, N. P., Structure of the MDM2 oncoprotein bound to the p53 tumor suppressor transactivation domain. *Science* **1996**, *274*, 948–953.
128. Vousden, K. H.; Lu, X., Live or let die: the cell's response to p53. *Nat. Rev. Cancer* **2002**, *2*, 594–604.
129. Harris, S. L.; Levine, A. J., The p53 pathway: positive and negative feedback loops. *Oncogene* **2005**, *24*, 2899–2908.
130. Hoe, K. K.; Verma, C. S.; Lane, D. P., Drugging the p53 pathway: understanding the route to clinical efficacy. *Nat. Rev. Drug Discov.* **2014**, *13*, 217–236.
131. Aeluri, M.; Chamakuri, S.; Dasari, B.; Guduru, S. K. R.; Jimmidi, R.; Jogula, S.; Arya, P., Small molecule modulators of protein–protein interactions: selected case studies. *Chem. Rev.* **2014**, *114*, 4640–4694.
132. Sheng, C.; Dong, G.; Miao, Z.; Zhang, W.; Wang, W., State-of-the-art strategies for targeting protein-protein interactions by small-molecule inhibitors. *Chem. Soc. Rev.* **2015**, *44*, 8238–8259.
133. Milroy, L.-G.; Grossmann, T. N.; Hennig, S.; Brunsveld, L.; Ottmann, C., Modulators of protein–protein interactions. *Chem. Rev.* **2014**, *114*, 4695–4748.
134. Walensky, L. D.; Bird, G. H., Hydrocarbon-stapled peptides: principles, practice, and progress. *J. Med. Chem.* **2014**, 57, 6275-6288.
135. Kumar, E. A.; Chen, Q.; Kizhake, S.; Kolar, C.; Kang, M.; Chang, C. A.; Borgstahl, G. E. O.; Natarajan, A., The paradox of conformational constraint in the design of Cbl(TKB)-binding peptides. *Sci. Rep.* **2013**, *3*, 1639.
136. DeLorbe, J. E.; Clements, J. H.; Whiddon, B. B.; Martin, S. F., Thermodynamic and structural effects of macrocyclic constraints in protein−ligand interactions. *ACS Med. Chem. Lett.* **2010**, *1*, 448–452.

137. Weber, F.; Brune, S.; Börgel, F.; Lange, C.; Korpis, K.; Bednarski, P. J.; Laurini, E.; Fermeglia, M.; Pricl, S.; Schepmann, D.; Wünsch, B., Rigidity versus flexibility: is this an issue in σ1 receptor ligand affinity and activity? *J. Med. Chem.* **2016**, *59*, 5505–5519.
138. Fasan, R.; Dias, R. L. A.; Moehle, K.; Zerbe, O.; Vrijbloed, J. W.; Obrecht, D.; Robinson, J. A., Using a β-hairpin to mimic an α-helix: cyclic peptidomimetic inhibitors of the p53–HDM2 protein–protein interaction. *Angew. Chem. Int. Ed.* **2004**, *43*, 2109–2112.
139. Udugamasooriya, D. G.; Spaller, M. R., Conformational constraint in protein ligand design and the inconsistency of binding entropy. *Biopolymers* **2008**, *89*, 653–667.
140. Park, Y. M., CD36, a scavenger receptor implicated in atherosclerosis. *Exp. Mol. Med.* **2014**, *46*, e99.
141. Pepino, M. Y.; Kuda, O.; Samovski, D.; Abumrad, N. A., Structure-function of CD36 and importance of fatty acid signal transduction in fat metabolism. *Annu. Rev. Nutr.* **2014**, *34*, 281–303.
142. Jimenez, B.; Volpert, O. V.; Crawford, S. E.; Febbraio, M.; Silverstein, R. L.; Bouck, N., Signals leading to apoptosis-dependent inhibition of neovascularization by thrombospondin-1. *Nat. Med.* **2000**, *6*, 41–48.
143. Febbraio, M.; Silverstein, R. L., CD36: Implications in cardiovascular disease. *Int. J. Biochem. Cell Biol.* **2007**, *39*, 2012–2030.
144. Hsieh, F.-L.; Turner, L.; Bolla, J. R.; Robinson, C. V.; Lavstsen, T.; Higgins, M. K., The structural basis for CD36 binding by the malaria parasite. *Nat. Commun.* **2016**, *7*, 12837.
145. Demers, A.; McNicoll, N.; Febbraio, M.; Servant, M.; Marleau, S.; Silverstein, R.; Ong, H., Identification of the growth hormone-releasing peptide binding site in CD36: a photoaffinity cross-linking study. *Biochem. J.* **2004**, *382*, 417–424.
146. Kar, N. S.; Ashraf, M. Z.; Valiyaveettil, M.; Podrez, E. A., Mapping and characterization of the binding site for specific oxidized phospholipids and oxidized low density lipoprotein of scavenger receptor CD36. *J. Biol. Chem.* **2008**, *283*, 8765–8771.
147. Camanni, F.; Ghigo, E.; Arvat, E., Growth hormone-releasing peptides and their analogs. *Front. Neuroendocrinol.* **1998**, *19*, 47–72.
148. Momany, F. A.; Bowers, C. Y. Computer-assisted modeling of xenobiotic growth hormone secretagogues. *Growth Hormone Secretagogues* **1996**, Springer New York, NY, USA.
149. McDowell, R. S.; Elias, K. A.; Stanley, M. S.; Burdick, D. J.; Burnier, J. P.; Chan, K. S.; Fairbrother, W. J.; Hammonds, R. G.; Ingle, G. S.; Jacobsen, N. E.; Mortensen, D. L.; Rawson, T. E.; Won, W. B.; Clark, R. G.; Somers, T. C., Growth hormone secretagogues: characterization, efficacy, and minimal bioactive conformation. *Proc. Natl. Acad. Sci.* **1995**, *92*, 11165–11169.
150. Zega, A., Azapeptides as pharmacological agents. *Curr. Med. Chem.* **2005**, *12*, 589–597.
151. Proulx, C.; Sabatino, D.; Hopewell, R.; Spiegel, J.; Ramos, Y. G.; Lubell, W. D., Azapeptides and their therapeutic potential. *Future Med. Chem.* **2011**, *3*, 1139–1164.
152. Havlir, D. V.; O'Marro, S. D., Atazanavir: New option for treatment of HIV infection. *Clin. Infect. Dis.* **2004**, *38*, 1599–1604.
153. Tal-Gan, Y.; Freeman, N. S.; Klein, S.; Levitzki, A.; Gilon, C., Metabolic stability of peptidomimetics: *N*-methyl and aza heptapeptide analogs of a PKB/Akt inhibitor. *Chem. Biol. Drug Des.* **2011**, *78*, 887–892.
154. Lee, H.-J.; Park, H.-M.; Lee, K.-B., The β-turn scaffold of tripeptide containing an azaphenylalanine residue. *Biophys. Chem.* **2007**, *125*, 117–126.
155. Ottersbach, P. A.; Schnakenburg, G.; Gutschow, M., Induction of chirality: experimental evidence of atropisomerism in azapeptides. *Chem. Commun.* **2012**, *48*, 5772–5774.
156. Sabatino, D.; Proulx, C.; Klocek, S.; Bourguet, C. B.; Boeglin, D.; Ong, H.; Lubell, W. D., Exploring side-chain diversity by submonomer solid-phase aza-peptide synthesis. *Org. Lett.* **2009**, *11*, 3650–3653.
157. Sabatino, D.; Proulx, C.; Pohankova, P.; Ong, H.; Lubell, W. D., Structure–activity relationships of GHRP-6 azapeptide ligands of the CD36 scavenger receptor by solid-phase submonomer azapeptide synthesis. *J. Am. Chem. Soc.* **2011**, *133*, 12493–12506.
158. Proulx, C.; Picard, É.; Boeglin, D.; Pohankova, P.; Chemtob, S.; Ong, H.; Lubell, W. D., Azapeptide analogues of the growth hormone releasing peptide 6 as cluster of differentiation 36

receptor ligands with reduced affinity for the growth hormone secretagogue receptor 1a. *J. Med. Chem.* **2012**, *55*, 6502–6511.
159. Zhang, J.; Mulumba, M.; Ong, H.; Lubell, W. D., Diversity-oriented synthesis of cyclic azapeptides by A3-macrocyclization provides high-affinity CD36-modulating peptidomimetics. *Angew. Chem. Int. Ed.* **2017**, *56*, 6284–6288.
160. Altschuh, D.; Vix, O.; Rees, B.; Thierry, J., A conformation of cyclosporin A in aqueous environment revealed by the X-ray structure of a cyclosporin-Fab complex. *Science* **1992**, *256*, 92–94.
161. Jiménez-Barbero, J.; Canales, A.; Northcote, P. T.; Buey, R. M.; Andreu, J. M.; Díaz, J. F., NMR determination of the bioactive conformation of peloruside a bound to microtubules. *J. Am. Chem. Soc.* **2006**, *128*, 8757–8765.
162. Bockus, A. T.; Lexa, K. W.; Pye, C. R.; Kalgutkar, A. S.; Gardner, J. W.; Hund, K. C. R.; Hewitt, W. M.; Schwochert, J. A.; Glassey, E.; Price, D. A.; Mathiowetz, A. M.; Liras, S.; Jacobson, M. P.; Lokey, R. S., Probing the physicochemical boundaries of cell permeability and oral bioavailability in lipophilic macrocycles inspired by natural products. *J. Med. Chem.* **2015**, *58*, 4581–4589.
163. Gharbi-Benarous, J.; Ladam, P.; Delaforge, M.; Girault, J.-P., Conformational analysis of major metabolites of macrolide antibiotics roxithromycin and erythromycin A with different biological properties by NMR spectroscopy and molecular dynamics. *J. Chem. Soc. Perkin Trans. 2* **1993**, 2303–2321.
164. Volpe, D., Drug-permeability and transporter assays in Caco-2 and MDCK cell lines. *Future Med. Chem.* **2011**, *3*, 2063–2077.
165. Bertho, G.; Gharbi-Benarous, J.; Delaforge, M.; Girault, J.-P., Transferred nuclear Overhauser effect study of macrolide–ribosome interactions: correlation between antibiotic activities and bound conformations. *Bioorg. Med. Chem.* **1998**, *6*, 209–221.
166. Bachet, B.; Brassy, C.; Mornon, J.-P., [O-(Dioxa-2,5 hexyl) oxime]-9 de l'erythromycine A hydratee. *Acta Crystallogr., Sect. C* **1988**, *44*, 112–116.
167. Gharbi-Benarous, J.; Delaforge, M.; Artaud, I.; Girault, J.-P., Analysis of the ^{1}H and ^{13}C NMR spectra of the novel macrolide antibiotic roxithromycin. Structure and conformation in solution. *Magn. Res. Chem.* **1990**, *28*, 846–855.
168. Gharbi-Benarous, J.; Delaforge, M.; Jankowski, C. K.; Girault, J. P., A comparative NMR study between the macrolide antibiotic roxithromycin and erythromycin A with different biological properties. *J. Med. Chem.* **1991**, *34*, 1117–1125.
169. Gharbi-Benarous, J.; Ladam, P.; Delaforge, M.; Girault, J.-P., A conformational exploration of the protonated and unprotonated macrolide antibiotic roxithromycin: comparative study by molecular dynamics and NMR spectroscopy in solution. *J. Chem. Soc. Perkin Trans. 2* **1992**, 1989–2006.
170. Holstein, J. J.; Luger, P.; Kalinowski, R.; Mebs, S.; Paulman, C.; Dittrich, B., Validation of experimental charge densities: refinement of the macrolide antibiotic roxithromycin. *Acta Crystallogr., Sect. B* **2010**, *66*, 568–577.
171. Mallet, F.; Petit, S.; Lafont, S.; Billot, P.; Lemarchand, D.; Coquerel, G., Solvent exchanges among molecular compounds. *J. Therm. Anal. Calorim.* **2003**, *73*, 459–471.
172. Schlunzen, F.; Zarivach, R.; Harms, J.; Bashan, A.; Tocilj, A.; Albrecht, R.; Yonath, A.; Franceschi, F., Structural basis for the interaction of antibiotics with the peptidyl transferase centre in eubacteria. *Nature* **2001**, *413*, 814–821.

13 APPENDICES

Appendix I. The 20 naturally occurring amino acids and their one- and three-letter acronyms.

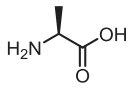

Alanine
Ala
A

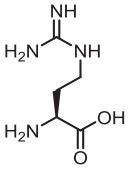

Arginine
Arg
R

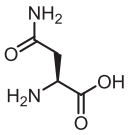

Asparagine
Asn
N

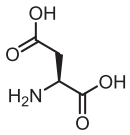

Aspartic acid
Asp
D

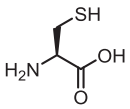

Cysteine
Cys
C

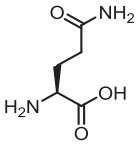

Glutamine
Gln
G

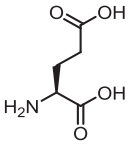

Glutamic acid
Glu
E

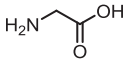

Glycine
Gly
G

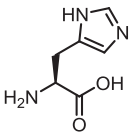

Histidine
His
H

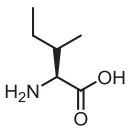

Isoleucine
Ile
I

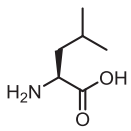

Leucine
Leu
L

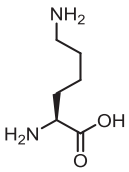

Lysine
Lys
K

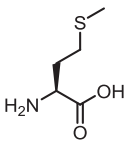

Methionine
Met
M

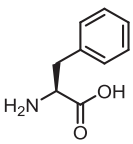

Phenylalanine
Phe
F

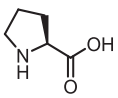

Proline
Pro
P

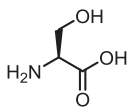

Serine
Ser
S

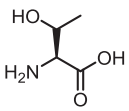

Threonine
Thr
T

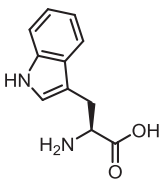

Tryptophan
Trp
W

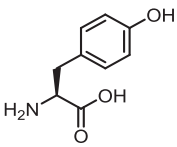

Tyrosine
Tyr
Y

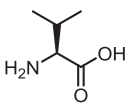

Valine
Val
V

Appendix II. Synthesis of **3** and **4**.

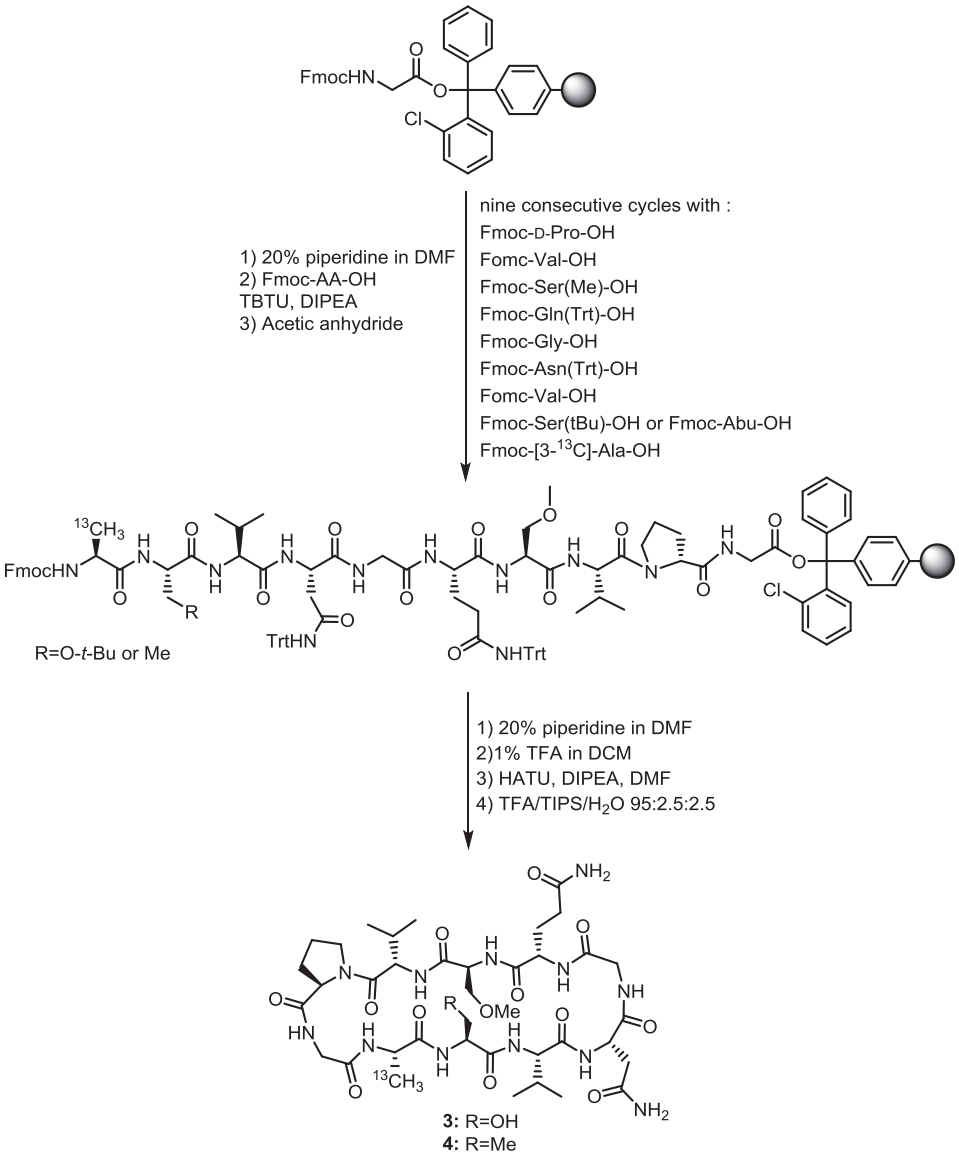

Appendix III. Synthesis of **5** and **6**.

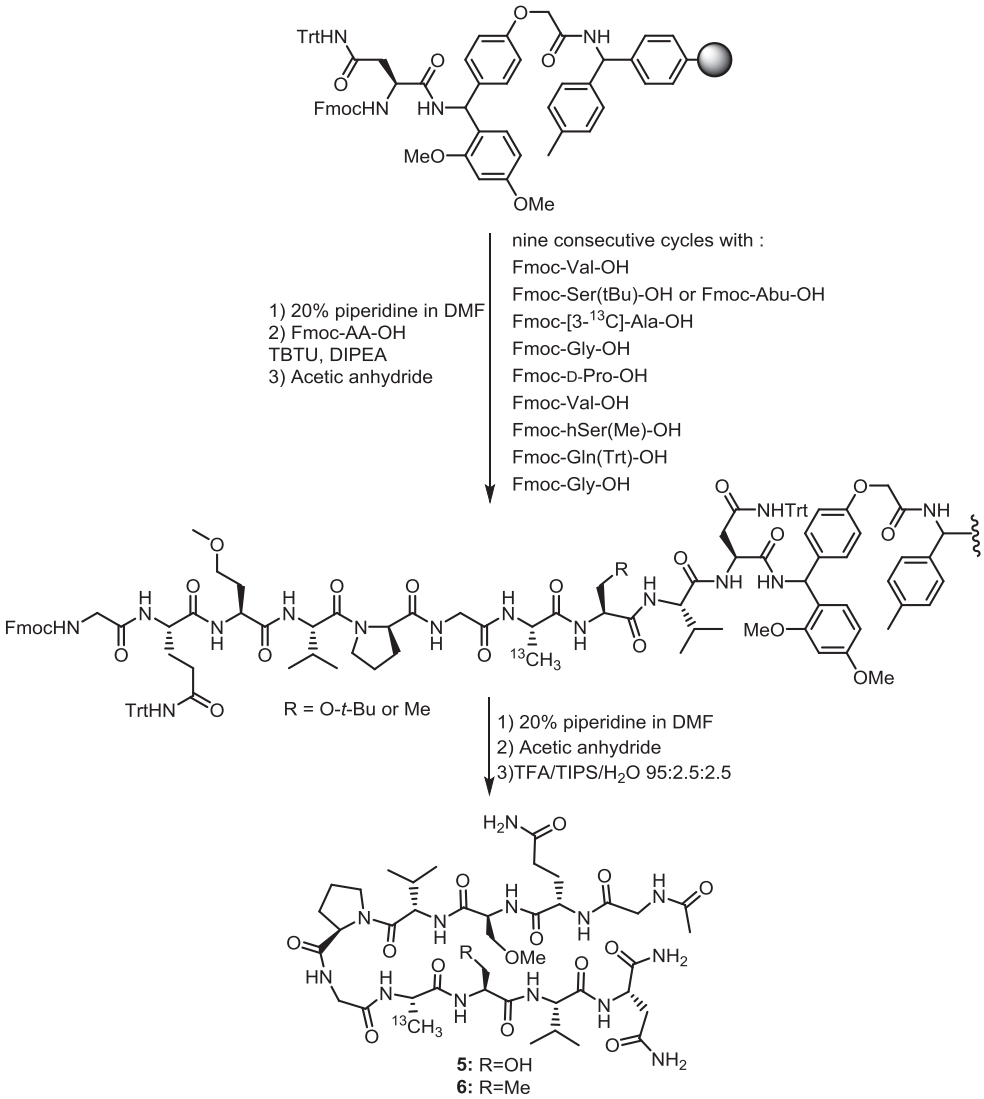

Appendix IV. Synthesis of **7** and **8**.

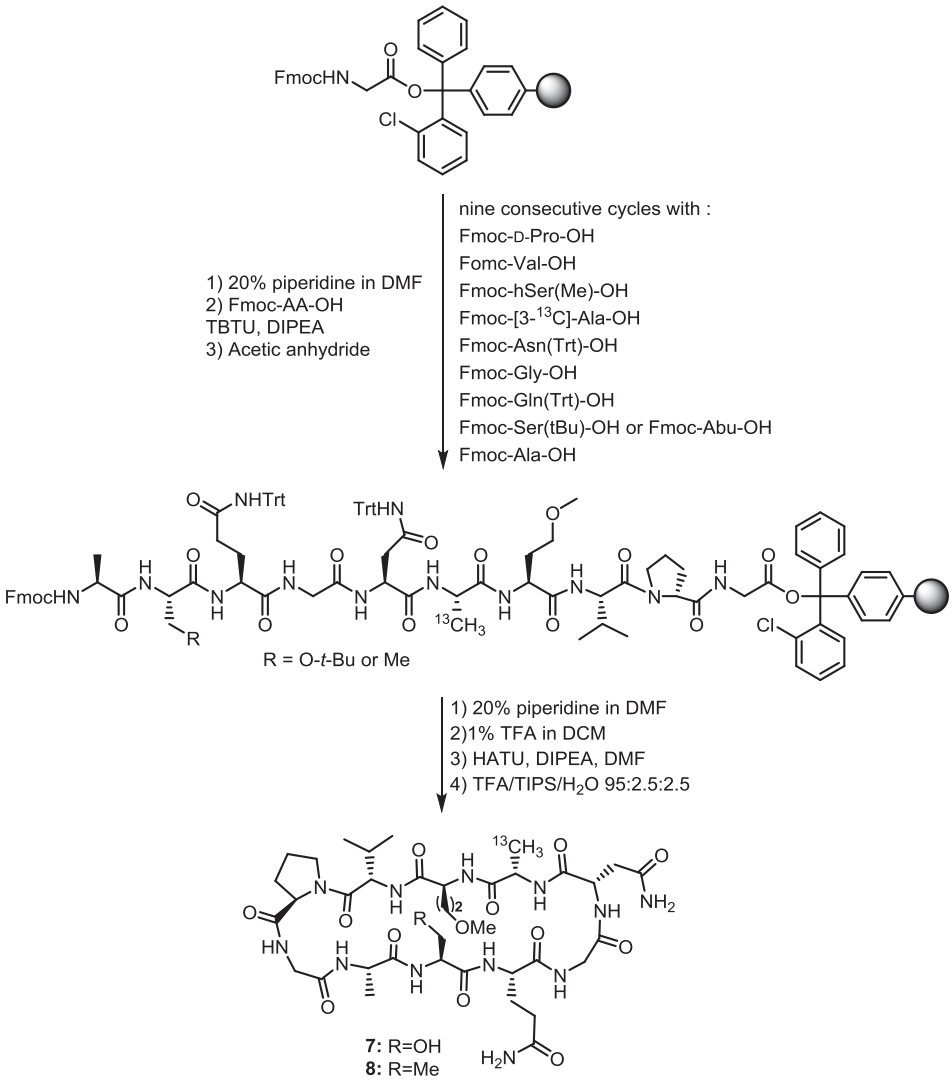

Appendix V. The input ensemble for the Ala(Cl)3 and Ser(Me)8 side chain NAMFIS analysis of peptide **9.**

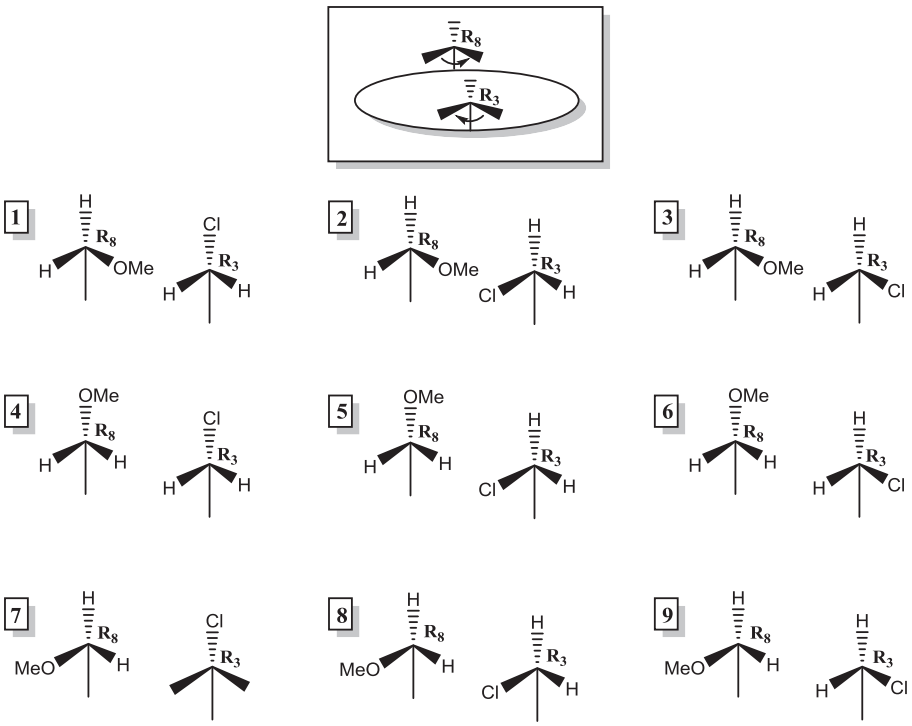

Figure A1. The input ensemble for the NAMFIS analysis of peptide **9**, with the Ala(Cl)3 and Ser(Me)8 interactions as constrains. The ensemble was generated by rotating the Cα—Cβ bond, as indicated by the arrows in the schematic β-hairpin in the square.

Appendix VI. Synthesis of **11**.

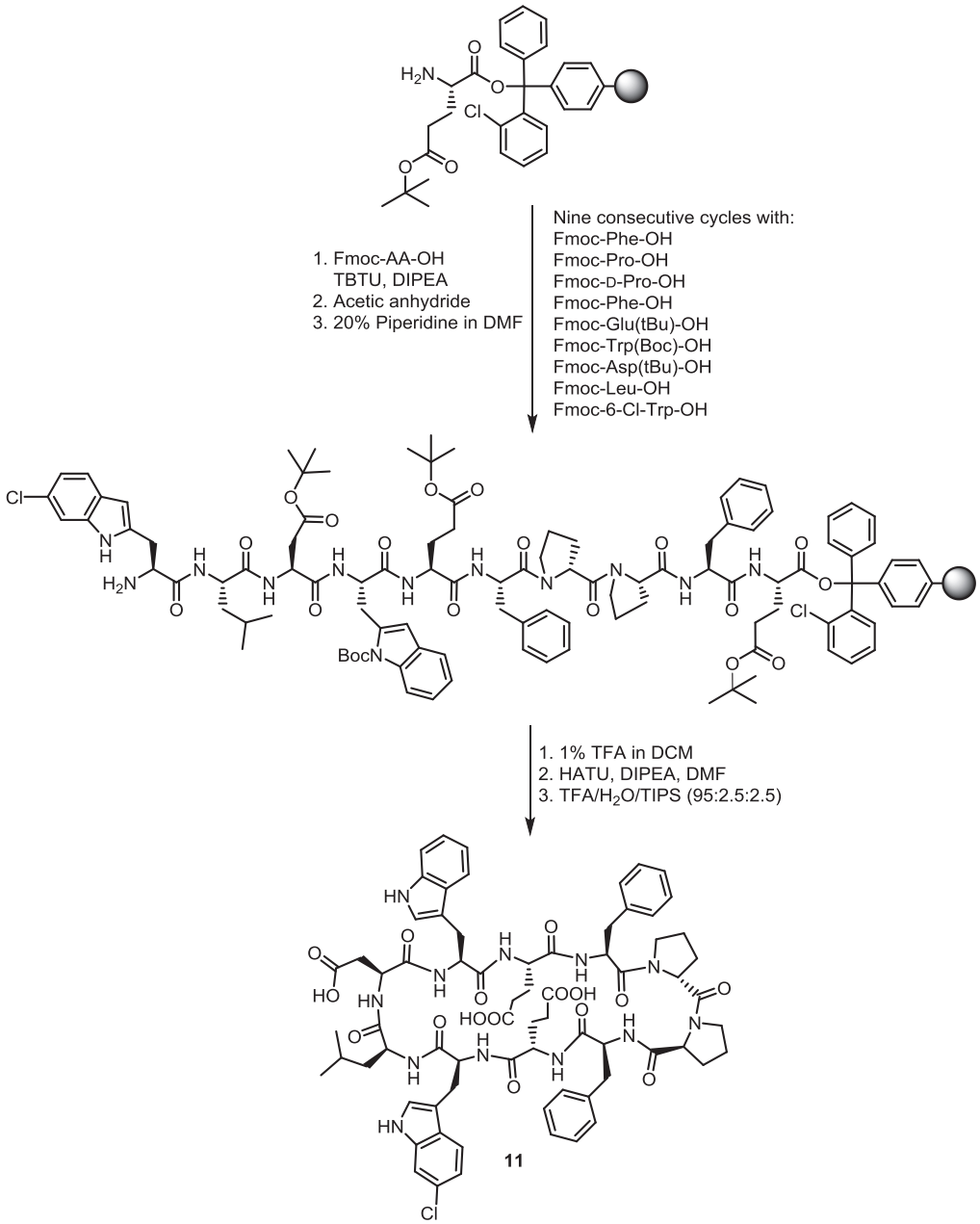

Appendix VII. Synthesis of **12** and **13**.

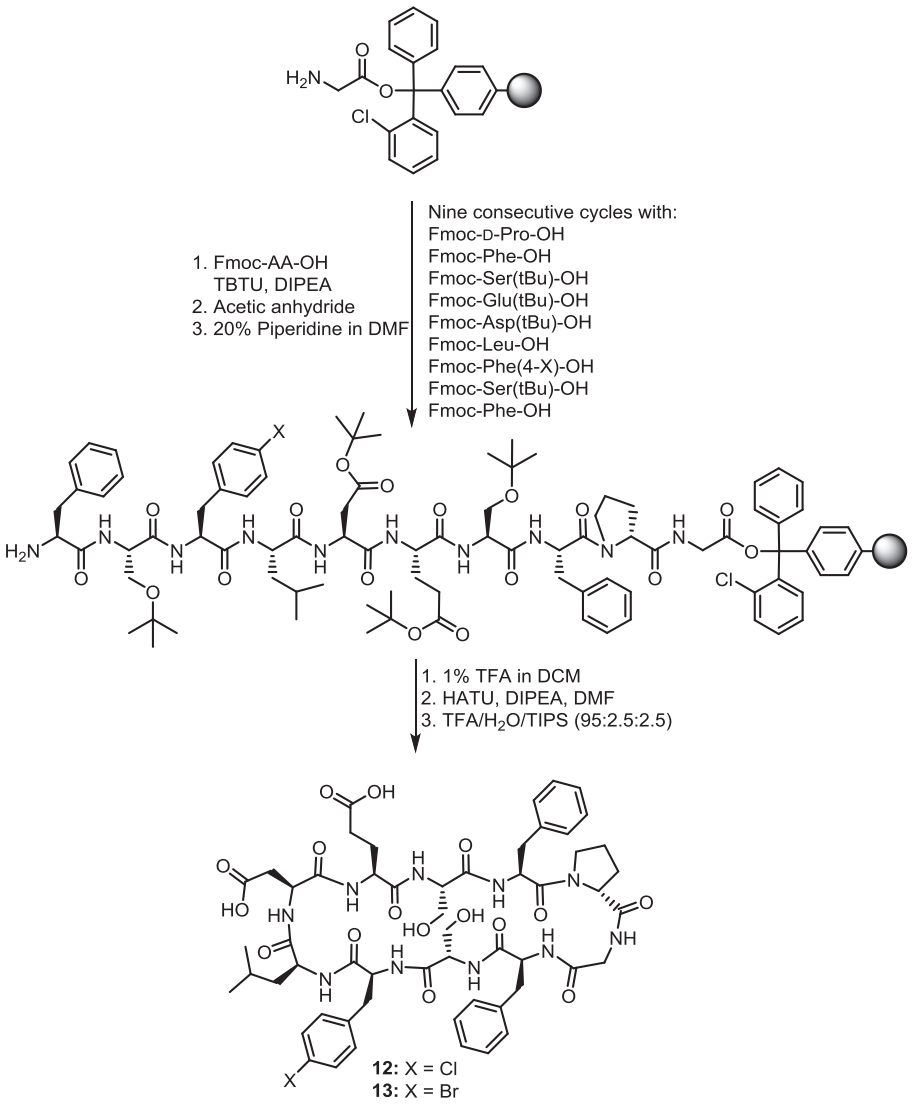

Appendix VIII. Synthesis of **14**.

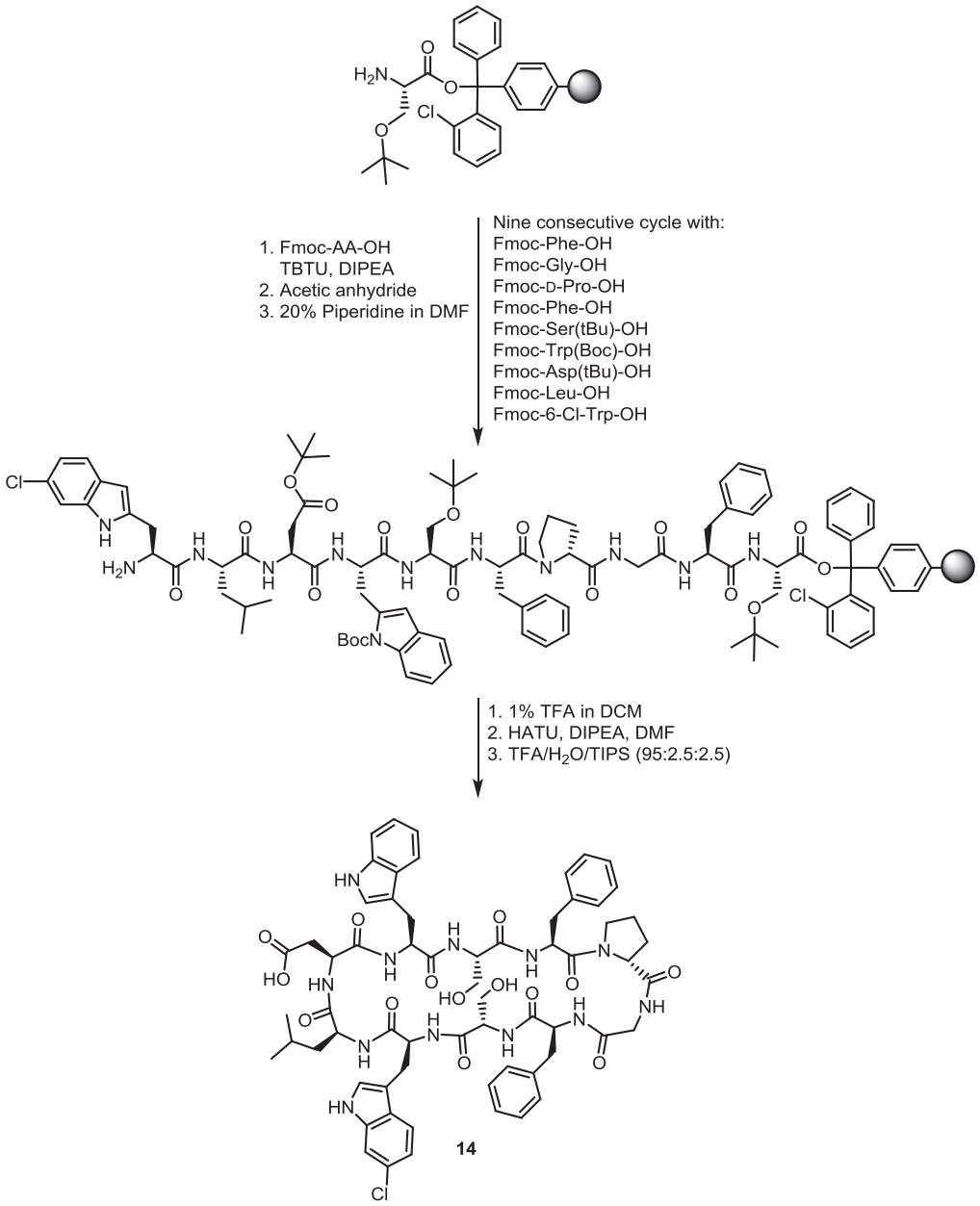

Appendix IX. [1]H NMR assignment for Roxithromycin.

Proton assignments were derived from TOCSY, NOESY, COSY, and HSQC NMR spectra recorded at 25 °C on a 900 MHz BRUKER Avance III HD NMR spectrometer equipped with a TCI cryoprobe.

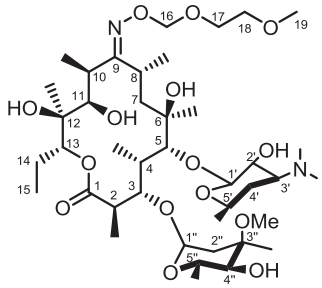

Table A1. [1]HNMR assignment (ppm) of roxithromycin in $CDCl_3$ and D_2O.

	Macrocycle			Sugars	
	$CDCl_3$	D_2O		$CDCl_3$	D_2O
1	-	-	1'	4.43	4.6
2	2.9	3.06	2'	3.49	3.53
2-Me	1.18	1.23	2'-OH	3.28	-
3	3.98	3.84	3'	2.49	3.48
4	2.03	2.02	3'-NMe_2	-	2.86
4-Me	1.09	1.07	4'	1.70, 1.27	2.12, 1.57
5	3.54	3.53	5'	3.5	3.89
6	-	-	5'-Me	1.23	1.31
6-Me	1.49	1.44	1"	4.84	4.95
7	2.35, 1.58	1.67, 4.56	2"	2.36, 1.56	2.53, 1.68
8	3.75	3.74	3"-Me	1.24	1.25
8-Me	1.03	1.14	3"-OMe	3.31	3.32
9	-	-	4"	3.02	3.23
10	2.67	2.94	4"-OH	2.21	
10-Me	1.19	1.19	5"	4	4.13
11	3.82	3.68	5"-Me	1.28	1.31
11-OH	4.31	-			
12	-	-			
12-Me	1.14	1.23			
12-OH	3.14	-			
13	5.1	5.14			
14	1.92, 1.47	1.87, 1.55			
15	0.85	0.85			
16	5.19, 5.17	5.22, 5.19			
17	3.80, 3.72	3.84			
18	3.57, 3.56	3.64			
19	3.42	3.4			

Appendix X. Interproton distances for Roxithromycin.

NOE build-ups were recorded without solvent suppression with mixing times of 100, 200, 300, 400, 500, 600, and 700 ms. The relaxation delay was set to 2.5 s, and 16 scans were recorded with 16384 data points in the direct dimension and 512 data points in the indirect dimension. Distances were calculated using geminal methylene protons (1.78 Å) as reference. The NOE peak intensities were calculated according to ([cross peak1 × cross peak2]/[diagonal peak1 × diagonal peak2])$^{0.5}$. At least 4 mixing times giving a linear ($R^2 > 0.97$) initial build-up rate (σ_{ij}) were used. The interproton distances (r_{ij}) were calculated according to the equation $r_{ij}=r_{ref}(\sigma_{ref}/\sigma_{ij})^{(1/6)}$.

Table A2. Interproton distances (Å) for roxithromycin derived from NOE build-up measurements in $CDCl_3$.

No.	Proton A	Proton B	σ	R^2	Distance rAB (Å)
1	13	11	0.0000091	0.99	2.31
2	3	5	0.0000250	0.99	1.95
3	11	4	0.0000013	0.99	3.19
4	2	4	0.0000110	0.99	2.24
5	3	4	0.0000130	0.99	2.18
6	11	10	0.0000147	0.99	2.13
7	10	7B	0.0000049	0.99	2.61
8	8	6Me	0.0000357	0.98	1.84
9	2	4Me	0.0000314	0.99	1.88
10	10	8Me	0.0000335	0.99	1.86
11	10	12Me	0.0000475	0.99	1.75
12	5	4Me	0.0000021	0.98	2.94
13	5	6Me	0.0000257	0.98	1.94
14	1"	2"A	0.0000068	0.99	2.43
15	1"	2Me	0.0000435	0.99	1.78
16	1"	3	0.0000310	0.99	1.88
17	1'	5'	0.0000272	0.98	1.92
18	1'	3'	0.0000464	0.99	1.76
19	4"	5"Me	0.0000235	0.99	1.97
20	1'	4Me	0.0000138	0.99	2.15
21	5	5"	0.0000071	0.99	2.41
22	11	12Me	0.0000075	0.97	2.44
ref.	2"A	2"B	0.0000433	0.99	1.78
ref.	17A	17B	0.0000380	0.76	1.76

Table A3. Interproton distances (Å) for roxithromycin derived from NOE build-up measurements in D_2O.

No.	Proton A	Proton B	σ	R^2	Distance rAB (Å)
1	13	11	0.0000193	0.99	2.93
2	11	4	0.0000623	0.99	2.41
3	2	4	0.0000314	0.99	2.70
4	10	4	0.0000035	0.98	3.90
5	3	5	0.0000235	0.99	2.84
6	5	4	0.0000110	0.99	3.22
7	3	2	0.0000084	0.99	3.37
8	3	4	0.0000167	0.99	3.00
9	11	10	0.0000426	0.99	2.57
10	13	12Me	0.0000036	0.98	3.89
11	3	2Me	0.0000060	0.99	3.56
12	10	8Me	0.0000073	0.99	3.45
13	10	12Me	0.0000243	0.99	2.82
14	2	4Me	0.0000131	0.98	3.13
15	5	6Me	0.0000228	0.98	2.85
16	3	6Me	0.0000038	0.98	3.85
17	3	4Me	0.0000018	0.99	4.35
18	10	8Me	0.0000364	0.98	2.64
19	4	6Me	0.0000029	0.98	4.02
20	1"	2	0.0000018	0.98	4.35
21	1'	4Me	0.0000185	0.99	2.95
22	1'	5"	0.0000660	0.99	2.39
23	1'	3"Me	0.0000080	0.99	3.40
24	1'	6Me	0.0000028	0.98	4.04
ref.	2"A	2"B	0.0003853	0.99	1.78
ref.	4'A	4'B	0.0004024	0.98	1.77

Appendix XI. MCMM conformational search of Roxithromycin.

The conformational searches were performed using the Monte Carlo algorithm with intermediate torsion sampling, 50 000 Monte Carlo steps, and a RMSD cut-off set to 2.0 Å, followed by molecular mechanics energy minimization with the software Macromodel (v.9.1) as implemented in the Schrödinger package. The energy minimization was performed using the Polak-Ribiere type conjugate gradient (PRCG) with maximum iteration steps set to 5000. All conformations within 42 kJ/mol from the global minimum were saved. The results of the four independent searches performed using OPLS-2005 or Amber* as force field, and with $CHCl_3$ and H_2O as solvation model, are given below. The ensembles from the conformational searches were combined, and elimination of redundant conformations by comparisons of the heavy atom coordinates applying the RMSD cutoff 1-1.5 Å was performed. These ensembles were combined and redundant conformations were eliminated again, giving the ensemble used for NAMFIS analysis. To this ensemble the three available crystal structures of roxithromycin were added (CSD: FUXYOM,[166] EWETUV[171] and KAHWAT[170]).

Table A4. Results of the MCMM conformational analysis.

		Number of conformations		
		Total[a]	Within 12.6 kJ/mol[b]	Following redundant conformer elimination[c]
$CHCl_3$	OPLS	177	13	62
	Amber*	197	25	
H_2O	OPLS	172	14	38
	Amber*	127	14	

[a]Total number of unique conformations found. The global minimum was found for all investigated compounds at least 30 times. [b]Conformations found within 12.6 kJ/mol (3.0 kcal/mol) of the global minimum. [c]Conformations obtained after redundant conformation elimination with the RMSD cutoff 1.5 Å ($CHCl_3$) and 1.Å (H_2O) for heavy atoms. These ensembles were again combined and reduced by redundant conformer elimination (RMSD cutoff = 1.5 Å) giving the ensemble used as input in the NAMFIS analysis (66 conformers).

Appendix XII. NAMFIS analysis of Roxithromycin.

Solution ensembles were determined by fitting the experimentally measured distances to those back-calculated for computationally predicted conformations following previously described protocols. CH_2 signals were treated according to the equation $d=(((d_1^{-6})+(d_2^{-6}))/2)^{-1/6}$, and methyl signals according to $d=(((d_1^{-6})+(d_2^{-6})+(d_3^{-6}))/3)^{-1/6}$. The NAMFIS ensemble analyses were validated using standard methods, that is through evaluation of the reliability of the conformational restraints by the addition of 10% random noise to the experimental data, by the random removal of individual restraints, and by comparison of the experimentally observed and back-calculated distances. Since the orientations of flexible parts of molecules are not as well predicted by the conformational searches as the more rigid parts, only macrocycle interactions were included in the initial NAMFIS analyses, corresponding to distance 1-13 for $CDCl_3$ and distance 1-19 for D_2O (Table A2 and A3).

Table A5. Experimentally determined and back-calculated (NAMFIS) interproton distances (Å).

MCMM $CDCl_3$		MCMM + X-ray $CDCl_3$		MCMM D_2O		MCMM + X-ray D_2O	
Exp.	Calc.	Exp.	Calc.	Exp.	Calc.	Exp.	Calc.
2.31	2.80	2.31	2.79	2.93	2.90	2.93	2.85
1.95	2.57	1.95	2.58	2.41	2.82	2.41	2.87
3.19	3.67	3.19	2.50	2.70	2.44	2.70	2.39
2.24	2.63	2.24	2.54	3.90	4.00	3.90	3.80
2.18	2.53	2.18	2.35	2.84	2.32	2.84	2.30
2.13	2.68	2.13	2.56	3.22	2.91	3.22	2.96
2.61	2.94	2.61	2.42	3.37	2.90	3.37	2.73
1.84	2.59	1.84	2.57	3.00	2.62	3.00	2.66
1.88	2.57	1.88	2.48	2.57	2.68	2.57	2.69
1.86	2.70	1.86	2.64	3.89	2.96	3.89	3.07
1.75	2.72	1.75	2.52	3.56	3.26	3.56	3.31
2.94	3.14	2.94	3.63	3.45	3.55	3.45	3.38
1.94	2.66	1.94	2.72	2.82	2.74	2.82	2.78
				3.13	2.70	3.13	2.78
				2.85	2.81	2.85	2.83
				3.85	3.93	3.85	3.90
				4.35	3.90	4.35	3.88
				2.64	2.97	2.64	2.86
				4.02	2.58	4.02	2.62
RMS=0.61		RMS=0.60		RMS=0.49		RMS=0.48	